



UNIVERSIDAD DE PUERTO RICO  
RECINTO DE RÍO PIEDRAS  
SENADO ACADÉMICO

Comité de Búsqueda y Consulta del Senado Académico para la  
Designación del Rector o Rectora del Recinto de Río Piedras

DOCUMENTOS SOMETIDOS POR LOS  
NOMINADOS Y NOMINADAS

**Ana R. Guadalupe Quiñones**

17 de agosto de 2010

# **Curriculum Vitae**

Department of Chemistry, P.O. Box 23346  
University of Puerto Rico, Río Piedras Campus '10 AUG 16 P 1 :13  
San Juan, Puerto Rico 00931-3346

Work Phone (787) 764-0000, ext. 7822  
Business Cell Phone: (787) 373-7676  
Personal Cell Phone: (787) 460-0193  
E-mail: [anlupe@uprrp.edu](mailto:anlupe@uprrp.edu)

## ANA R. GUADALUPE QUIÑONES

### SUMMARY OF QUALIFICATIONS

1998 Professor of Chemistry, University of Puerto Rico, Río Piedras Campus

### EDUCATION

1987-88 Postdoctoral - University of North Carolina, Chapel Hill, North Carolina.  
1984-87 Ph.D. in Analytical - Electrochemistry, Cornell University, Ithaca, New York.  
1981-84 M.Sc. in Analytical Chemistry - University of Puerto Rico, Río Piedras Campus  
1974-79 B.Sc. in Chemistry - University of Puerto Rico, Río Piedras Campus

### LANGUAGES

English and Spanish

### PROFESSIONAL EXPERIENCE

2009 Acting Chancellor, University of Puerto Rico, Río Piedras Campus  
2001-2009 Dean of Graduate Studies and Research, University of Puerto Rico, Río Piedras Campus  
1999-2000 Director, Office of Academic Affairs, Vice Presidency for Research and Academic Affairs, UPR-Central Administration  
1994-98 Coordinator of the Chemistry Graduate Program, University of Puerto Rico, Río Piedras Campus  
1998 Professor - University of Puerto Rico, Río Piedras Campus  
1992-98 Associate Professor - University of Puerto Rico, Río Piedras Campus  
1988-92 Assistant Professor - University of Puerto Rico, Río Piedras Campus  
1982-84 Instructor - Interamerican University, Río Piedras, Puerto Rico  
1981-82 Teacher Assistant - University of Puerto Rico, Río Piedras Campus  
1979-81 Laboratory Instructor - University of the Sacred Heart, Santurce, Puerto Rico

## PROFESSIONAL MEMBERSHIPS

---

American Chemical Society, Puerto Rico Chapter: Treasurer 1996 and President 1998  
Puerto Rico Science Teachers Association: President 1991-93

## AWARDS RECEIVED

---

1984-85      Cornell University Minority Fellowship  
1986-87      Johnson Foundation Fellowship  
1987-88      North Carolina Minority Postdoctoral Scholarship  
1997          Academic Excellence and Productivity Award, Academic Senate, University of  
Puerto Rico, Río Piedras Campus

## CONTINUED EDUCATION

---

### *Research*

1986          Workshop: *Microelectrodes*, Penn State University, Pennsylvania  
1988          Collaborative Work: *Polymer Modified Electrodes*, Grenoble, France  
1989          NSF - *Summer Polymer Course for Undergraduate Faculty*, Rensselaer Polytechnic  
Institute, Nueva York  
1994          Howard Hughes Medical Institute - *Workshop in DNA Recombinant Technology* -  
Mayaguez Campus, University of Puerto Rico  
1997          Workshop: *Molecular Modeling and Computational Chemistry* - University of  
Massachusetts, Amherst, Massachusetts  
1997          Course on *Scanning Electron Microscopy and X-Rays Microanalysis*, University of  
New York at New Paltz, New York  
1998          Workshop: *Contemporary Biomaterials through Precise Control of Macromolecular  
Chemistry and Architecture*, College of Mary and Williams, Virginia  
1999          Workshop: *Advanced Polymers through Macromolecular Engineering*, College of  
Mary and Williams, Virginia

### *Education and Administration*

2000          Workshop on the *Role of the Executive Administrator*, University of Puerto Rico,  
Central Administration  
2000          *Outcomes Based Assessment and Accreditation Conference*, Middle States  
Commission on Higher Education, Condado Plaza, San Juan, Puerto Rico  
2000          Conference in *Problem Based Learning*, Samford Institute, Alabama  
2000          Workshops in *Program Review and Graduate School Database*, Annual Meeting,  
Council of Graduate Schools, New Orleans, Louisiana

- 2000 *Quality Assurance in Higher Education*, Annual Meeting, Middle States Association of College and Schools, Philadelphia, Pennsylvania
- 2000 Executive Training Course in *Project Management*, ExecTrain, San Juan, P.R.
- 2002 Workshop in *Assessment in Higher Education*, NCTLA Assessment Institutes - Penn State University, Center for the Study of Higher Education, San Juan, Puerto Rico
- 2003 Summer Institute in *Educational Fundraising*, Council for the Advancement and Support of Education, Dartmouth College, New Hampshire
- 2007 *Survival Skills and Ethics Program*, University of Pittsburgh, Snowmass, Colorado
- 2007 *Recruiting and Retaining Adult and Graduate Students: Mastering Techniques to Increase Market Share*, Aslanian Group: Experts in Adult Learning, San Francisco, CA
- 2008 *Teaching Research Ethics Annual Workshop*, University of Indiana, Indiana, Bloomington

## **SCIENTIFIC AND PROFESSIONAL PRESENTATIONS**

---

More than 100 scientific and professional presentations, most of them working in collaboration with undergraduate and graduate students.

## **SUPERVISED THESES**

---

- 1991 *The Homogeneous Electrocatalytic Enzyme Coupled Oxidation of L(-) Malate using [Ru(tpy)(bpy)(H<sub>2</sub>O)](NO<sub>3</sub>)(PF<sub>6</sub>) as a Mediator*, Neftalí Rivera, MS
- 1993 *Estudio de la oxidación electroquímica de NADH en presencia de un sistema enzima -mediador*, Yanira Colón, MS
- 1994 *Activated Carbon Paste: Electrochemical Characterization and Application to Biosensors*, Noel Motta, PhD
- 1995 *Insulin Delivery from Glucose Responsive Membranes of Copolymers of 4-Vinylpyridine and Vinylferrocene*, Sonia A. Soto, MS
- 1996 *Polymeric Films of Mixed Cyano-Pyridyl Complexes of Iron(II)*, Vanessa Rivera, M.S.
- 1997 *An NADH Sensor Based on Lipoamide Dehydrogenase and its Coupling to Lactate Dehydrogenase*, Carmen Colón, MS
- 1997 *Development of a Biosensor for Hydrogen Peroxide Detection*, María E. Morales, MS
- 2000 *Ruthenium Polypyridyl Complexes as Molecular Probes for Dehydrogenases and Nucleic Acid Research*, Neftalí Rivera, PhD
- 2001 *Electrochemical Production of Copper Nanoparticles Using Block Copolymers as Templates and Their Catalytic Activity in CO<sub>2</sub> Electroreduction*, Sandra González, MS
- 2002 *L-Cysteine Methyl ester-Modified Sol-gel Graphite Screen-Printed Electrode as a Chemical Sensor for the Determination of Hg(II) in Aqueous Solutions*, Magaly Cintrón, MS
- 2004 *Rhodium and Ruthenium Polypyridyl Complexes and Their Applications in the Non-Enzymatic Regeneration of NADH*, Zhiqin Ji, PhD
- 2006 *Electrochemical Studies and Binding Parameters of the Interaction of Electroactive Polyelectrolytes with Nucleic Acids*, José N. Carrasquillo, PhD

2006 *Electrochemical Preparation and Physicochemical Characterization of Porous Silicon and Anodic Films of Porous SiO<sub>2</sub>*, Mariem Rosario, PhD

## CONSULTATIONS

---

1989, 1994, 1996 Special Proposal Review Committee, USA National Institute of Health  
1993, 1996 Member of the Scientific Affairs Committee of Puerto Rico Industry-University Consortium  
1996 - Reviewer for the J. of Electroanalytical Chemistry, Electroanalysis, J. of the Brazilian Chemical Society, Macromolecules, and Journal of the American Chemical Society  
2003 Chair, Council of Higher Education Commission for the License Renewal of the University of Sacred Heart, Santurce, PR  
2000, 2004 National Science Foundation Proposal Panel Reviewer  
2005-2007 NIH Instrumentation and Systems Development Study Section, Bioengineering and Technologies Integrated Review Group  
2005-2009 Member, Committee of Minorities in Graduate Education, USA Council of Graduate Schools  
2006-2009 Member, Educational Testing Service: GRE Executive Board and Committee on Minorities in Graduate Education

## OTHER ACTIVITIES

---

1990-91 Judge in the Puerto Rico Humanities and Scientific Symposium, PR Science Teachers Association  
1990-91 Judge in the Symposium on Scientific Research for High School Students, PR Science Teachers Association  
1991-92 Member of the Organizing Committee of the Second & Third State Conference for the Professional Improvement of Puerto Rico Science and Mathematics Teachers, Caribe Hilton Hotel, San Juan, P. R.  
1991-92 PIVES - Coordinator of Scientific Research Activities for High School Students, Resource Center for Science and Engineering, University of Puerto Rico  
1990 Chair, First Mini-Gordon Conference in Electrochemistry, Lajas, P. R.  
1992 to date NSF/AMP Undergraduate Research Mentor  
1993-94 Member of the Committee of Graduate Academic Affairs, Chemistry Graduate Program, University Puerto Rico, Río Piedras Campus  
1996-98 Member of the Department of Chemistry, Personnel Committee, University Puerto Rico, Río Piedras Campus  
1995 Workshop on Ethics in Teaching and Research - Teacher Assistants Traineeships - University of Puerto Rico, Río Piedras Campus  
1995-98 Teacher in the Review Section in Analytical Chemistry and Instrumental Analysis for the PR Chemists License Exam - Colegio de Químicos de Puerto Rico  
1995-97 Representative of the Faculty of Natural Sciences in the Advisory Council of Graduate Studies and Research, University of Puerto Rico, Río Piedras Campus

1996 Chautauqua Short Course in Chemical Sensors and Biosensors, Sponsored by NSF -  
Resource Center for Science & Engineering, University of Puerto Rico  
1998 American Chemical Society Coordinator of Project SEED

## **AWARDED GRANTS**

---

### *Research*

NIH-SUBE: Interfacial Dynamics of Electron Transfer Reactions of Proteins, 1988-1992, \$152,000  
Industry University Consortium: Fundamental Studies of Homogeneous and Heterogeneous Electrocatalysts, 1989-90, \$16,200  
UPR-FIPI: Fundamental Studies of Heterogeneous Electrocatalysts, 1989-90, \$4,500  
UPR-FIPI: Electrochemical and Spectroscopical Studies of Multifunctional Microstructures Assembled on Electrode Surfaces, 1990-93, \$18,000  
NIH-SUBE: Interfacial Dynamics of Electron Transfer Reactions of Proteins, 1992-96, \$163,139  
Industry University Consortium: Coupling of Enzymatic and Electrochemical Reactions for Controlled Drug Release, 1992-93, \$49,170  
Abbott Pharmaceutical Laboratories: Alternative Methods for the Determination of Compounds of Clinical Relevance, 1993-94, \$36,250  
Industry University Consortium: Toward a Rationale Design of Polymeric Membranes for the Controlled Release of Insulin, 1994-96, \$68,156  
NSF-EPSCoR: Supramolecular Chemistry on Electrode Surfaces, 1994-95, \$41,193  
DoE-EPSCoR: Polymer Supported Copper Particles as Electrocatalysts: Morphological Effects on Catalytic Activity, 1994-96, \$102,340  
NIH-MBRS: Reactivity and Energetics of Dehydrogenase Enzymes and Redox Mediators, 1996-2000, \$130,279  
DoE-EPSCoR: Electrocatalysis on Polymer - Metal Nanoparticles Composites, 1996-00, \$253,976  
NSF-EPSCoR: Surface Confined Binuclear Transition Metal Complexes, 1995-99, \$116,416  
Industry University Consortium: Multicomponent Drug Delivery Vehicles of Nanoscale Dimensions, 1996-98, \$62,633  
EPA-EPSCoR: Development of Peptide Nucleic Acids Biosensors for the Detection of Faecal Coliforms in Drinking Water, 2000-02, \$270,000  
NSF-PREM: Penn University and UPR-Humacao Partnership for Research and Education in Materials, 2002-7, \$250,000  
NSF-PREM: Penn University and UPR-Humacao Partnership for Research and Education in Materials, 2009-2014, \$300,000

### *Education and Administration*

NSF-REU	Hands-On Experiences in Modern Chemical Instrumentation, 1997-2004, \$ 486,000.00
NSF-EESE	Preparing Current and Future Researchers to Understand the Ethical Parameters of Research, from Inception to Dissemination, 2008-2010, \$299,956
USA-DE Title V (graduate)	Expanding Graduate Education and Achieving Success for Hispanics at UPR-Río Piedras Through Distance Education, 2009-2014, \$2,873,651
NSF Advance	ADVANCE Institutional Transformation Award: Empowering Science Women and Building an Inclusive and Responsive Science Community to Foster Faculty Development at the Colleges of Natural and Social Sciences, \$2.5M, (For resubmission)

### **PUBLICATIONS**

---

1. Guadalupe A.R., Abruña H.D., Electroanalysis with Chemically Modified Electrodes, *Anal. Chem.*, 1985, 57, 142.
2. Wier L.M., Guadalupe A.R., Abruña H.D., Multiple Use Polymer Modified Electrode for Electroanalysis of Metal Ions in Solution, *Anal. Chem.*, 1985, 57, 2009.
3. Guadalupe A.R., Wier L.M., Abruña H.D., Analytical Applications of Polymer Modified Electrodes, *American Laboratory*, 1986, 18(8), 102.
4. Guadalupe A.R., Abruña H.D., Organic Electroanalysis with Chemically Modified Electrodes, *Anal. Letters*, 1986, 19(15&16), 1613.
5. Guadalupe A.R., Jhaveri S.S., Liu K. E., Abruña H.D., Electroanalysis of Primary Amines with Chemically Modified Carbon Paste Electrodes, *Anal. Chem.* 1987, 59, 2436.
6. Potts K.T., Usifer D.A., Guadalupe A.R., Abruña H.D., 4-Vinyl, 6-Vinyl and 4'-Vinyl-2,2':6'2"-Terpyridinyl Ligands: Their Synthesis, Transition Metal Coordination Chemistry and Electrochemistry, *J.A.C.S.*, 1987, 109, 3961.
7. Guadalupe A.R., Usifer D.A., Potts K.T., Abruña H.D., Charge Transport and Novel Chemical Pathways of Electrodes Modified with Electropolymerized Layers of  $[\text{Co}(\text{vtpy})_2]^{2+}$  *J.A.C.S.*, 1988, 110, 3462.
8. Guadalupe A. R., Usifer D. A., Potts K. T., Abruña H.D., Novel Chemical Pathways at Chemically Modified Electrodes in Chemically Modified Surfaces, Vol. 2, D. E. Leyden, ed., Gordon & Breach, Holland, 1988.
9. Guadalupe A.R., Liu K. E., Abruña H.D., Transport Properties of Cationic Dyes in Nafion Films: Unusually High Diffusion Coefficients and Aggregations Effects, *Electrochimica Acta*, 1991, 36(5/6), 881.

10. Adeyerim S. A., Dovletoglon A., Guadalupe A. R., Meyer T.J., Redox and Spectral Properties of the Four-Electron Oxidant trans-[Ru(tpy)(O)<sub>2</sub>(H<sub>2</sub>O)](ClO<sub>4</sub>)<sub>2</sub>, *Inorg. Chem.*, 1992, 31, 1375.
11. Guadalupe, A.R.; Chen, X.; Sullivan, B.P.; Meyer, T.J., Oxo Complexes, pH Effects and Catalysis in Films Formed by Electropolymerization, *Inorg. Chem.*, 1993, 32, 5502.
12. Motta, N.; Guadalupe, A.R. Activated Carbon Paste Electrodes for Biosensors, *Anal. Chem.*, 1994, 66, 566.
13. Rivera, N.; Colón, Y.; Guadalupe, A. R. Ruthenium Complexes as Redox Mediators for Malate and Lactate Dehydrogenases, *Bioelectrochem. & Bioenergetics*, 1994, 34, 169.
14. Martínez, F.; Murray, M.; Guadalupe, A.R. Polymer Modified Electrodes for Metal Ion Sensors - Symposium in "Transducer Active Polymers" - Division of Polymeric Materials: Science and Engineering - ACS National Meeting, Fall 1994, Washington, DC, page 583.
15. Guo, Y.; Guadalupe, A.R. Direct Electrochemistry of Horseradish Peroxidase Adsorbed on Glassy Carbon Electrode from Organic Solvents, *The Royal Society of Chem., Chemical Communications*, 1997, page 1437.
16. Devenney, M.; Wost, L.A.; Gould, S.; Guadalupe, A.R.; Sullivan, P.B.; Gaspar, J.V.; Leasure, R.L.; Gardner, J.R.; Meyer, T.J. Excited States Interactions in Electropolymerized Thin Films of Ru<sup>II</sup>, Os<sup>II</sup>, and Zn<sup>II</sup> Polypyridyl Complexes, *J. of Phys. Chem. A*, 1997, 101, 4535.
17. Guo, Y.; Guadalupe, A.R. Electroanalytical Applications of Screen-Printable Surfactant-Induced Sol-Gel Graphite Composites, Sensors and Actuators, *Chemical Part B Chemical*, 1998, 46(3) 213.
18. Colón, C.; Guadalupe, A.R. Cobalt Polypyridyl Complexes as Redox Mediators for Lipoamide Dehydrogenase, *Electroanalysis*, 1998, 10(9), 621.
19. Guo, Y.; Guadalupe A.R. Preconcentration and Voltammetry of Mercury on a Functionalized Sol-Gel Thin Film Modified Glassy Carbon Electrode, *J. Pharm. Biomed. Anal.*, 1999, 19, 175-181.
20. Guo, Y.; Guadalupe A.R. On-site Characterization of Electrocrystallized Platinum Particles on Carbon and Sol-gel Thin Film Modified Carbon Surfaces, *Langmuir*, 1999, 15(3), 759-762.
21. Zhiqin J.; Guadalupe A.R. Reusable Doped Sol-gel Graphite Electrodes for Metals Ions Determination, *Electroanalysis*, 1999, 11(3), 167-176.
22. Guo, Y.; Guadalupe, A.R. Aerogel from Metastable Lamellar Surfactant/Sol-gel Composite, *Chem. Comm*, 1999, 315-316.
23. Guo, Y.; González S.; Guadalupe A.R.\* Substrate Dependent Colloidal Organization, *Journal of Colloid and Interface Science*, 1999.
24. Zhiqin, J., Yongkui, A., Guadalupe, A.R., and Songping D.H. Structure of cis-Dichlorobis (1,10-phenanthroline) Rhodium(III) Perchlorate, *New Crystal Structures*, NCS 214(1999), 1999.
25. Guo, Y.; Guadalupe, A.R.\* Chemical-Derived Prussian Blue So-Gel Composite Thin Films, *Chem.Mater.*, 11(1), 135-140, 1999.
26. Soni, R.K.; Fonseca L.F.; Resto, O.; Guadalupe A.R. and Weisz S.Z. Electropolymerization in Porous Silicon Film, *Mat. Res. Sc. Proc.*, 536, 197, 1999.
27. Alejandro, F.; Guadalupe A.R. Crystal Structure of 2,2'-bipyridine  $\eta^4$  - 1,5-cyclooctadiene Rhodium (I), hexafluorophosphate, *Z. Crystallography*, NCS 214, 463-464, 1999

28. Zhiqin, J.; Songping, H.; Guadalupe, A.R. \* Synthesis, X-ray Structures, Spectroscopic and Electrochemical Properties of Ruthenium (II) Complex Containing 2,2'- Bipyrimidine, *Inorganica Chimica Acta*, 305, 127-134, 2000.
29. Rosario-Canales, M.; Resto, O.; Fonseca, L.; Guadalupe, A.R. Physicochemical Characterization of Porous Silicon Surfaces Etched in Salt Solutions of Varying Compositions and pH, *Mater. Res. Soc. Proc.*, 762, 2003.
30. Muñoz, L. and Guadalupe, A.R. Morphological Studies of Oligonucleotide Probes Covalently Immobilized at Polystyrene Modified Surfaces, *J. of Biotechnology*, 118, 233-245, 2005.
31. Santiago, M.; Vélez, M.; Borrero, S.; Díaz, A.; Hofmann, C.; Guadalupe, A. R. \*; Colón, J. \* Amperometric Ethanol Biosensor Based on Bis((1,10-phenanthroline-5,6-dione)2,2'-bipyridine)ruthenium(II)-exchanged Zirconium Phosphate Modified Carbon Paste Electrodes, *Electroanalysis*, 18(6), 559-572, 2006.
32. Díaz, M.; Rosado, A.; del Pilar, J; Vega, E\*.; Guadalupe, A.R. Design, Construction and Analytical Characterization of a DNA Sensor for the Detection of *Salmonella*, *Polymeric Materials: Science and Engineering*, 98, 448-449, 2008.
33. Santiago, M. B.; Daniel, G.A.; David, A.; Guadalupe, A.R. \* ; Colón, J. L.\* Effect of Enzyme and Cofactor Immobilization on the Response of Ethanol Amperometric Biosensors Modified with Layered Zirconium Phosphate, *Electroanalysis*, 22(10), 1097-1105, 2010.
34. Cardona, R.A.; Hernández, K.; Pedró, L.E.; Otaño, M.; Montes, I. \*, Guadalupe, A. R.\* Electrochemical and Spectroscopical Characterization Of Ferrocenyl Chalcones, *J. of the Electrochemical Society*, 157(8), F104-110, 2010.
35. Rosario-Canales, M.; Rivera-Sánchez, M; Fonseca, L.F.; Resto, O.; Guadalupe, A.R. Synthesis and Characterization of Porous Silicon Surfaces in Base Media, **manuscript under revision.**
36. Feng, M.; Alejandro, F.; González, F.L.; Guadalupe, A.R. Electrochemical and Spectroscopic Studies of the Chemical Interaction and Binding of Poly-[Fe (4-vinyl-4'-methyl-2, 2-bipyridine)<sub>3</sub>]Cl<sub>2</sub> to Calf-Thymus DNA, **manuscript under revision.**
37. Díaz, M.; Rosado, A.; del Pilar, J; Vega, E\*.; Guadalupe, A.R. \* A Biosensor for Salmonella: Surface and Electrochemical Characterization, **manuscript in preparation.**

## **PATENTS**

---

Electroanalytical Applications of Screen-Printable Surfactant-Induced Sol-Gel Graphite Composites, A.R. Guadalupe and Y. Guo, USA Patent 6231920B1 – May 15, 2001

Revised August 2010

## **Publicaciones**



## Electrochemical and Spectroscopical Characterization of Ferrocenyl Chalcones

Rocío A. Cardona,\* Kenneth Hernández, Laura E. Pedró, Myrna R. Otaño, Ingrid Montes, and Ana R. Guadalupe<sup>†</sup>

Department of Chemistry, University of Puerto Rico, Río Piedras Campus, San Juan 00931-3346, Puerto Rico

We report on the electrochemical and spectroscopical characterization of 10 ferrocenyl chalcones. These compounds were synthesized via the Claisen-Schmidt condensation from acetylferrocene and the corresponding benzaldehyde or pyridine carboxaldehyde. The compounds were obtained in good yields (>60%) and purified by recrystallization. All compounds exhibit a quasi-reversible electrochemical behavior and chemical reversibility, as evidenced by  $\Delta E_p$  of 72–90 mV and  $I_{pa}/I_{pc}$  values equal to 1.0–1.17. The redox formal potential ( $E^{0'}$ ) for these compounds range between 665 and 774 mV. The heterogeneous electron-transfer rate constants calculated from the Nicholson method are in the range of  $(2.0\text{--}4.4) \times 10^{-2}$  cm/s. Their diffusion coefficients are on the order of  $(1.65\text{--}3.7) \times 10^{-3}$  cm<sup>2</sup>/s, and the number of electrons transferred equals 1. 1-ferrocenyl-3-(*p*-*N,N*-dimethylaminophenyl)prop-2-en-1-one shows a behavior similar to dimethylaniline and undergoes electropolymerization, producing cationic oligomers and dimeric species. The UV/visible spectra show the characteristic bands for aromatic systems in the UV region (200 and 280 nm) and bands in the visible (400 and 500 nm). The molar absorbance coefficient ( $\epsilon$ ) values are in the ranges  $(2.1\text{--}7.5) \times 10^4$  L/(mol cm) for  $\lambda_{max}$  of 200–300 nm and  $(1.8\text{--}17.6) \times 10^2$  L/(mol cm) for  $\lambda_{max}$  of 300–500 nm.

© 2010 The Electrochemical Society. [DOI: 10.1149/1.3439669] All rights reserved.

Manuscript submitted December 15, 2009; revised manuscript received April 12, 2010. Published June 15, 2010.

Ferrocene derivatives have been extensively studied for many reasons. First, they exhibit the well-defined one-electron redox process that is characteristic of ferrocene. The redox process is electrochemically reversible or quasi-reversible, and the formal redox potential ( $E^{0'}$ ) depends on the nature of the substituents attached to the cyclopentadienyl rings.<sup>1,2</sup> Through a variety of synthetic routes, derivatives can be made with tunable redox and spectroscopical properties.<sup>2,3</sup> They have found applications in different fields such as biosensors,<sup>4–5</sup> drug delivery systems,<sup>6</sup> electrocatalysts,<sup>7,8</sup> and optoelectronics,<sup>9</sup> among others.

A family of ferrocene derivatives that have drawn considerable attention from scientists in recent years is that of the ferrocenyl chalcones (FCs).<sup>10–12</sup> These compounds not only possess the redox activity of ferrocene, but they also show intense colors.<sup>12</sup> An FC is a compound where ferrocene is linked to an aromatic group through an enone moiety. Several derivatives of FCs have been synthesized and characterized structurally.<sup>10–13</sup> More recently, studies on FCs have focused on their biological properties, in particular their potential antiplasmodial and anticancer activity.<sup>11</sup>

In our case, we are interested in exploiting these compounds for applications in biosensing and electrocatalysis. For that purpose, we conducted a study of the electrochemical and UV/visible (UV/vis) behavior of several FCs (Fig. 1). To the best of our knowledge, few studies have been published using FCs for these applications.

### Experimental

**Chemicals.**— Ferrocene (98%), acetylferrocene (95%), 3-nitrobenzaldehyde (99%), 4-nitrobenzaldehyde (98%), 4-methoxybenzaldehyde (98%), 4-chlorobenzaldehyde (98%), 4-(dimethylamino) benzaldehyde ( $\geq 99\%$ ), 2-fluorobenzaldehyde (97%), 3-fluorobenzaldehyde (97%), 2-pyridinecarboxaldehyde (99%), 3-pyridinecarboxaldehyde (98%), 4-pyridinecarboxaldehyde (97%), tetrabutylammonium perchlorate (TBAP), acetonitrile (ACN)-*d*<sub>3</sub> (99.6% D), chloroform-*d* (99.8% D), acetone, and ethanol (American Chemical Society grade) were obtained from Aldrich. ACN (Burdick and Jackson) was dried over 4 Å molecular sieves. Diamond paste (no. 40-6244) and metadi fluid (no. 40-6032) were

from Buehler Co. Nanopure water (17 MΩ cm, Barnstead) was used in all experiments. Thin-layer chromatography (TLC) was done with 250 μm Al<sub>2</sub>O<sub>3</sub> plates (Whatman).

**Synthesis and characterization of the compounds.**— FCs were synthesized in Dr. I. Montes' laboratory following the Claisen-Schmidt reaction, as previously published.<sup>11,14,15</sup> <sup>1</sup>H and <sup>13</sup>C NMR spectra were taken in a 500 MHz Bruker-AV spectrometer, while the UV/vis spectra were done in a Perkin-Elmer (Lambda 35) spectrophotometer.

**Synthesis of FCs.**— 1 mmol of acetylferrocene was added to a 50 mL erlenmeyer flask and dissolved in a 1:1 ethanol/water solution with 10 mmol of NaOH at room temperature. In another flask, 1 mmol of the desired aromatic derivative was mixed with 3–5 mL of ethanol. The acetylferrocene solution was added slowly to the solution of the substituted benzaldehyde or pyridine carboxaldehyde under continuous stirring. The reaction progress was followed by TLC until completion. The resultant precipitate was collected by vacuum filtration and recrystallized. Compounds 2a and 2e were recrystallized from acetone, 2d from ethanol, and 2j from 1:1 ethanol/water. Mixtures of 1:1 acetone/water were used to recrystallize compounds 2b, 2f, 2g, 2h, 2i, and 2k, while a 2:1 mixture was used for compound 2c.

**Methylation of DMAPP.**— In a round flask, 1 mmol of 1-ferrocenyl-3-(*p*-*N,N*-dimethylaminophenyl) prop-2-en-1-one (DMAPP) and 8 mmol of sodium bicarbonate were dissolved in 2-methyl tetrahydrofuran. The mixture was stirred under N<sub>2</sub>, while 16 mmol of dimethylsulfate was added dropwise. After 1 h stirring at room temperature, the temperature was raised to 60°C for 2 h. The resulting precipitate was collected and dried. The purification was done by recrystallization from 1:1 acetone/water mixture.

**Electrochemistry.**— All electrochemical experiments were done in a BAS 100 B/W. A three-electrode electrochemical cell was used with Pt (area = 0.0197 cm<sup>2</sup>) or glassy carbon (area = 0.080 cm<sup>2</sup>), Ag/AgCl (NaCl 3 M), and nichrome as the working, reference, and counter electrodes, respectively. The Pt electrode surface was polished with diamond paste/metadi fluid in a microcloth and rinsed with water. Subsequently, the electrode was cycled in 1 M H<sub>2</sub>SO<sub>4</sub> solution from –200 to 1200 mV at 100 mV/s for 50 cycles, rinsed with water and air dried.

For each compound, a 10 mL of  $\sim 1 \times 10^{-3}$  M solution was prepared in 0.1 M TBAP/ACN. Cyclic voltammetry (CV) was run for each compound at scan rates of 20, 50, 100, 200, 500, 1000, and

\* Electrochemical Society Student Member.

<sup>†</sup> E-mail: anlupe@uprrp.edu

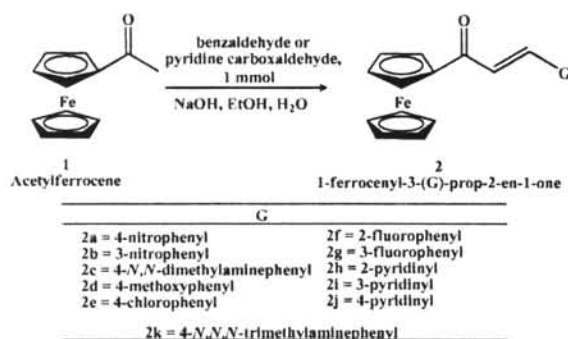


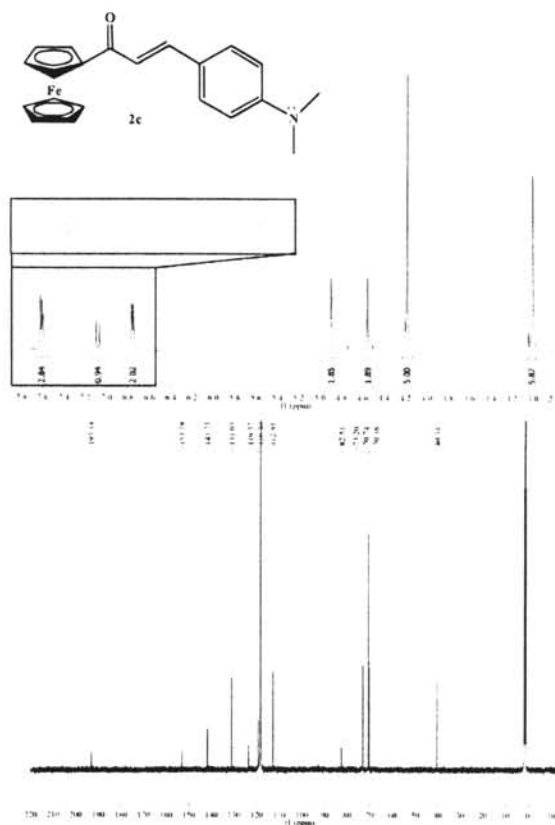
Figure 1. Synthesis of FCs.

2000 mV/s. 1 and 10 cycles were done for each scan rate, and the electrode was cleaned between scan rates. Each experiment was run three times, every time with a fresh solution. The background was recorded for each compound under the same experimental conditions of the sample. The cell was degassed with  $N_2$  for 10–15 min before each measurement. To determine the number of electrons transferred, a 10 mL TBAP 0.1 M/ACN solution containing  $\sim 1 \times 10^{-3}$  M of both ferrocene and the FC was prepared. A CV of the solution was recorded at 100 mV/s between 0 and 1200 mV. Chronocoulometry (CC) was done in a similar solution but without the ferrocene to determine the diffusion coefficient of the compounds. The applied potential pulse was from 200 to 1200 mV for 250 ms.

**UV/vis spectroscopy.**—The molar extinction coefficients of the most prominent UV/vis bands of the compounds were calculated from calibration curves following Beer's law. A  $1 \times 10^{-3}$  M stock solution of each compound was prepared in ACN followed by dilutions with concentrations in the  $(2-1000) \times 10^{-6}$  M range. Absorption spectra of all compounds were taken from 190–820 nm. The cell path was 1.00 cm.

### Results and Discussion

**Synthesis and chemical characterization.**—The FCs differ in the aromatic derivative attached to the double bond. The *o*- and *m*-fluorophenyl derivatives (2f, 2g) have not been reported until now. All the compounds were obtained in good yields (>60%) and were characterized by  $^1H$  and  $^{13}C$  NMR after purification. Figure 2 shows the  $^1H$  and  $^{13}C$  NMR spectra of DMAPP (2c). The  $^1H$  NMR shows three characteristic regions: the ferrocene [ $\delta$  (ppm) = 4.894 (s, 2H), 4.555 (s, 2H), 4.184 (s, 5H)], the *p*-*N,N*-dimethylaminophenyl [ $\delta$  (ppm) = 7.612 (d,  $J$  = 9 Hz, 2H), 6.758 (d,  $J$  = 8.5 Hz, 2H), 3.003 (s, 6H)], and the double bond [ $\delta$  (ppm) = 7.600 (d,  $J$  = 13.5 Hz, 1H), 7.082 (d,  $J$  = 15.5 Hz, 1H)].  $^{13}C$  NMR spectra show the expected number of signals according to the number of carbon atoms with chemical shifts as follows: ferrocene [ $\delta$  (ppm) = 82.59, 73.19, 70.78, 70.36], *p*-*N,N*-dimethylaminophenyl [ $\delta$  (ppm) = 153.07, 131.02, 112.90, 40.38], the carbonyl [ $\delta$  (ppm) = 193.13], and double bond [ $\delta$  (ppm) = 141.72, 123.62]. All FC compounds showed signals corresponding to these three distinct regions. The  $^1H$  chemical shifts corresponding to the ferrocene and double-bond regions were basically unaltered by the aromatic derivatives. As expected, the  $^1H$  chemical shifts of the aromatic derivative changed depending on the substituents on the phenyl or the position of the nitrogen atom in the pyridine. Similar results were observed for the  $^{13}C$  NMR where the ferrocene, carbonyl, and double-bond signals did not change significantly. The  $^{13}C$  NMR for the aromatic derivative followed the expected pattern depending on the compound molecular structure. Our results compare favorably with previously published values by Sol-

Figure 2.  $^1H$  and  $^{13}C$  NMR of DMAPP (2c) in  $CD_3CN$ .

canoia and co-workers.<sup>16</sup> See tables in the supporting information section<sup>17</sup> for a summary of the spectral analysis of the studied compounds.

**Electrochemical characterization.**—The redox activity of the FCs was studied using CV and CC. Figure 3A–C shows the CVs,  $I_{pa}$  vs the square root of the sweep rate curve (insert  $\log I_{pa}$  vs  $\log v$ ), and the Anson plot of DMAPP (2j) (insert:  $Q$  vs time, ms). The same electrochemical measurements were done for all FCs. Table 1 summarizes the electrochemical parameters of all the compounds.

The number of electrons transferred was determined by comparing the cathodic peak currents for ferrocene and each individual FC from a cyclic voltammogram of a solution containing both compounds at the same concentration and correcting by differences in their diffusion coefficients. Using this approach, from the Randles and Sevcik equation,<sup>15</sup> assuming a comparable rate of heterogeneous electron transfer ( $k_e$ ), the  $n$  values ranged from 0.87 to 1.47. Based on these data, we conclude that all FC compounds exhibit the expected  $1e^-$  redox process centered on the ferrocene moiety.

The formal redox potential ( $E^{0'}$ ) of the FCs varies from +665 mV for DMAPP (2c) to +773 mV for the 2-pyridinyl derivative (2h). Compared to ferrocene ( $E^{0'}$ ), the  $E^{0'}$  values are higher by at least +206 mV (DMAPP) to +314 mV (2-pyr). These  $E^{0'}$  changes can be explained by electronic effects. As reported by Wu and collaborators,<sup>11</sup> the carbonyl group on FCs is highly polarized, and as such it withdraws electron density from the ferrocene moiety, making its oxidation more difficult, a fact that is reflected on higher  $E^{0'}$  values. Simultaneously, but to a lesser extent, the substituents also exert an electronic influence by modulating the electron withdrawing capacity of the carbonyl group; this explains the small but

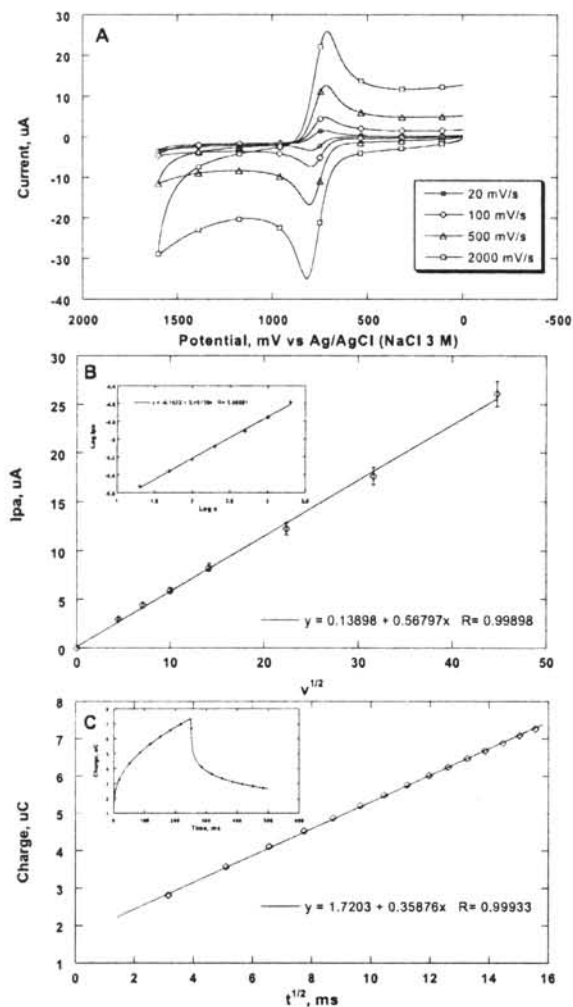


**Figure 3.** Cyclic voltammograms of a solution of 2j (1.00 mM) in 0.101 M TBAP/ACN at a platinum working electrode: (A) voltammogram at various scan rates, (B)  $I_{pa}$  vs  $v^{1/2}$  (insert:  $\log I_{pa}$  vs  $\log v$ ), and (C) Anson plot (insert:  $Q$  vs time).

still significant  $E^{0'}$  differences among the various derivatives. This is consistent with our observation that the nitro derivatives (Hammett values of  $\sigma_p = 0.81$  and  $\sigma_m = 0.71$ ) exhibit higher  $E^{0'}$  (as expected for electron withdrawing groups), while an electron donating substituent such as *N,N*-dimethylamino (Hammett value of  $\sigma_p = -0.63$ ) shows a lower  $E^{0'}$ . In general, the  $\log E^{0'}$  correlates satisfactorily ( $r = 0.935$ ) with the corresponding Hammett values<sup>12,19,20</sup> or the various substituents (see Fig. 4).

The  $I_{pc}/I_{pa}$  ratio, with the exception of the DMAPP (vide infra), is close to 1, showing that the redox process of the FCs is chemically reversible. The  $\Delta E_p$  values range between 72 and 90 mV, which is higher than the expected Nernstian value of 59 mV per electron, indicating that the redox process is electrochemically quasi-reversible.<sup>18</sup> The plots of  $I_{pc}$  (or  $I_{pa}$ ) vs the square root of the sweep rate shows a linear dependence, and the slopes of the plots of  $\log I_{pc}$  (or  $I_{pa}$ ) vs  $\log$  sweep rate are close to 0.5, evidencing that the redox process is diffusion controlled. The diffusion coefficients ( $D_{ox}$ ) are between  $1.65$  and  $3.7 \times 10^{-5}$  cm<sup>2</sup>/s, which closely agrees with the  $D_{ox}$  of ferrocene,  $2.4 \times 10^{-5}$  cm<sup>2</sup>/s.<sup>21</sup>

**Electropolymerization of DMAPP.**—Figure 5A shows the CV of 1 mM DMAPP derivative in 0.1 M ACN/TBAP. We observe three well-defined oxidations with (a)  $E_{pa} = +694$  mV, (b)  $+974$  mV, and (c)  $+1521$  mV and a cathodic process with (e)  $E_{pc} = +632$  mV. On top of the cathodic wave, there is a barely discernible shoulder around (d)  $+760$  mV. Figure 5B shows that on reversing the potential at  $+850$  mV, there is only one reversible wave with  $E^{0'} = +665$  mV. We assigned this wave to the oxidation and reduction of the ferrocene nucleus in the DMAPP in analogy with other FCs. The (b) second and (c) third oxidations, which are chemically irreversible are assigned to the successive loss of the nitrogen electrons in the *p-N,N*-dimethylamino group. The shoulder at (d)  $+760$  mV corresponds to the reduction of the cationic radical that is produced after the first oxidation of this group.

Figure 5C shows that on continuous cycling (50 cycles), the original waves [(a)–(e)] started to decrease with the peak at (c)  $+1521$  mV, decreasing faster than the others. Concurrently, we observe a small anodic wave growing between (f) 1070 and 1400 mV with a cathodic counterpart between (g) 900 and 1300 mV. The background current close to (h) 0 mV increases toward the negative potentials. We attribute these changes to the electropolymerization of DMAPP similar to what happens in the electrochemically induced polymerization of *N,N*-dimethylaminoaniline (DMA). Oyama and co-workers<sup>22</sup> reported the electrochemical oxidation of DMA, a compound that is structurally similar to the R group in DMAPP. DMA oxidizes electrochemically at  $+800$  and  $+1000$  mV vs saturated sodium chloride calomel electrode in 0.5 M Na<sub>2</sub>SO<sub>4</sub>. The first oxidation generates a radical cation (DMA<sup>•+</sup>) that oxidizes further into a dication (DMA<sup>2+</sup>). On continuous cycling, DMA<sup>•+</sup> electropolymerizes forming an electroinactive cationic polymeric film at the electrode surface.

**Table I.** Electrochemical parameters of the FCs.

Compound	$E^{0'}$ (mV/s)	$n$	$D_{ox}$ ( $\times 10^{-5}$ ) (cm <sup>2</sup> /s)	$I_{pc}/I_{pa}$	$\Delta E_p$ (mV)	Slope $\log I_{pa}$ vs $\log v$
2a	723.667 ± 0.001	0.93 ± 0.01	2.17 ± 0.01	1.01 ± 0.01	72.000 ± 0.0001	0.453
2b	722.69 ± 0.02	0.88 ± 0.01	3.33 ± 0.01	1.1 ± 0.4	90.00 ± 0.02	0.487
2c	664.50 ± 0.02	—	—	2.0 ± 0.5	47.67 ± 0.03	0.433
2d	680.833 ± 0.002	0.87 ± 0.02	3.7 ± 0.8	1.1 ± 0.1	86.333 ± 0.002	0.478
2e	691.50 ± 0.01	0.90 ± 0.02	3.4 ± 0.1	1.17 ± 0.04	75.67 ± 0.01	0.487
2f	699.00 ± 0.01	1.44 ± 0.13	1.65 ± 0.2	1.1 ± 0.2	79.67 ± 0.02	0.471
2g	693.00 ± 0.01	1.47 ± 0.10	1.73 ± 0.08	1.1 ± 0.1	79.333 ± 0.004	0.467
2h	773.17 ± 0.02	0.90 ± 0.01	3.17 ± 0.01	1.0 ± 0.2	72.000 ± 0.004	0.400
2i	733.667 ± 0.004	1.25 ± 0.01	2.80 ± 0.01	1.11 ± 0.04	83.33 ± 0.01	0.473
2j	760.000 ± 0.004	0.91 ± 0.01	3.12 ± 0.01	1.0 ± 0.2	82.67 ± 0.01	0.467
2k	692.66 ± 0.02	—	—	1.0 ± 0.7	74.00 ± 0.01	0.455

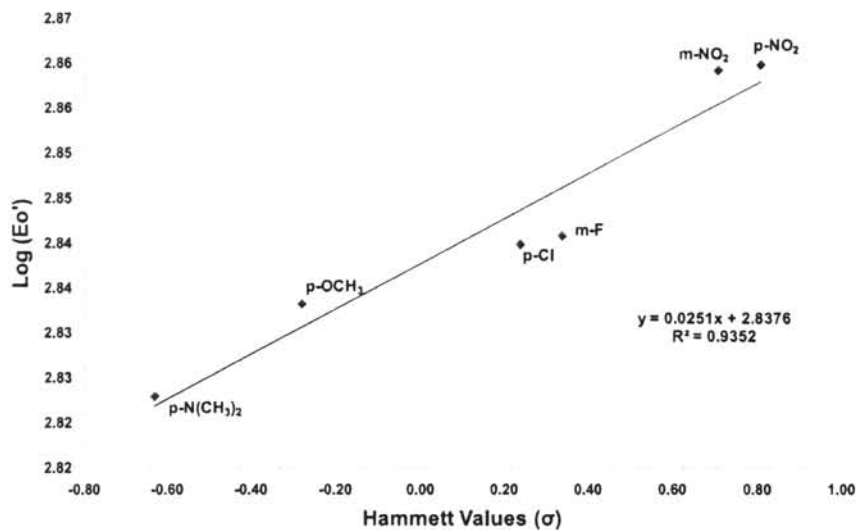


Figure 4. Hammett plot for ferrocene derivatives [ $\log$  of  $E_o'$  as a function of Hammett values ( $\sigma$ )].

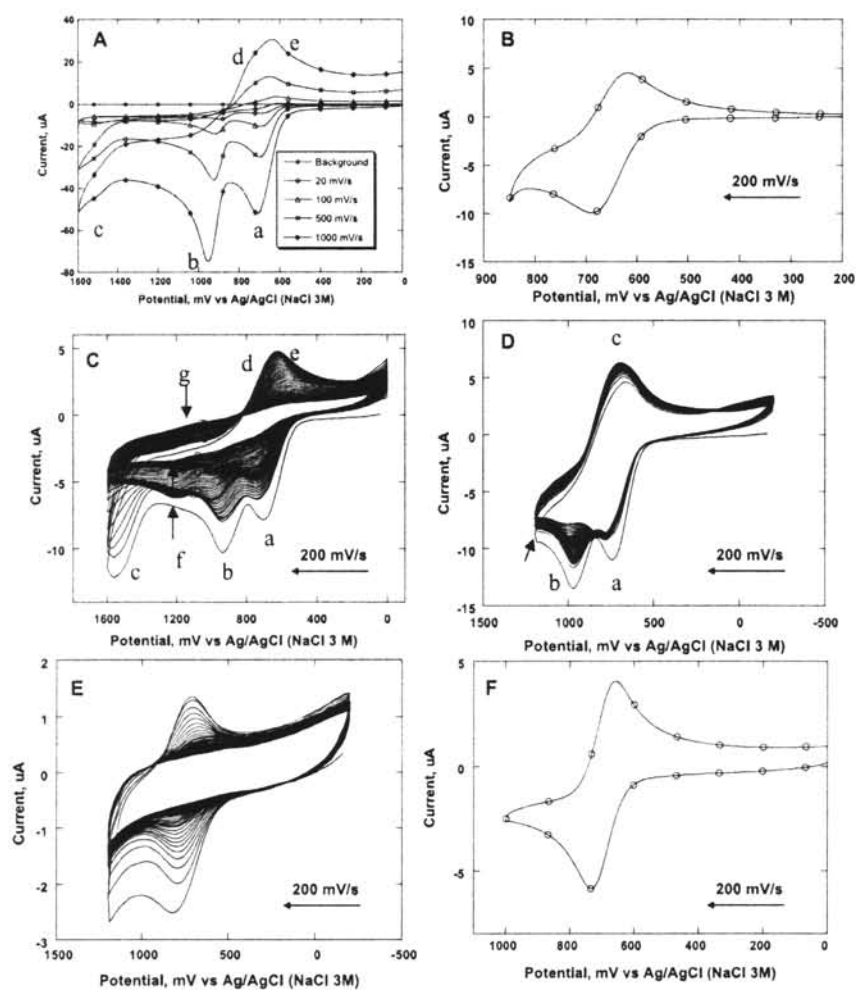
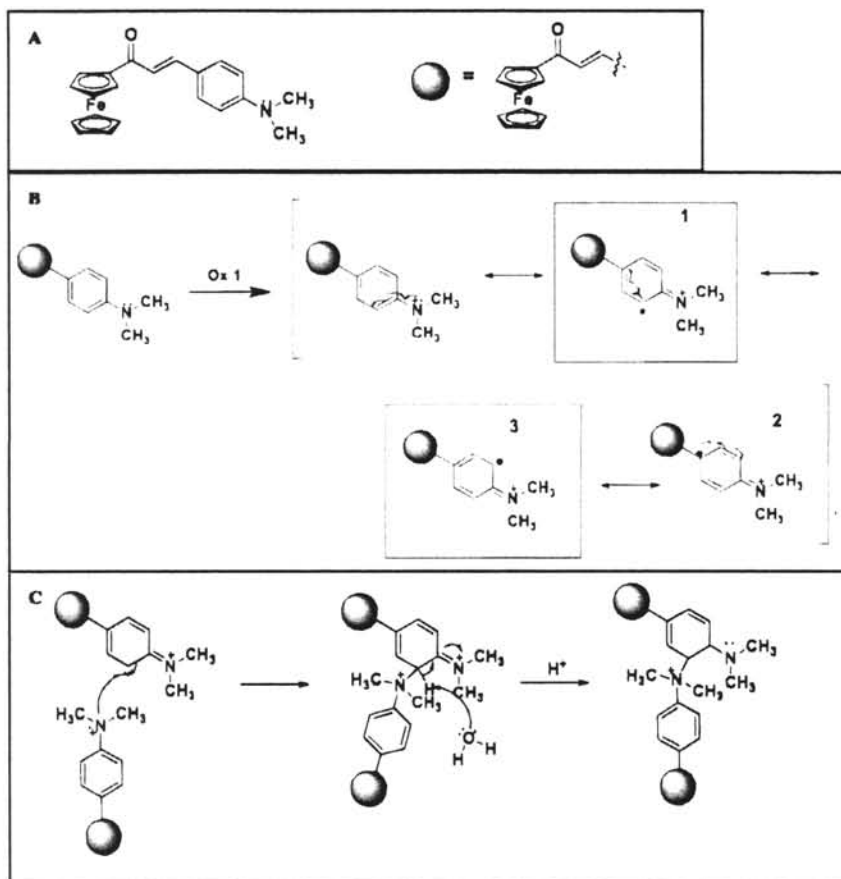


Figure 5. CV at a platinum electrode of  $1.00 \times 10^{-3}$  M compounds (2c) and (2k) in 0.101 M TBAP/ACN: For (2c), (A) 1 cycle at 20, 100, 500, 2000 mV/s, (B) 200 mV/s in the window potential of ferrocene oxidation, (C) 50 cycles at 200 mV/s 0–1600 mV/s scan window, (D) 50 cycles at 200 mV/s 0–1200 mV/s scan window, (E) 50 cycles at 200 mV/s in supporting electrolyte only after cycling in (D), and (F) voltammogram of (2k) at 200 mV/s.



**Figure 6.** Proposed mechanism for electrochemical polymerization of DMAPP: (A) DMAPP molecular structure, (B) DMAPP resonance structures, and (C) formation of the DMAPP dimer: Head to ortho position attack (likewise happens for the meta position).

In analogy to Oyama's results, we propose that the small wave that grows between +900 and +1400 mV (g, h) corresponds to the oxidation and the reduction of a dimeric species produced by the chemical reaction of two radical monocations generated after the first oxidation of the *N,N*-dimethylamino group. The increment in background signal at 0 mV could result from the reduction of protons produced during the electropolymerization. The production of cationic oligomers, which are soluble in ACN, or the formation of an electroactive polymeric film might be the reason for the voltammetric waves fading away eventually.

An experiment where the potential was cycled 50 times between +0 and +1200 mV showed that the wave corresponding to the ferrocene nucleus decrease slightly while the one due to the first DMAPP redox process decreased steadily (Fig. 5D). When this electrode was removed from the solution, dried in air, and put in an ACN solution with supporting electrolyte only, a voltammetric wave with  $E^{0'} = +696$  mV was observed (Fig. 5E). As before (Fig. 5C), this wave decreases continuously until it disappears completely. In this experiment, the observation of the ferrocene signal is the reason for losing the ferrocene signal is the formation of low molecular weight cationic species.

As has been reported for DMA,<sup>22</sup> we propose that DMAPP undergoes electrochemical polymerization after its first oxidation. The electropolymerization results in the formation of a film at the glassy carbon electrode. Contrary to the DMA case, DMAPP electropolymerization does not produce a high molecular weight polymer because the *p* position is not available. The formation of the oligomers occurs through the chains growth at the meta positions. These positions are sterically hindered thus decreasing the probability of the

formation of a high MW polymer (Fig. 6A-C). This is consonant with what has been observed for DMA and aniline.<sup>13,23</sup> In both cases, the polymerization preferably occurs through a head to tail attack initiated by the cation radical. Although the polymerization also occurs at the ortho positions relative to the amino and dimethylamino groups, the polymer grows mainly at the para position. In our case, the para position is sterically hindered because of the presence of the ferrocenyl moiety.

When the DMAPP is quaternized with dimethylsulfate (Fig. 5F), only one voltammetric wave is observed with a  $E^{0'} = +693$  mV. Likewise, the quaternization of the DMAPP prevents its electrochemical polymerization.

*Electron-transfer heterogeneous rate constant ( $k_s$ ).*—To determine the heterogeneous electron-transfer rate constant ( $k_s$ ), we treated the CV data according to Nicholson.<sup>24</sup> We constructed a working curve of  $\Delta E_p n$  ( $n = 1e^-$ ) as a function of  $\log \Psi$  using the values for  $\Delta E_p n$  (V) and  $\Psi$  published by Nicholson. The equation for this curve is  $\Delta E_p n = -0.02\Psi^3 + 0.0536\Psi^2 - 0.0545\Psi + 0.083$ . By taking the product of the  $n$  and  $\Delta E_p$  values of each compound and substituting in the cubic equation, we obtained the  $\Psi$  values. The  $k_s$  was calculated from the following equation

$$k_s = \Psi [D_o \pi (F/RT) v]^{1/2} [(D_o/D_R)^{\alpha/2}]$$

where  $\Psi$  is the value obtained from the cubic equation,  $D_o$  is the diffusion coefficient ( $\text{cm}^2/\text{s}$ ),  $F$  is the Faraday constant (96,500 C/mol),  $R$  is 8.314472 J/mol K,  $T$  is 298 K, and  $\alpha = 0.5$ .  $D_o/D_R$  is assumed to be equal to 1. Table II summarizes the values of  $k_s$  for all

**Table II. Heterogeneous electron-transfer rate constants ( $k_s$ ) for the FCs.**

Compound	$k_s$ (cm/s)
2a	$(0.027 \pm 0.003)$
2b	$(0.042 \pm 0.004)$
2c	—
2d	$(0.024 \pm 0.003)$
2e	$(0.037 \pm 0.002)$
2f	$(0.023 \pm 0.005)$
2g	$(0.024 \pm 0.002)$
2h	$(0.020 \pm 0.009)$
2i	$(0.027 \pm 0.004)$
2j	$(0.044 \pm 0.007)$

the compounds. The  $k_s$  are between 0.020 to 0.044 cm/s. When compared to the  $k_s$  reported for ferrocene of 0.035–0.076 cm/s,<sup>21</sup> the values for the FCs are comparable and in accordance with previous papers.

**UV/vis spectra and absorption coefficients.**— Figure 7A–D shows the UV/vis spectra of the compounds grouped by the nature of the aromatic derivative. Table III summarizes the absorption coefficients for the most prominent bands in the spectra. With few exceptions,

all FCs showed three bands in the UV region and one in the visible region. The absorption coefficients ranges from  $1.8 \times 10^2$  to  $7.5 \times 10^4$  L mol<sup>-1</sup> cm<sup>-1</sup>.

It can also be observed in the spectra that the region between 275–328 nm is variable for all FCs. This region corresponds to the  $n - \pi^*$  electronic transition attributed to the carbonyl. As pointed out in the electrochemical section, these differences demonstrate the effect that the electrodonating and electrowithdrawing substituents exert on the carbonyl polarization.<sup>12</sup>

Different from ferrocene which is yellow-orange solid, all FC solids exhibit a strong purple reddish color. The color of the ACN solution was the same as the solid. Some of the FCs exhibit solvatochromism. The solutions were stable for 24 h without protecting them from the room light.

### Conclusion

In this study, we demonstrated the synthesis and characterization of 10 FCs. Our results show that all compounds are chemically reversible  $I_{pa}/I_{pc} = 1.0$ –1.17 for all compounds except DMAP and are electrochemically quasi-reversible,  $\Delta E_p = 72$ –90 mV. The  $n$  and  $D_{ox}$  values reported agree with the values published for ferrocene ( $1e^-$ ,  $D_{ox} = 2.4 \times 10^{-5}$  cm<sup>2</sup>/s).<sup>21</sup> The  $k_s$  values ranges 0.020–0.044 cm/s compared to 0.035–0.076 cm/s values for ferrocene.

The DMAPP electrochemical parameters were difficult to obtain because the proximity of the ferrocene and first DMAPP redox process and the complication introduced by its electropolymerization.

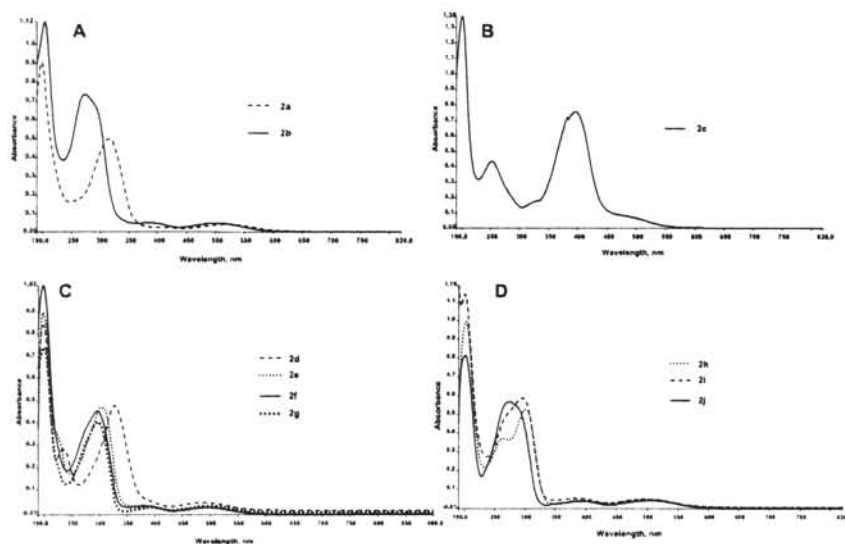


**Figure 7.** UV/vis spectra of  $2.0 \times 10^{-5}$  M compounds (2a–2j) in ACN for: (A) 2a and 2b, (B) 2c, (C) 2d–2g, and (D) 2h–2j.

**Table III. Absorption coefficients of FCs.**

Compound	$\lambda_{max}$ (nm)	$\epsilon (\times 10^4)$ (L/mol cm)	$\lambda_{max}$ (nm)	$\epsilon (\times 10^4)$ (L/mol cm)	$\lambda_{max}$ (nm)	$\epsilon (\times 10^2)$ (L/mol cm)	$\lambda_{max}$ (nm)	$\epsilon (\times 10^2)$ (L/mol cm)
2a	198.82	$5.2 \pm 0.3$	—	—	315.46	$290 \pm 1$	517.55	$20.3 \pm 0.5$
2b	204.24	$5.7 \pm 0.5$	280.87	$3.7 \pm 0.3$	390.05	$15.6 \pm 0.8$	503.30	$16.8 \pm 0.8$
2c	200.17	$7.5 \pm 0.2$	252.39	$2.44 \pm 0.05$	393.44	$421 \pm 9$	—	—
2d	199.17	$5.7 \pm 0.3$	—	—	328.33	$280 \pm 2$	488.06	$16.1 \pm 0.3$
2e	199.17	$3.8 \pm 0.2$	303.11	$2.1 \pm 0.2$	384.89	$17.6 \pm 0.6$	497.23	$15.8 \pm 0.5$
2f	199.94	$5.6 \pm 0.1$	295.47	$2.2 \pm 0.3$	386.42	$16.5 \pm 0.1$	498.00	$15.4 \pm 0.1$
2g	201.46	$3.4 \pm 0.2$	297.00	$2.0 \pm 0.1$	387.94	$16.1 \pm 0.7$	497.23	$15.5 \pm 0.6$
2h	201.53	$6.2 \pm 0.9$	301.22	$2.9 \pm 0.1$	390.73	$15.6 \pm 0.2$	500.59	$16.1 \pm 0.1$
2i	201.53	$6.5 \pm 0.3$	296.47	$3.29 \pm 0.04$	391.41	$1.8 \pm 0.3$	493.81	$1.8 \pm 0.3$
2j	199.49	$4.7 \pm 0.6$	275.45	$3.1 \pm 0.2$	394.80	$14.4 \pm 0.3$	506.70	$16.5 \pm 0.3$

The electropolymerization of DMAPP results in cationic oligomers that are soluble and not suitable for further polymerization and the formation of polymeric films at electrode surface.

We report that the substituent in the aromatic ring influences the  $E^{0'}$  of the FCs by modulating to a certain extent the polarization of the carbonyl group. This result is consistent with the UV/vis variations in the  $n - \pi^*$  region that corresponds to the carbonyl absorption.

In summary, FCs with tunable redox and spectroscopical properties can be produced by the reaction of acetylferrocene and appropriate derivatives of aromatic aldehydes. These compounds could be used as electrochemical and optical labels in sensor arrays. We are currently exploring ways to immobilize these compounds at electrode surfaces and studying their applications in biosensing and electrocatalysis.

#### Acknowledgments

We thank Linda Vargas, Yesenia Enríquez, and Tanya L. Díaz for their assistance with preliminary studies. Rocío del A. Cardona thanks NSF-PREM (NSF-DMR-0934195) and NIH-RISE (2R 25 GM 061151) for their kind support. K.H. acknowledges the support from NIH-MARC (5T 34 GM 07821). M.O. acknowledges the support from Pfizer Pharmaceuticals.

University of Puerto Rico assisted in meeting the publication costs of this article.

#### References

1. S. M. Batterjee, M. I. Marzouk, M. E. Aazab, and M. A. El-Hashash, *Appl. Organomet. Chem.*, **17**, 291 (2003).
2. E. Coutouli-Argyropoulou, C. Sideris, and G. Kokkinidis, *J. Organomet. Chem.*, **691**, 3909 (2006).
3. P. Debroy and S. Roy, *Coord. Chem. Rev.*, **251**, 203 (2007).
4. T. Ihara, Y. Maruo, S. Takenaka, and M. Takagi, *Nucleic Acids Res.*, **24**, 4273 (1996).
5. T. S. Zatsepin, S. Y. Andreev, T. Hianik, and T. S. Oretskaya, *Russ. Chem. Rev.*, **72**, 537 (2003).
6. C. M. Jewell, M. E. Hays, Y. Kondo, N. L. Abbott, and D. M. Lynn, *J. Controlled Release*, **112**, 129 (2006).
7. S. Mu, *Synth. Met.*, **139**, 287 (2003).
8. J.-B. Raoof, R. Ojani, and A. Kiani, *J. Electroanal. Chem.*, **515**, 45 (2001).
9. I. Willner, V. Pardo-Yissar, E. Katz, and K. T. Ranjiti, *J. Electroanal. Chem.*, **497**, 172 (2001).
10. A. Shah, A. M. Khan, R. Qureshi, F. L. Ansari, M. F. Nazar, and S. S. Shah, *Int. J. Mol. Sci.*, **9**, 1424 (2008).
11. X. Wu, E. R. T. Tiekink, I. Kostetski, N. Kocherginsky, A. L. C. Tan, S. B. Khoo, P. Wilairat, and M.-L. Go, *Eur. J. Pharm. Sci.*, **27**, 175 (2006).
12. S. Tomá, A. Gáplovsky, and I. Pavlík, *Monatsh. Chem.*, **116**, 479 (1985).
13. A. Shah, R. Qureshi, A. M. Khan, F. L. Ansari, and S. Ahmad, *Bull. Chem. Soc. Jpn.*, **82**, 453 (2009).
14. S. J. Ji, S. Y. Wang, Z. L. Shen, and M. F. Zhou, *Chin. Chem. Lett.*, **14**, 1246 (2003).
15. S. J. Ji, S. Y. Wang, and Z. L. Shen, *Chin. Chem. Lett.*, **14**, 663 (2003).
16. E. Solčániová, S. Toma, and A. Fiedlerová, *Org. Magn. Reson.*, **14**, 181 (1980).
17. See supplementary material at <http://dx.doi.org/10.1149/1.3439669> (E-JESOAAN-157-027008) for additional information.
18. P. T. Kissinger and W. R. Heineman, *J. Chem. Educ.*, **60**, 702 (1983).
19. J. E. Heffner, J. C. Raber, O. A. Moe, and C. T. Wigal, *J. Chem. Educ.*, **75**, 365 (1998).
20. B. M. Smith and J. March, *March's Advanced Organic Chemistry: Reaction, Mechanism and Structure*, 5th ed., pp. 368–375, John Wiley & Sons, New York (2001).
21. A. M. Bond, T. L. E. Henderson, D. R. Mann, T. F. Mann, W. Thormann, and C. G. Zoski, *Anal. Chem.*, **60**, 1878 (1988).
22. N. Oyama, T. Ohsaka, and T. Shimizu, *Anal. Chem.*, **57**, 1526 (1985).
23. M. Leclerc, J. Guay, and L. H. Dao, *Macromolecules*, **22**, 649 (1989).
24. R. S. Nicholson, *Anal. Chem.*, **37**, 1351 (1965).

# Design, Construction and Analytical Characterization of a DNA Sensor for the Detection of *Salmonella*

Madeline Diaz Serrano<sup>1</sup>, Arellys Rosado<sup>1</sup>, Joselyn del Pilar<sup>1</sup>, Esther Vega<sup>2</sup> and Ana R.Guadalupe<sup>1</sup>

<sup>1</sup> Department of Chemistry, University of Puerto Rico, Rio Piedras Campus, San Juan, Puerto Rico, 00931-3346

<sup>2</sup> Department of Biology, P.O. Box CUH 100 Rd 908, University of Puerto Rico, Humacao Campus, Humacao, Puerto Rico, 00791

## INTRODUCTION

*Salmonella* is one of the most aggressive food pathogens directly related with public health<sup>1</sup>. Every year 70 millions persons are infected and 500 died in the USA. The analytical methods for the detection of *Salmonella* are laborious and require several days for results. During this time portions of food may have been distributed, marketed, sold and eaten before a problem is even detected. Alternative analytical methods are necessary to overcome these drawbacks and to detect *Salmonella* routinely in water and food products with timely confirmation of the infection.<sup>2,3</sup>

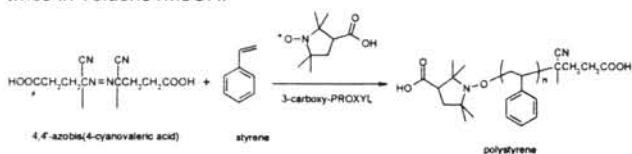
DNA sensors are attractive compared to other detection systems because they can be mass produced at low cost, in a variety of sizes and shapes; their response can be characterized theoretically and their analytical characteristics can be tailored to a particular need.<sup>4</sup> Here, we propose a strategy towards the preparation of a *Salmonella* DNA sensor array.

Our research objective is to build an electrochemical biosensor array to detect *Salmonella*. To accomplish this goal, we used polystyrene-modified carbon electrode surfaces as the platform for the construction of nucleic acid sensors. We anchored *Salmonella* genes (probes) onto these surfaces and hybridized them with their complementary sequences (targets). The hybridization reaction was followed electrochemically using ferrocene labels.

## EXPERIMENTAL

**Reagents.** Styrene was distilled in vacuum prior to the polymerization. 4,4'-azobis(4-cyanovaleric acid) (CVA) (Sigma) and 3-Carboxy-Proxyl (3CP), 1,3-dicyclohexyl carbodiimide (DCC) and N-hydroxysuccinimide (Aldrich) were used for the styrene polymerization and functionalization and LiOH (Aldrich) were used to titrate the polymers. The probe sequence SAMLA15C: (35 mer, 5'-/5AmMC12/CCTTCCTGAAGA CATGCCTGAAACAAAGTATGGC-3' was purchased from IDT DNA Technologies.

**Di-Carboxylic Polystyrene Synthesis.** CVA, 3CP and styrene were mixed in a crystal ampoule in DMF as the solvent.<sup>4</sup> This mixture was vacuum sealed after four freeze-pump-thaw cycles. The ampoule was placed in an oil bath at -130°C for 96h. After this time, the polymers were recovered and purified by dissolution/precipitation twice in Toluene /MeOH.



Scheme 1. Di-carboxylic polystyrene synthesis.

**Molecular Weights Determination.** The molecular weights ( $M_n$  and  $M_w$ ) and the polydispersity ( $M_w/M_n$ ) of each polymer were determined by Size Exclusion Chromatography (SEC) (Hewlett Packard 1100 LC) with three detectors: a Light Scatterer (mini DAWN

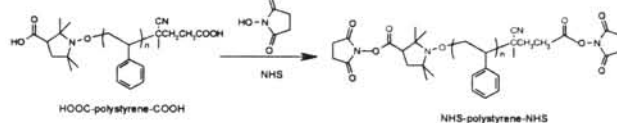
Tristar), a UV Spectrometer and Interferometric refract (Optilab DS). Tetrahydrofuran (THF) was the eluent at flow rate of 1.0 ml/min. Two Styragel columns (Waters) with effective molecular weight ranges of 500-30,000 (HT3) and 5,000-600,000 (HT4) connected in series were used for the polymers separation.

**Di-carboxylic Functionality Calculation.** The carboxylic group's number in each polystyrene chain was determined by LiOH titration. The average functionality ( $F$ ) was calculated as follows:

$$F = \frac{C_{LiOH} V_{LiOH} MW_{Polymer}}{m_{polymer}} \quad (1)$$

where  $F$  is the average functionality or  $-COOH$  numbers,  $C$  is the LiOH concentration (mol/L),  $V$  is the volume of LiOH (L),  $MW$  is the polymer molecular weight (g/mol) and  $m$  is the polymer mass (g).

**Derivatization of COOH-PS-COOH.** A derivatization of the polystyrene chains with N-hydroxysuccinimide was done to enhance the carboxylic group reactivity toward the amine group. The reactants molar ratios were 2.5: 2.5: 1 (NHS: DCC: Polymer).



Scheme 2. Derivatization of di-carboxylic polystyrene.

**Platform Preparation and Characterization.** Gold films were cut to ~1 cm<sup>2</sup> and cleaned with sonication in acetone, and deionized water and dried with N<sub>2</sub>. Polymer solutions (5.0% w/v) were prepared in 1,1,2-trichloroethane. For the polymers, a 4μL aliquot was spin coated at 3,000 rpm for 1 min.

**Oligonucleotide Immobilization and Characterization.** The oligonucleotide SALMA15C solution was prepared in 0.2M sodium carbonate (pH 9.66). The buffer was autoclaved before its use. 50μL of oligonucleotide solution was deposited over the polymer 24,710g/mol (AFM experiments) and incubated at 4°C for 24h.

## RESULTS AND DISCUSSION

**Characterization of Polymers.** The polystyrene chains were synthesized by living free radical polymerization using 3-carboxy-2,2,5,5,-tetramethyl-1-pyrro[di]nyloxy (3CP) as a TEMPO analog radical. (Scheme 1) This strategy provides at least one functional end group ( $-COOH$ ) through the symmetric cleavage of CVA and one ( $-COOH$ ) by the 3CP radical. The number of  $-COOH$  groups were determined by the LiOH titration. The functionality range was 2-3.5. Titration also results showed that the polymer functionality ( $\#-COOH/chain$ ) increases as the molecular weights increases.

10 AUG 16 P 2:22

RECIBIDO  
SERVIDO ACADEMICO  
RECINTO RIO PIEDRAS UPR

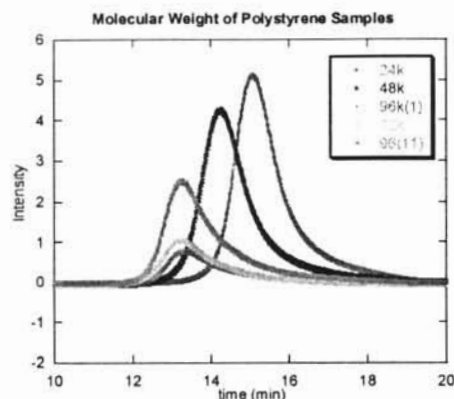


Figure 1. Size Exclusion Chromatography of COOH-PS-COOH Samples.

Table 2. Polymer Titrations

Mn (teo) (g/mol)	V LiOH (L)	Mn (SEC) (g/mol)	Mn/Mw	F
24,000	4.83E-05	24,710	1.113	2.00+0.06
48,000	3.87E-05	43,637	1.154	2.8+0.3
72,000	2.50E-05	79,895	1.231	3.37+0.03
96,000	2.90E-05	72,213	1.162	3.4+0.2
96,000	2.90E-05	71,700	1.201	3.5+0.4

[LiOH] = 0.09335M

The characterization of polystyrene samples before and after their modification was done with IR techniques, the characteristic bands were: C-H aromatics and aliphatic ( $2800-3500\text{ cm}^{-1}$ ), C=C aromatics ( $1400-1490\text{ cm}^{-1}$ ) and carbonyl band at  $1743\text{ cm}^{-1}$ .

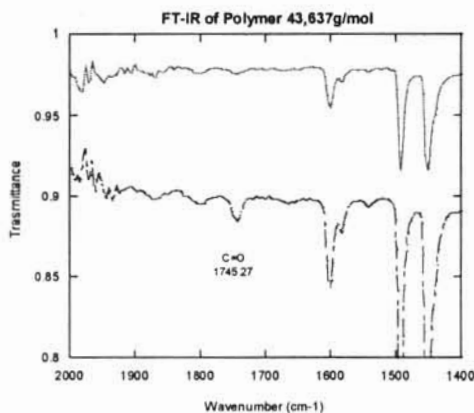


Figure 2. FT-IR spectrum of PS-(NHS)<sub>2</sub>.

**Polystyrene Modification on Gold Substrate.** NHS- derivatized polystyrene sample were placed over gold substrate by spin coating. In figure 3, complete coverage of the surface was obtained with  $4\text{ }\mu\text{L}$  of 5.0%w/v polymers solutions. An AFM images showed a gold substrate (A) with globular morphology due to gold aggregates. Image (B) showed polymers  $24,710\text{ g/mol}$  with smooth and small roughness surface.

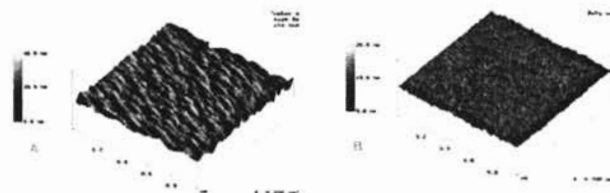


Figure 3. Atomic force microscopy for (A) bare gold RMS roughness:  $1.218\text{ nm}$  and spin-coated polystyrene films; (B) MW  $24,710\text{ g/mol}$  PMS roughness:  $0.606\text{ nm}$ .

#### CONCLUSION

In summary, the polystyrene polymerizations were successful completed. The characterization by HPLC-SEC was done, with molecular weights going from  $24,710-79,869\text{ g/mol}$  and polydispersity values 1.1 to 1.2. Variations in molecular weights and functionality were obtained in polymers with Mw greater than  $48\text{K g/mol}$ . The polymer  $24,710\text{ g/mol}$  modification was successful obtained and characterized. Modifications of gold substrates with the polymers were determined by AFM, the images showed a smooth surface with roughness of  $1.0-0.5\text{ nm}$ .

We expect to produce a methodology for the construction of electrochemical biosensors based on the use of *Salmonella* DNA-functionalized polymeric films with spatial resolution, high reproducibility and high sensitivity. We expect this array to be portable and user-friendly. This strategy could then be extended to the development of biosensors for other microorganisms.

#### ACKNOWLEDGEMENTS

We are grateful to Dr. Pinto (Department of Physics, UPR, Humacao) and Oscar Resto (Department of Physics, UPR, Rio Piedras) for the technical support with the AFM studies. We thank the Materials Characterization Center for the access to the FT-IR facilities.

#### REFERENCES

1. U.S. Food and Drug Administration, <http://www.cfsan.fda.gov>. Accessed January 2006.
2. Pathirana, S. T.; Barbaree, J.; Chin, B. A.; Hartell, M. G.; Neely, W. C.; Vodyanov, V., *Biosensors & Bioelectronics* 2000, 15, 135-141.
3. Jenikova, G.; Pazlarova, J.; Demnerova, K., *Internat Microbiol* 2000, 3, 225-229.
4. Muñoz, L.; Guadalupe, A. R.; Vega, E., *Journal of Biotechnology* 2005, 118, 233-245.



ELSEVIER

Available online at [www.sciencedirect.com](http://www.sciencedirect.com) AUG 16 P 1 : 1

SCIENCE @ DIRECT®

Journal of  
 BIOTECHNOLOGY

Journal of Biotechnology 118 (2005) 233–245

[www.elsevier.com/locate/jbiotec](http://www.elsevier.com/locate/jbiotec)

## Morphological studies of oligodeoxyribonucleotides probes covalently immobilized at polystyrene modified surfaces

Lisa Muñoz-Serrano<sup>a</sup>, Ana R. Guadalupe<sup>a,\*</sup>, Esther Vega-Bermudez<sup>b</sup>

<sup>a</sup> Department of Chemistry, P.O. Box 23346, University of Puerto Rico, Río Piedras Campus, San Juan, PR 00931-3346, USA

<sup>b</sup> Department of Biology, P.O. Box CUH 100 Rd 908, University of Puerto Rico, Humacao Campus, Humacao, PR 00791, USA

Received 22 September 2004; received in revised form 29 April 2005; accepted 4 May 2005

### Abstract

The immobilization of short ss-DNA (18- and 36-mer) and their hybridization were studied at gold and glassy carbon substrates modified with low molecular weight (~12, 18 and 24 kg/mol) polystyrene thin films. Amino-modified DNA was attached to the surface by reaction with succinimide ester groups bound to the polystyrenes. A ferrocene modified DNA target was used to confirm the probe-target hybridization. Atomic force microscopy studies showed significant morphological changes after probe immobilization and hybridization compared to the featureless structure of the polystyrene film. Single-stranded DNA samples had a globular morphology with an average density of 3.8 and 2.2 ( $\times 10^{11}$ ) globules/cm<sup>2</sup> for the 18- and 36-mer, respectively. The formation of a porous structure with a 2.0 and 1.0 ( $\times 10^{11}$ ) average pore density corresponding to the 18- and 36-mer was observed after hybridization. A surface composition analysis was done by X-ray photoelectron spectroscopy to confirm and support the images interpretation. Ferrocene oxidation (+323 mV/18-mer, +367 mV/36-mer, versus Ag/AgCl) proved the presence of ds-DNA at the modified surfaces.

© 2005 Elsevier B.V. All rights reserved.

**Keywords:** DNA sensors; AFM; Nanostructures; Polymers; Biointerfaces

### 1. Introduction

DNA arrays or gene chip technology has definitely emerged as one of the most promising methods for the detection of bacterial, viral or genetic diseases (Wang,

2000; Paleček and Fojta, 2001; Pividori et al., 2000). The specific recognition of target gene sequences with complementary oligodeoxyribonucleotide (ODN) probes that are attached to a solid support is the basis of this chip technology. The optimal performance of DNA arrays depends on the orientation and spatial arrangement of the probes at the surface (Wang, 2000). Both orientation and steric effects affect the hybridization efficiency, and therefore sensor analytical parameters such as sensitivity, detection limit and response time.

\* Corresponding author. Tel.: +1 787 764 0000x5967; fax: +1 787 763 6011.

E-mail address: [a.guadalupe@degi.rpp.upr.edu](mailto:a.guadalupe@degi.rpp.upr.edu) (A.R. Guadalupe).

In principle, higher responses and lower detection limits are expected when more targets are successfully hybridized.

The immobilization of DNA on electrode surfaces have been done using different strategies including adsorption and covalent attachment to carbon electrodes (Pividori et al., 2000; de-los-Santos-Alvarez et al., 2002; Pedano and Rivas, 2003), conjugation of avidin and biotinylated DNA (Dupont-Filliard et al., 2001; Niemeyer et al., 2001; Riepl et al., 2002) and gold-thiol linkage (Hashimoto et al., 1994; Ihara et al., 1997; Kelley et al., 1997; Hashimoto et al., 1998; Yu et al., 2001; Patolsky et al., 2001; Takenaka et al., 2000; Mucic et al., 1996; Nakayama et al., 2002; Anne et al., 2003; Satjapipat et al., 2001; Hianik et al., 2001). Among these methods, thiol chemisorption is the most widely used. However, Tarlov and others have shown that thiolated ODNs orient themselves perpendicular (one-point attachment) and parallel (multiple-point attachment) to the surface (Herne and Tarlov, 1997; Steel et al., 2000). This random orientation affects the stability and reproducibility of the sensors response. To overcome this problem, Tarlov and other research groups used a second thiol reagent to form a mixed monolayer composed of the HS-ODNs and HS-organic molecules (Satjapipat et al., 2001; Hianik et al., 2001; Herne and Tarlov, 1997; Steel et al., 2000). The HS-organic molecules act to eliminate undesired interactions of the HS-ODNs probes with the bare gold surface. This procedure enhances the sensor performance in comparison to the thiol-ODNs solo system, but significant variations in the hybridization response still occur. Even when the desired ODN orientation is achieved at the surface, its specific location and distribution is still questionable. There is a need for new methods that precisely tailored the position of ODNs probes at surfaces to build high-density sensor arrays with greater sensitivity.

Our research goal is to prepare polymers with a precise control of the surface density and spatial distribution of DNA on surfaces. We believe that by varying and controlling the molecular weight of the polymers, it could be possible to control the amount of DNA on the surface and consequently its hybridization efficiency. It is known that block copolymers can organize on surfaces with different morphologies in an orderly fashion. In this report, we present results on the use of DNA-polystyrene-DNA block copolymers as a strat-

egy to create such surfaces. Atomic force microscopy (AFM) was used to study ODNs immobilization and hybridization in DNA-polystyrene-DNA polymer films at gold surfaces. AFM can provide information regarding ODNs structural arrangement on solid supports as has been previously demonstrated (Kelley et al., 1998; Yokota et al., 1999; Sun and Yokota, 2000; Huang et al., 2001; Mourougou-Candoni et al., 2003). Thin films of different molecular weight polystyrenes functionalized with a succinimide ester were used to anchor amino-modified ODNs. The hybridization event was monitored deliberately modifying the complementary target with a ferrocene derivative. Results on the ODNs surface density, size distribution, orientation and on polymer morphology are presented before and after the hybridization event. The uniqueness of this method is the simplicity of the surface modification, and the potential for controlling the probes' spatial location and for producing polymer membranes with multiple and different end-functional groups. With this method, it is possible to produce sensor arrays using  $\mu$ -contact and ink-jet printing techniques.

## 2. Experimental

### 2.1. Chemicals

Styrene was distilled in vacuum prior to polymerization. 4,4'-Azobis(4-cyanovaleric acid) (Sigma) and 3-carboxy PROXYL (3CP), 1,3-dicyclohexyl carbodiimide and *N*-hydroxysuccinimide (Aldrich) were used for the polymerization and subsequent functionalization of polystyrene. Dimethylformamide, tetrahydrofuran, methanol and chloroform were all HPLC grade. Ferrocene carboxylic acid (95%) was obtained from Alfa Aesar. 1,4-Dioxane, 1,1,2-trichloroethane, methyl sulfoxide, silica gel (200–400 mesh, 60 Å) and Sephadex G-25 were purchased from Aldrich. Amino-modified ODN: 5'-NH<sub>2</sub>-(CH<sub>2</sub>)<sub>12</sub>-CTA TGC ACG TTC CGG TAT-3' (18-mer) and 5'-NH<sub>2</sub>-(CH<sub>2</sub>)<sub>12</sub>-CTA TGC ACG TTC CGG TAT TGC CTA TTC ACG TAT CGG-3' (36-mer), the amino-modified complementary sequences; 5'-NH<sub>2</sub>-(CH<sub>2</sub>)<sub>12</sub>-ATA CCG GAA CGT GCA TAG-3' and 5'-NH<sub>2</sub>-(CH<sub>2</sub>)<sub>12</sub>-CCG ATA CGT GAA TAG GCA ATA CCG GAA CGT GCA TAG-3' and the non-complementary sequences; 5'-GTA TTC GCC CGA TGT ACA-3' and 5'-NH<sub>2</sub>-(CH<sub>2</sub>)<sub>12</sub>-CCC

Table 1  
Nitroxide-mediated living radical polymerization of styrene with 4,4'-azobis(4-cyanovaleric acid) and 3-carboxy PROXYL

Rxn	Styrene (mL)	CVA (mg)	3CP (mg)	$M_n$ (g/mol)	$M_w/M_n$	COOH/ chain
1	4.0	68.9	113.9	11520	1.11	1.37
2	8.0	71.1	114.4	17500	1.07	1.59
3	12.0	70.4	113.2	24470	1.04	1.98

AAG CGA GCT GCT A-3' were purchased from IDT DNA Technologies. Spectra Por/CE pre-treated (MWCO 2000) dialysis membranes were obtained from Spectrum. All aqueous solutions were prepared with nanopure water (Barnstead, 18 M $\Omega$ /cm). Other reagents were at least analytical reagent grade.

### 2.2. Nitroxide-mediated living radical polymerization of styrene with 3-carboxy PROXYL and 4,4'-azobis(4-cyanovaleric acid) as initiator

Three styrene polymers with different molecular weight were synthesized as indicated in Table 1. The general procedure was to mix 4,4'-azobis(4-cyanovaleric acid) (CVA), 3-carboxy-PROXYL and styrene in a glass ampoule followed by dissolution with 10 mL dimethylformamide (DMF). The molar ratio of 3CP to initiator (CVA) was 2.44. The ampoules were vacuum sealed after four freeze-pump-thaw cycles and placed in an oil bath at  $\sim$ 130  $^{\circ}$ C. After 96 h, the polymers were recovered and purified by dissolution/precipitation twice in DMF/MeOH. The white solids were placed in a vacuum line until dryness. The polymers were analyzed by IR spectroscopy (Nicolet Magna 750) in KBr pellets.

### 2.3. Size exclusion chromatography

The polymer molecular weight and polydispersity was determined by size exclusion chromatography (Hewlett Packard 1100 LC). A light-scattering (miniDAWN Tristar) and an interferometric refractometer (Optilab DSP) both from Wyatt Technology were used as the detection system to determine  $M_w$  and  $M_n$ , respectively. Two Styragel columns (Waters) with an effective molecular weight range of 500–30,000 (HT3) and 5000–600,000 (HT4) were connected in series. The eluent was THF (flow rate: 1.0 mL/min). Polymer solutions (0.5%, w/v) were dis-

solved in filtered THF. Prior to injection, the samples were filtered with a PVDF syringe filter, 0.2  $\mu$ m (Whatman).

### 2.4. Titration of dicarboxylated polystyrene

LiOH was titrated with KHP and phenolphthalein. An amount of dried polymer (50–60 mg) was dissolved in 5 mL of chloroform. To this solution, 0.2 mL of methanol and two drops of phenolphthalein (0.5 wt% in EtOH) were added following the procedure described by Polymer Source Inc. (Canada). The polymer solution was titrated with 0.1 M LiOH until the indicator color changed. The average COOH functionality ( $F$ ) was calculated as follows:

$$F = \frac{C_{\text{LiOH}} \times V_{\text{LiOH}} \times \text{MW}_{\text{polymer}}}{\text{Grams of polymer}} \quad (1)$$

Titration results were (MW/ $F$ ): 11,520/1.37; 17,500/1.59; 24,470/1.98.

### 2.5. Derivatization of dicarboxylated polystyrene

The polymer sample and *N*-hydroxysuccinimide (NHS) were dissolved in 5 mL DMF. 1,3-Dicyclohexyl carbodiimide (DCC) was dissolved in 5 mL DMF. The DCC solution was added dropwise to the polymer solution. The mixture was left for 24 h at RT with continuous stirring. The reactants molar ratio was 2:2:1 corresponding to NHS, DCC and the polymer, respectively. The polymer was precipitated in methanol and purified twice by dissolution/precipitation in chloroform/MeOH. The product was placed in a vacuum dessicator until dryness.

### 2.6. Synthesis of *N*-hydroxysuccinimide ester of ferrocene carboxylic acid

The derivatization of ferrocene carboxylic acid was done as described by Takenaka et al. (1994). First,

0.51 g (2.46 mmol) of DCC were dissolved in 10 mL of 1,4-dioxane while 0.51 g (2.21 mmol) of the ferrocene-COOH and 0.31 g (2.70 mmol) of NHS were dissolved with 35 mL of 1,4-dioxane. The DCC solution was added dropwise to the ferrocene solution and the reaction was allowed to proceed at RT for 24 h. The reaction byproduct was removed by filtration. The product was recovered rotoevaporating the solution to dryness. The solid was dissolved in a small amount of chloroform and chromatographed on silica gel with chloroform as eluent. The purified solid yielded 89% (0.71 g). IR (KBr pellets) experimental: 1769, 1739, 1214 and 1077  $\text{cm}^{-1}$ ; expected (Takenaka et al., 1994): 1770, 1740, 1220 and 1080  $\text{cm}^{-1}$ .

### 2.7. Synthesis of ferrocenyl oligonucleotides (18- and 36-mer)

The succinimide ester of ferrocene (9.85 mg, 30.11  $\mu\text{mol}$ ) was dissolved in 1.0 mL of methyl sulfoxide. The H<sub>2</sub>N-18mer was dissolved in 800  $\mu\text{L}$  of 0.2 M sodium carbonate buffer (pH 9.5). The Ester solution (400  $\mu\text{L}$ ) was added to the H<sub>2</sub>N-18mer solution. The mixture was left for 16 h at 4 °C, after which, it was chromatographed on a Sephadex G-25 column using deionized water/carbonate buffer (50/50) as eluent. The fraction (~3 mL) with yellow color was dialyzed against water to remove salt excess and unreacted reagents and finally freeze-dried. The final product was stored in the refrigerator until use. The same procedure was followed for the H<sub>2</sub>N-36mer.

### 2.8. Preparation of succinimide-polystyrene-succinimide polymer films

Polymer solutions (5.0%, w/v) were prepared in 1,1,2-trichloroethane. After sonication for 30 min, the solutions were filtered with a PVDF syringe filter. The final solutions were tightly closed and left at room temperature until use. Gold substrates (from Thermo Electron Corporation) were cut to ~1  $\text{cm}^2$  and cleaned with sonication in acetone, followed by deionized water (both for 30 min), and dried with N<sub>2</sub>. For the three polymers, a 4  $\mu\text{L}$  aliquot was deposited over the substrate, and then spin coated at 3000 rpm for 1 min. The samples were placed in a vacuum line overnight. The film thickness (measured by profilometry) ranges from 0.30 to 0.70  $\mu\text{m}$ .

### 2.9. Oligonucleotides immobilization and hybridization

For the immobilization of the ODN, 50  $\mu\text{L}$  of 50  $\mu\text{M}$  NH<sub>2</sub>-ODN in 0.2 M sodium carbonate (pH 9.5) was deposited over the polymer sample. The attachment of ODNs will occur at the primary amine linker at this pH (Ontko et al., 1999). One set of polymer film samples (MW: 11,520; 17,500 and 24,470 g/mol) were used for the H<sub>2</sub>N-18mer immobilization and another set for the H<sub>2</sub>N-36mer. The samples were incubated at 4 °C for 24 h. The films were rinsed with deionized water, then with ~20 mL of 0.2 M PBS (pH 6.9), and again with deionized water. The samples were placed in a vacuum line for 24 h. For the hybridization of the immobilized probes, 50  $\mu\text{L}$  of 50  $\mu\text{M}$  ferrocenyl-ODN in 0.2 M PBS (pH 6.9) were placed over the sample that had the complementary probe sequence. The samples were incubated at ~55 °C for 10 min and left at RT for 24 h. The films were rinsed with deionized water, followed by PBS and deionized water and then placed in a vacuum line for 24 h. The same hybridization procedure was done with a non-complementary sequence using a sample that contained the H<sub>2</sub>N-18mer probe.

### 2.10. Atomic force microscopy

AFM images were collected at room conditions using a NanoScope MultiMode™ Scanning Probe Microscope from Digital Instruments. The imaging was performed using the tapping mode at a scan frequency of 1–2 Hz with silicon etched probes from Veeco Metrology. The collected images were flatten and analyzed using the Nanoscope III software.

### 2.11. X-ray photoelectron spectroscopy

XPS measurements were performed on a 5600 PHI Multisystem. The polychromatic X-ray radiation source was Mg K $\alpha$  at 15 kV and 400 W. The pass energy was maintained for each conclusive set of analysis. Survey and multiplex spectra were obtained with pass energy of 93.9 and 58.7 eV, respectively. The instrument was calibrated with Au and Cu standard samples. The reported spectra sections were corrected considering the C 1s peak (284.5 eV) as an internal standard. The quantitative evaluation was done with the AC-

ACCESS PHI software, based on atomic sensitive factors for each specific transition of certain elements.

### 2.12. Osteryoung square wave voltammetry

The electrochemistry of ferrocene-ds-DNA attached to the polymer membranes was studied by Osteryoung square wave voltammetry using a BAS 100B voltammetric analyzer. The experiments were carried out in 0.2 M PBS (pH 6.9) with 0.1 M NaCl at room temperature under a N<sub>2</sub> stream. The Glassy C working electrode was polished with Metadi diamond paste and washed thoroughly with water under sonication before use. A carbon electrode was used instead of a gold electrode because the gold showed an oxidation peak close to the oxidation potential of the ferrocene label under our experimental conditions. The electrode surface was modified exactly as described for the gold surface, but using 2 μL of the polymer sample. For the immobilization and hybridization steps, 20 μL each of H<sub>2</sub>N-ODN and Fc-ODN solutions were used. A non-complementary H<sub>2</sub>N-ODN probe was immobilized and exposed to Fc-ODN following the same procedure described above for the complementary system. The counter and reference electrodes were a Nichrome wire and Ag/AgCl, respectively.

## 3. Results and discussion

### 3.1. Characterization and derivatization of the polymers

Fig. 1 shows the size exclusion chromatography of three polystyrenes prepared by nitroxide-mediated living radical polymerization. The polydispersity of the polymers was 1.04–1.11 for molecular weights ranging from 24,470 to 11,520 g/mol (Table 1). The elution

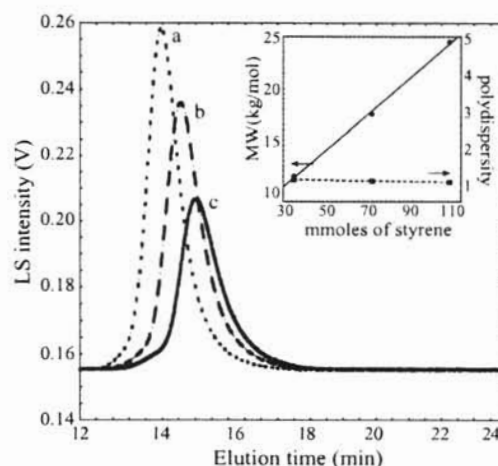
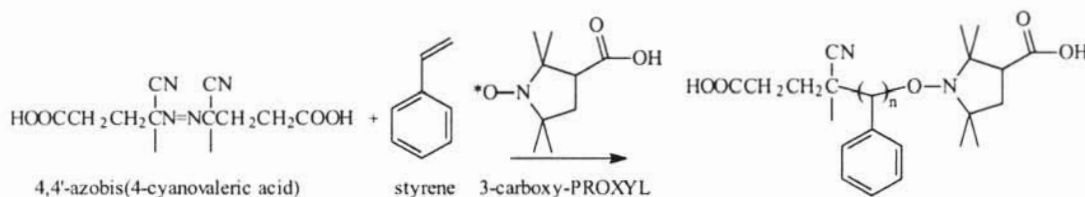


Fig. 1. Size exclusion chromatography of the polymers prepared by nitroxide-mediated living radical polymerization of styrene with 3-carboxy PROXYL and cyanovaleric acid as initiator. (a) 24,470 g/mol, PD 1.04; (b) 17,500 g/mol, PD 1.07; and (c) 11,520 g/mol, PD 1.11. Inset: dependency of the molecular weight and polydispersity with added monomer.

time increased as the molecular weight decreased as expected.

We synthesized monodisperse polystyrene with COOH groups at the polymer chain-ends. To accomplish this, we used CVA as a radical initiator and 3CP to control the growth of the polymer chains (see Scheme 1). CVA is an azo radical initiator with COOH groups at opposite ends of the azo functional group. 3CP is a TEMPO analog with a COOH group in the pyrrolidinyloxy ring. Together in the reaction vessel, CVA and 3CP initiate and terminate the polymer chains with a COOH group. Monodisperse polystyrene results from the use of 3CP following the same mechanism of other nitroxide reagents (Georges et al., 1993; Hawker, 1994; Veregin et al., 1995; Ohno et al., 1998; Hawker et al., 2001). Homopolymers with a variety of functionalities have been successfully synthesized using similar



Scheme 1.

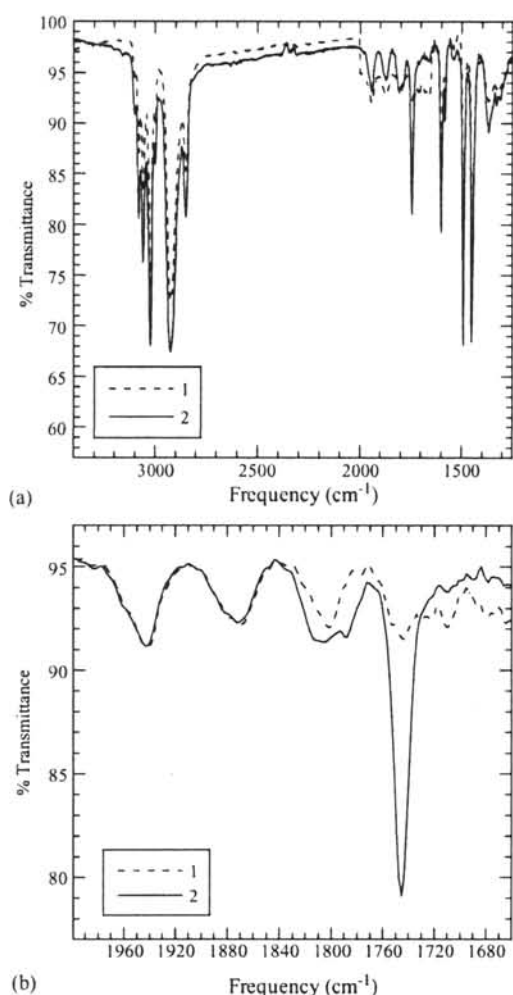


Fig. 2. Infrared spectra of dicarboxylated polystyrene (a.1), dicarboxylated polystyrene derivatized with *N*-hydroxysuccinimide (a.2), enlargement of the 2000–1660  $\text{cm}^{-1}$  for the dicarboxylated polystyrene (b.1) and dicarboxylated polystyrene derivatized with *N*-hydroxysuccinimide (b.2).

polymerization conditions (Ohno et al., 1998; Hawker et al., 2001).

Derivatization of the carboxylated polystyrene with NHS was done to form an active ester bond that eventually was reacted with the  $\text{NH}_2$ -ODNs. Fig. 2(a) shows the IR spectra of the carboxylated polystyrene (MW 11,520 g/mol) before (a.1) and after (a.2) the reaction with NHS. Both spectra show the characteristic polystyrene bands (e.g.: aromatics CH: 3081, 3059 and 3025  $\text{cm}^{-1}$ ; aliphatics CH: 2922 and 2848  $\text{cm}^{-1}$ ;

and aromatics C=C: 1600, 1492 and 1451  $\text{cm}^{-1}$ ). The predominant fingerprinting bands of monosubstituted polystyrene obscured the carbonyl band of the COOH end groups (Fig. 1(b)). After NHS-derivatization, the IR spectrum shows an enlarged peak at 1745  $\text{cm}^{-1}$  that was assigned to the carbonyl groups in the succinimide ester-polystyrene chains (Fig. 2(b)).

### 3.2. Preparation of polymer thin films on gold substrates

Optically transparent thin films of the NHS-derivatized polystyrenes were prepared over gold substrates by spin-coating. As seen in Fig. 3, complete coverage of the surface was obtained with 4  $\mu\text{L}$  of 5.0% (w/v) polymer solutions in 1,1,2-trichloroethane. An AFM image of the bare gold substrate (Fig. 3(a)) shows the gold aggregates that are characteristic of surfaces prepared by sputtering. A smooth surface with small roughness was observed for the polymer films (Fig. 3(b–d)).

### 3.3. Immobilization of the 18- and 36-mer probes and hybridization with their complementary sequences

Fig. 4 shows the AFM images of the samples after ODNs immobilization in the polymer film (MW 11,520 g/mol) and their respective size histograms. The immobilization of the 18- and 36-mers was done reacting the ODNs amino groups with the succinimide groups of the polymer membrane. For both cases, the images show that the ODNs collapsed at the membrane surface and adopt a globular morphology. The globules have the same height ( $\sim 2.0$ – $3.0$  nm), but differ significantly in diameter. The fact that there is a globular size distribution indicates that the ODNs randomly organize to form globules avoiding repulsive interactions. Considering that the dimensions of an 18 and 36-mer oligonucleotides are on the order of  $\text{\AA}$ , we conclude that each globule must consist of ODNs aggregates. Table 2 summarizes our AFM results. The globules diameter almost double for the 36-mer compared to the 18-mer ODNs suggesting that the ODN length dictates the aggregates size. There have been few reports presenting surface densities and distributions of short ss-DNA molecules using AFM. A surface den-

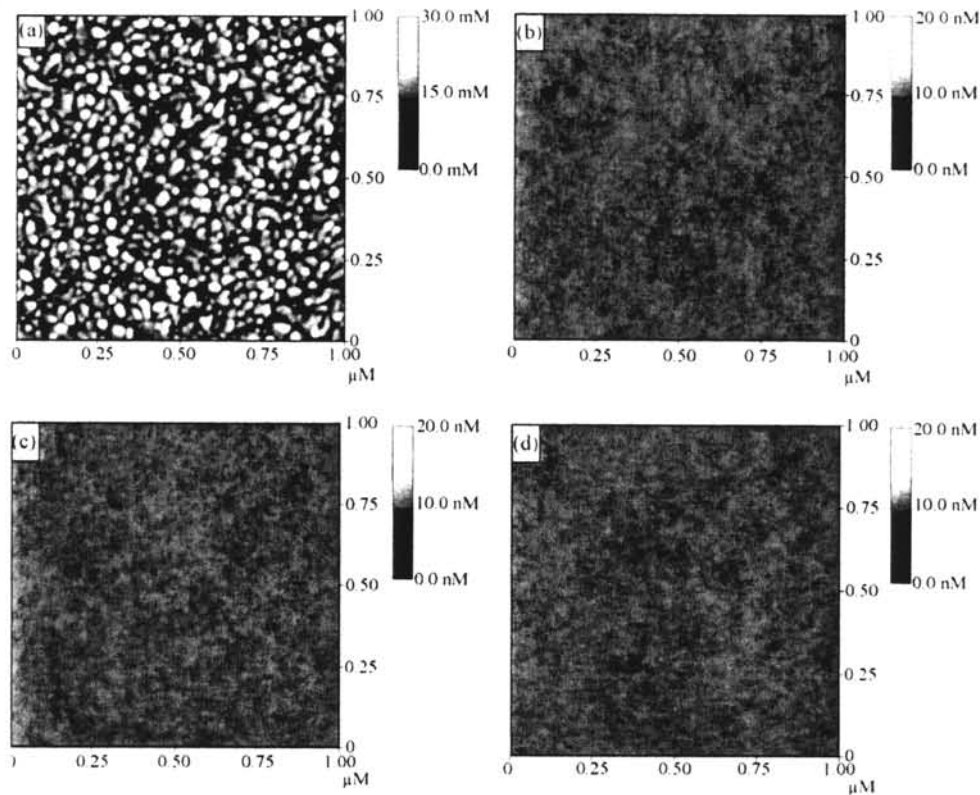


Fig. 3. Atomic force microscopy images for (a) bare gold RMS roughness: 1.293 nm and spin-coated polystyrene films; (b) MW 11,520 g/mol RMS roughness: 0.248 nm; (c) 17,500 g/mol RMS roughness: 0.215 nm and; (d) 24,470 g/mol RMS roughness: 0.267 nm over gold substrate.

sity of  $1.1 \times 10^{10}$  molecules/cm<sup>2</sup> for ODNs (17-mer) tethered at a gold substrate with diameters distribution of 26–40 nm was reported by Huang et al. (2001). DNA molecules domains with 15 nm diameter and a

density in the  $10^{11}$  molecules/cm<sup>2</sup> range for 25-mer thiolated oligonucleotides at gold substrates was presented by Mourougou-Candoni et al. (2003). These research groups have reported a globular morphology

Table 2  
Summary of atomic force microscopy imaging results

	18-mer			36-mer		
	11,520 <sup>a</sup>	17,500 <sup>a</sup>	24,470 <sup>a</sup>	11,520 <sup>a</sup>	17,500 <sup>a</sup>	24,470 <sup>a</sup>
Single-stranded						
Globules diameter <sup>b</sup>	14	13	12	25	27	23
Surface density <sup>c</sup>	3.80	3.56	3.68	2.20	1.68	2.04
Double-stranded						
Rings diameter <sup>b</sup>	10.5	11.5	11	11.5	11.5	12
Pores diameter <sup>b</sup>	23	25	25	24	28	24

<sup>a</sup> g/mol.

<sup>b</sup> Units: globules diameters, rings diameter and pores diameter (nm).

<sup>c</sup>  $\times 10^{11}$  globules/cm<sup>2</sup>.

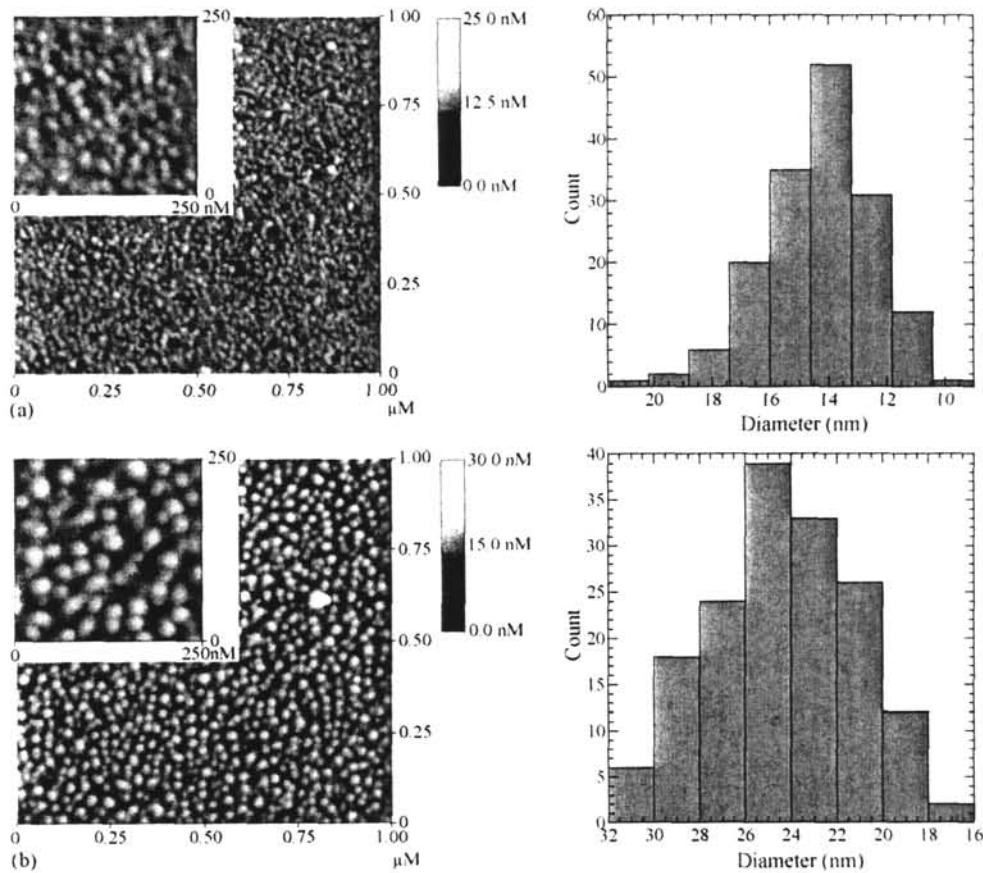


Fig. 4. Atomic force microscopy for polystyrene 11,520 g/mol after the immobilization of  $\text{NH}_2$ -ODNs: (a) 18-mer RMS roughness: 1.103 nm; and (b) 36-mer RMS roughness: 1.291 nm with their corresponding histograms.

for short ss-DNA at various substrates and under different sample preparation. This observation is important considering the known distortion effects produced by AFM tips during the imaging of biological samples (Yokota et al., 1999; Huang et al., 2001; Mourougou-Candoni et al., 2003).

Fig. 5 shows the AFM images for the samples after hybridization and their respective size histograms. It is evident that a different morphology resulted when the single-stranded ODNs reacted with their complementary sequence. The initial globular film morphology changed to a porous morphology with the formation of rings around pores. As shown in the histograms, the rings ( $\sim 10.5$ – $11.5$  nm) and pores ( $\sim 22$ – $28$  nm) diameter were comparable for the 18- and 36-mer. Interestingly, the pores diameters match the diameter of

the gold aggregates at the bare surface (20–30 nm, see Fig. 3(a)). We believe that an increment in electrostatic repulsions upon strands hybridization induces the film morphology changes resulting in a porous membrane templated by the gold aggregates. We speculate that this new morphology is a response of the system as it reaches a most stable molecular arrangement. The hybridization experiment was repeated with a non-complementary ODN sequence to verify that the observed morphological changes were a result of ODNs hybridization. Fig. 6 shows the AFM image of an 18-mer film sample that was treated with a non-complementary 18-mer sequence. From the comparison of Figs. 4 and 6, it is clear that the film retains a globular morphology before and after being treated with a non-complementary ODN sequence. The mor-

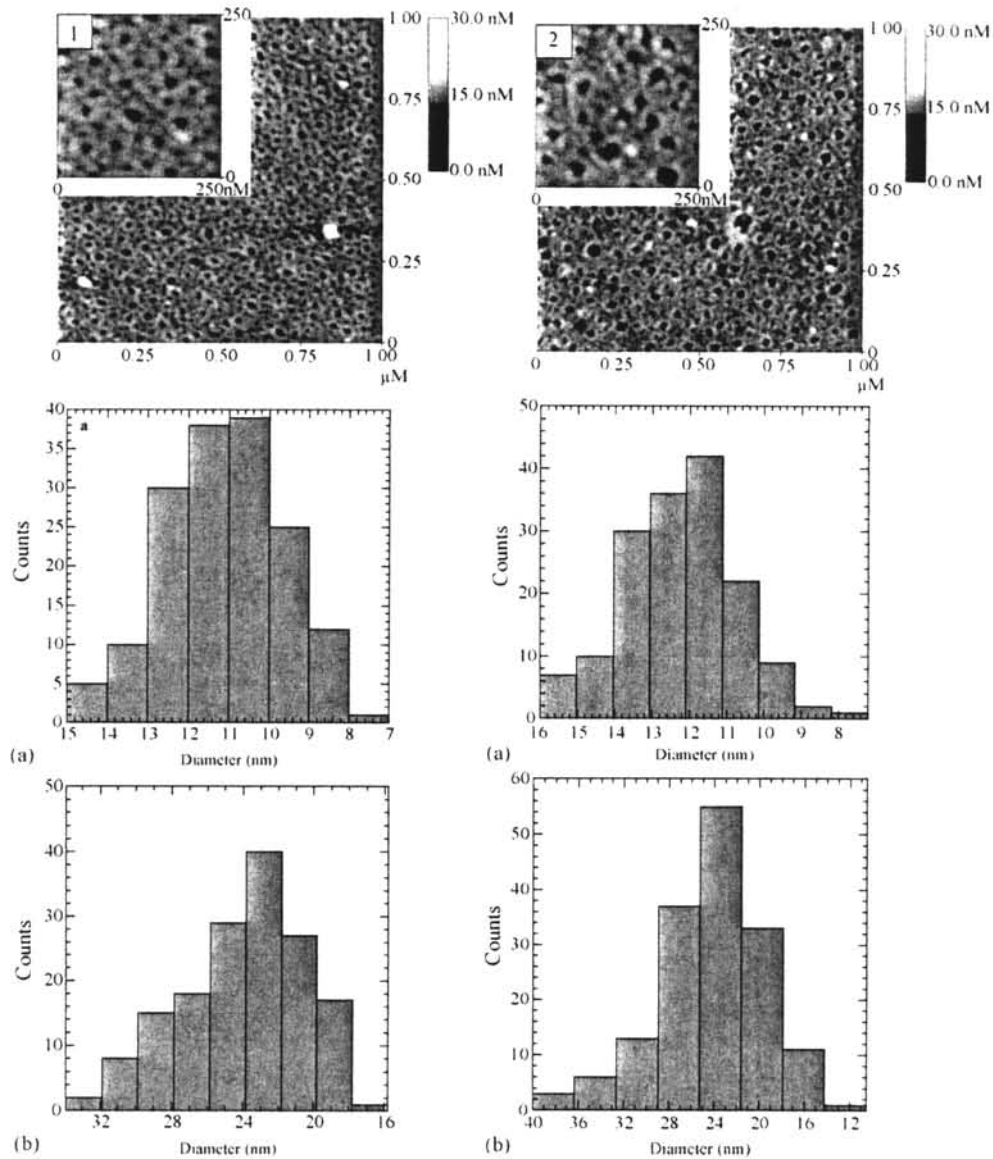


Fig. 5. Atomic force microscopy for polystyrene 11,500 g/mol after hybridization for (1) 18-mer and (2) 36-mer with the diameter histogram for (a) rings and (b) pores.

phological changes observed with the complementary ODNs were not observed with the non-complementary ones, proving that surface changes were a direct consequence of strands hybridization.

To substantiate the results obtained with AFM, the samples were further studied with X-ray photoelectron spectroscopy (XPS). Fig. 7 shows the XPS spectra in

the region of N 1s and P 2p for the substrate modified with the polymer membrane and after ODNs immobilization. No peaks were observed for the polymer modified substrate. After immobilization, the presence of nitrogen and phosphorous peaks were evident. The approximate molar ratio of nitrogen to phosphorous in DNA chains is 3.5 (Zhang et al., 2002). In our case,

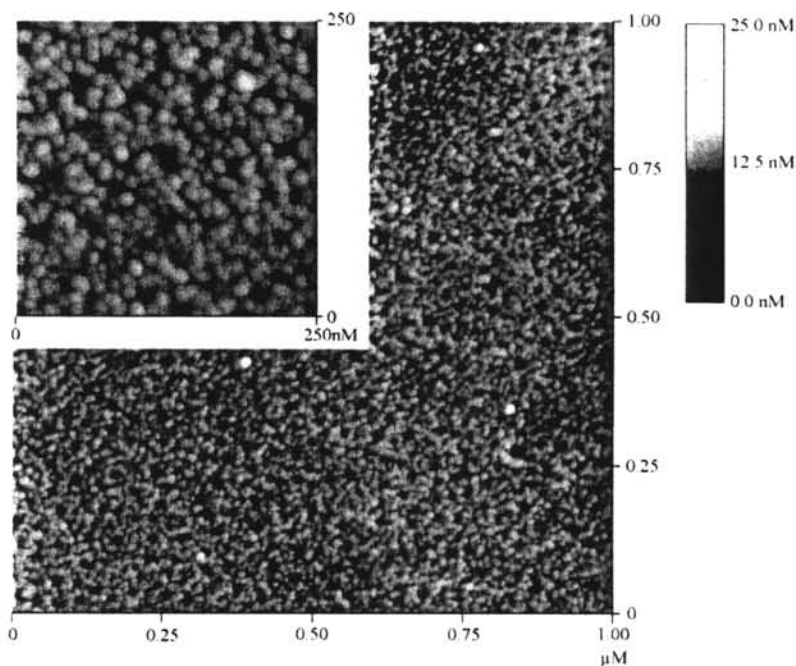


Fig. 6. Atomic force microscopy for polystyrene (11,520 g/mol) with a 18-mer probe treated with a non-complementary 18-mer ODN.

the ratio was 3.3, which confirms the presence of the ODNs at the surface.

Fig. 8 shows the XPS spectra in the Au 4f region. Two peaks were observed in this region as expected for bare gold. The peaks disappeared completely after modification with the polymer membrane and subsequent immobilization with the single-stranded probe. The Au 4f peaks were again visible after ODNs hybridization but with less intensity. This result strongly supports our hypothesis that on hybridization increased electrostatic repulsions induced a morphology change in the polymer film that results in the partial exposure of the bare gold surface.

We expected a dependency on the number of reactive points with molecular weight; that is, an increase in the number of reactive points per surface area with a decrease in the polymer molecular weight. That dependency was not observed. We believe that the differences in the molecular weight of the polymers studied were relatively small and hindered such dependency. We are currently studying the dependency between these variables (polystyrene molecular weight, surface density, spatial distribution) using higher molecular weights and longer DNA probes.

In addition, we observed that as the molecular weight increased, the polydispersity decreased and the titration results showed two  $-\text{COOH}$  per chain. We also observed that the polydispersity increased as the molecular weight decreased and that at the lowest molecular weight polymer the number of  $-\text{COOH}$  per group was mainly one. It is well known that in nitroxide-mediated living radical polymerization low molecular weight polymers have a tendency to high polydispersities (Veregin et al., 1995). This implies that in our experiments, two polymer chains of the lowest molecular weight will have approximately the same number of  $\text{COOH}$  groups as one polymer chain of the highest molecular weight. Thus, the surface densities of reactive points will remain the same in the range of polymer molecular weights that we studied.

#### 3.4. Electrochemical characterization of the modified surfaces

The hybridization of the immobilized probes in the presence of complementary and non-complementary sequences was studied by looking at the redox pro-

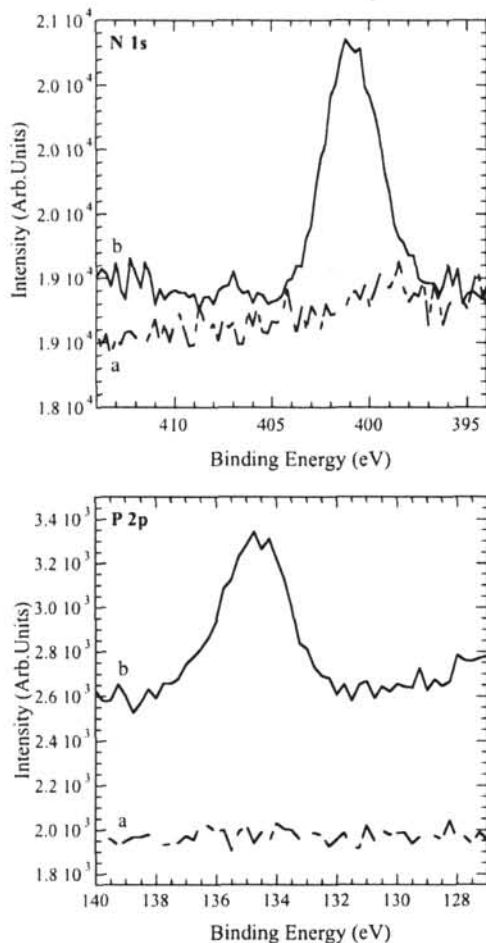


Fig. 7. XPS N 1s and P 2p spectra for (a) spin-coated polystyrene over gold and (b) after  $\text{NH}_2$ -oligonucleotide immobilization.

cess of a ferrocene label previously attached to the target sequence. The electrochemical behavior of the samples was studied using Osteryoung square wave voltammetry. Fig. 9(1 and 2) shows the voltammograms for the polymer membrane (MW 11,520 g/mol) with the 18- and 36-mer. As expected, no signal was observed for the single-stranded modified surfaces in PBS buffer (Fig. 9(1a and 2a)). Fig. 9(1b and 2b) shows the OSWV of the carboxylated polymer film in the presence of a ferrocene-labeled ODN. The absence of an electrochemical signal indicates that the target ODNs do not react or adsorb to the polymer films. This result verifies that the observed

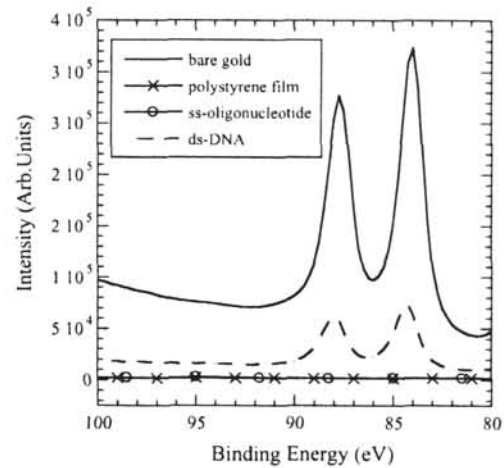


Fig. 8. XPS Au 4f spectra in bare gold, spin coated polystyrene over gold, after  $\text{NH}_2$ -ODN immobilization and after hybridization.

globular morphology is a result of the ODNs immobilization at the succinimidated polystyrene films. A small ferrocene oxidation peak was observed when the surfaces were placed in contact with the non-complementary sequence (Fig. 9(1c and 2c)). Since the probe and target sequences were non-complementary, the observed signal indicates the adsorption of a fraction of the targets to the electrode surfaces. However, a remarkable increase in the ferrocene oxidation peak is evident after hybridization with the complementary ODNs (Fig. 9(1d and 2d)). The adsorption signal is clearly insignificant compared to the hybridization signal.

The  $E_{p,a} = 320$  mV for the 18- and 36-mer ds-ODNs in solution (not shown). For the ds-DNA at the surface, the  $E_{p,a}$  were 323 and 367 mV for the 18- and 36-mer, respectively. There is a 47 mV difference for the 36-mer at the surface compared to the potential in solution. This difference was not observed for the ds-DNA 18-mer. Considering that both double stranded chains (18- and 36-mer) are separated from the surface by a  $\text{C}_{12}$  spacer and that this is also the case for the ferrocene label in the targets, it is reasonable to assume that a semifluid ODN layer is present at the surface. We then ascribed the potential difference observed in the 36-mer to a limited accessibility of the ferrocene label to the surface because the differences in length between the ds-DNA samples.

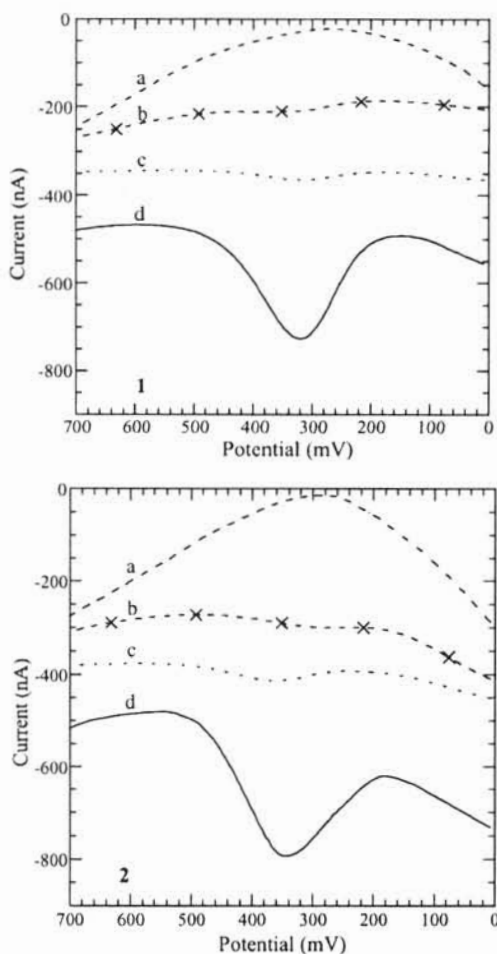


Fig. 9. Osteryoung square wave voltammetry of ds-DNA-ferrocene (1) 18-mer and (2) 36-mer for (a) blank (buffer solution), (b) complementary DNA in carboxylated polystyrene, (c) non-complementary DNA and (d) complementary DNA in PBS (pH 6.9) with 0.1 M NaCl. Reference and auxiliary electrodes: Ag/AgCl and Nichrome.

#### 4. Conclusion

In summary, a novel method for the immobilization of single-stranded DNA on polystyrene thin films was developed. This method allows the immobilization of ODNs in nanometric domains with a controlled separation distance. The robustness and stability of these polymer membranes make these supports good candidates for anchoring of ODNs at solid surfaces. Specifically, the use of functionalized polystyrene films could substantially reduce non-specific interactions between

the ODNs and the surface. The implications for nucleic acids arrays are multi-fold because high-density arrays could be designed and built at relatively low cost and with higher sensitivity if combined with polymer imprinting technologies and chemical signal amplification. The construction of DNA sensors, where the orientation, specific probe location and morphology at the surface is known, is essential for the improvement of hybridization efficiency and sensor sensitivity.

#### Acknowledgements

We gratefully acknowledge Dr. Luis Fonseca and Oscar Resto (Department of Physics, University of Puerto Rico, Río Piedras Campus) for the technical support with the AFM studies. We thank the Materials Characterization Center for the access to the FTIR facilities and Dr. Estevão Fachini for the assistance with the XPS measurements. This work was supported by DOE-EPSCoR Grant No. DE-FG02-01ER45868.

#### References

- Anne, A., Bouchardon, A., Moiroux, J., 2003. 3'-Ferrocene-labeled oligonucleotide chains end-tethered to gold electrode surfaces: novel model systems for exploring flexibility of short DNA using cyclic voltammetry. *J. Am. Chem. Soc.* 125, 1112–1113.
- de-los-Santos-Alvarez, P., Lobo-Castañón, M.J., Miranda-Ordieres, A.J., Tuñón-Blanco, P., 2002. Voltammetric determination of underivatized oligonucleotides on graphite electrodes based on their oxidation products. *Anal. Chem.* 74, 3342–3347.
- Dupont-Filliard, A., Roget, A., Livache, T., Billon, M., 2001. Reversible oligonucleotide immobilization based on biotinylated polypyrrole film. *Anal. Chim. Acta* 449, 45–50.
- Georges, M.K., Veregin, R.P.N., Kazmaier, P.M., Hamer, G.K., 1993. Narrow molecular weight resins by a free-radical polymerization process. *Macromolecules* 26, 2987–2988.
- Hashimoto, K., Ito, K., Ishimori, Y., 1994. Sequence-specific gene detection with a gold electrode modified with DNA probes and an electrochemically active dye. *Anal. Chem.* 66, 3830–3833.
- Hashimoto, K., Ito, K., Ishimori, Y., 1998. Microfabricated disposable DNA sensor for detection of hepatitis B virus DNA. *Sens. Actuators B* 46, 220–225.
- Hawker, C.J., 1994. Molecular weight control by a "living" free-radical polymerization process. *J. Am. Chem. Soc.* 116, 11185–11186.
- Hawker, C.J., Bosman, A.W., Harth, E., 2001. New polymer synthesis by nitroxide mediated living radical polymerizations. *Chem. Rev.* 101, 3661–3688.

- Herne, T.M., Tarlov, M.J., 1997. Characterization of DNA probes immobilized on gold surfaces. *J. Am. Chem. Soc.* 119, 8916–8920.
- Hianik, T., Gajdos, V., Krivanek, R., Oretskaya, T., Metelev, V., Volkov, E., Vadgama, P., 2001. Amperometric detection of DNA hybridization on a gold surface depends on the orientation of oligonucleotide chains. *Bioelectrochemistry* 53, 199–204.
- Huang, E., Satjapipat, M., Han, S., Zhou, F., 2001. Surface structure and coverage of an oligonucleotide probe tethered onto a gold substrate and its hybridization efficiency for a polynucleotide target. *Langmuir* 17, 1215–1224.
- Ihara, T., Nakayama, M., Murata, M., Nakano, K., Maeda, M., 1997. Gene sensor using ferrocenyl oligonucleotide. *Chem. Commun.*, 1609–1610.
- Kelley, S.O., Barton, J.K., Jackson, N.M., Hill, M.G., 1997. Electrochemistry of methylene blue bound to a DNA-modified electrode. *Bioconjug. Chem.* 8, 31–37.
- Kelley, S.O., Barton, J.K., Jackson, N.M., McPherson, L.D., Potter, A.B., Spain, E.M., Allen, M.J., Hill, M.G., 1998. Orienting DNA helices on gold using applied electric fields. *Langmuir* 14, 6781–6784.
- Mourougou-Candoni, N., Naud, C., Thibaudau, F., 2003. Adsorption of thiolated oligonucleotides on gold surfaces: an atomic force microscopy study. *Langmuir* 19, 682–686.
- Mucic, R.C., Herrlein, M.K., Mirkin, C.A., Letsinger, R.L., 1996. Synthesis and characterization of DNA with ferrocenyl groups attached to their 5'-termini: electrochemical characterization of a redox-active nucleotide monolayer. *Chem. Commun.*, 555–557.
- Nakayama, M., Ihara, T., Nakano, K., Maeda, M., 2002. DNA sensors using a ferrocene oligonucleotide conjugate. *Talanta* 56, 857–866.
- Niemeyer, C.M., Adler, M., Gao, S., Chi, L., 2001. Nanostructured DNA-protein aggregates consisting of covalent oligonucleotide-streptavidin conjugates. *Bioconjug. Chem.* 12, 364–371.
- Ohno, K., Tsujii, Y., Miyamoto, T., Fukuda, T., Goto, M., Kobayashi, K., Akaike, T., 1998. Synthesis of a well-defined glycopolymer by nitroxide-controlled free radical polymerization. *Macromolecules* 31, 1064–1069.
- Ontko, A.C., Armistead, P.M., Kircus, S.R., Thorp, H.H., 1999. Electrochemical detection of single-stranded DNA using polymer-modified electrodes. *Inorg. Chem.* 38, 1842–1846.
- Paleček, E., Fojta, M., 2001. DNA hybridization and damage. *Anal. Chem.*, 75A–83A.
- Patolsky, F., Lichtenstein, A., Willner, I., 2001. Electronic transduction of DNA sensing processes on surfaces: amplification of DNA detection and analysis of single-base mismatches by tagged liposomes. *J. Am. Chem. Soc.* 123, 5194–5205.
- Pedano, M.L., Rivas, G.A., 2003. Immobilization of DNA on glassy carbon electrodes for the development of affinity biosensors. *Biosens. Bioelectron* 18, 269–277.
- Pividori, M.I., Merkoçi, A., Alegret, S., 2000. Electrochemical genosensor design: immobilization of oligonucleotides onto transducer surfaces and detection methods. *Biosens. Bioelectron* 15, 291–303.
- Riepl, M., Enander, K., Liedberg, B., Schaferling, M., Kruschina, M., Ortigao, F., 2002. Functionalized surfaces of mixed alkanethiols on gold as a platform for oligonucleotide microarrays. *Langmuir* 18, 7016–7023.
- Satjapipat, M., Sanedrin, R., Zhou, F., 2001. Selective desorption of alkanethiols in mixed self-assembled monolayers for subsequent oligonucleotide attachment and dna hybridization. *Langmuir* 17, 7637–7644.
- Steel, A.B., Levicky, R.L., Herne, T.M., Tarlov, M.J., 2000. Immobilization of nucleic acids at solid surfaces: effect of oligonucleotide length on layer assembly. *Biophys. J.* 79, 975–981.
- Sun, H.B., Yokota, H., 2000. MutS-mediated detection of DNA mismatches using atomic force microscopy. *Anal. Chem.* 72, 3138–3141.
- Takenaka, S., Uto, Y., Kondo, H., Ihara, T., Takagi, M., 1994. Electrochemically active DNA probes: detection of target DNA sequences at femtomole level by high-performance liquid chromatography with electrochemical detection. *Anal. Biochem.* 218, 436–443.
- Takenaka, S., Yamashita, K., Takagi, M., Uto, Y., Kondo, H., 2000. DNA sensing on a DNA probe-modified electrode using ferrocenylnaphthalene diimide as the electrochemically active ligand. *Anal. Chem.* 72, 1334–1341.
- Veregin, R.P.N., Georges, M.K., Hamer, G.K., Kazmaier, P.M., 1995. Mechanism of living free radical polymerizations with narrow polydispersity: electron spin resonance and kinetic studies. *Macromolecules* 28, 4391–4398.
- Wang, J., 2000. From DNA biosensors to gene chips. *Nucl. Acids Res.* 28, 3011–3016.
- Yokota, H., Sunwoo, J., Sarikaya, M., van den Engh, G., Aebersold, R., 1999. Spin stretching of DNA and protein molecules for detection by fluorescence and atomic force microscopy. *Anal. Chem.* 71, 4418–4422.
- Yu, C.J., Wan, Y., Yowanto, H., Li, J., Tao, C., James, M.D., Tan, C.L., Blackburn, G.F., Meade, T.J., 2001. Electronic detection of single-base mismatches in DNA with ferrocene-modified probes. *J. Am. Chem. Soc.* 123, 11155–11161.
- Zhang, Z.L., Pang, D.W., Zhang, R.Y., Yan, J.W., Mao, B.W., Qi, Y.P., 2002. Investigation of DNA orientation on gold by EC-SSTM. *Bioconjug. Chem.* 13, 104–109.

# Effect of Enzyme and Cofactor Immobilization on the Response of Ethanol Oxidation in Zirconium Phosphate Modified Biosensors

Mitk'El B. Santiago,<sup>b</sup> Gabriel A. Daniel,<sup>a</sup> Amanda David,<sup>a</sup> Barbara Casañas,<sup>a</sup> Griselle Hernández,<sup>a</sup> Ana R. Guadalupe,<sup>a</sup> Jorge L. Colón<sup>a\*</sup>

<sup>a</sup> Department of Chemistry, P. O. Box 23346, University of Puerto Rico, Río Piedras, P. R. 00931-3346, USA

<sup>b</sup> Department of Chemistry, University of Puerto Rico at Cayey, 205 Avenida Antonio R. Barceló Cayey, PR 00736, USA

\*e-mail: jlcolon@uprrp.edu

Received: June 29, 2009

Accepted: January 1, 2010

## Abstract

Two different self-contained ethanol amperometric biosensors incorporating layered [Ru(phen)<sub>2</sub>bpy]<sup>2+</sup>-intercalated zirconium phosphate (ZrP) as the mediator as well as yeast-alcohol dehydrogenase (*y*-ADH) and its cofactor nicotinamide adenine dinucleotide (NAD<sup>+</sup>) were constructed to improve upon a design previously reported where only this mediator was immobilized in the surface of a modified electrode. In the first biosensor, a [Ru(phen)<sub>2</sub>bpy]<sup>2+</sup>-intercalated ZrP modified carbon paste electrode (CPE) was improved by immobilizing in its surface both *y*-ADH and NAD<sup>+</sup> using quaternized Nafion membrane. In the second biosensor, a glassy carbon electrode was modified with [Ru(phen)<sub>2</sub>bpy]<sup>2+</sup>-intercalated ZrP, *y*-ADH, and NAD<sup>+</sup> using Nafion as the holding matrix. Calibration plots for ethanol sensing were constructed in the presence and absence of ZrP. In the absence of ZrP in the surface of the modified glassy carbon electrode, leaching of ADH was observed as detected by UV-vis spectrophotometry. Ethanol sensing was also tested in the presence and absence of ascorbate to measure the selectivity of the sensor for ethanol. These two ethanol biosensors were compared to a previously reported one where the *y*-ADH and the NAD<sup>+</sup> were in solution, not immobilized.

**Keywords:** Alcohol dehydrogenase, Zirconium phosphate, Ethanol biosensor, Amperometric biosensor, Ruthenium complex, NAD<sup>+</sup>/NADH redox couple, Electron mediator, Biosensors

DOI: 10.1002/elan.200900329

10 AUG 16 P 1:14

RECIBIDO  
SERVIDO A AGENCIA  
RECINTO RÍO PIEDRAS UPR

## 1. Introduction

There is a need for fast and reliable methods for determining ethanol content [1–4]. The development of biosensors able to detect low concentrations of alcohols have attracted interest for some time [5–7]. Alcohol dehydrogenase (ADH) has been used in the past for the detection of ethanol for various industrial applications, including brewing and wine making [5–7]. Several approaches have been used for the construction of amperometric ethanol biosensors which include modified electrodes used with the enzyme in solution [8] or immobilized in the electrode surface [5, 9–12]. Immobilization of enzymes in rigid matrices has attracted attention for some time [13–16]. There are several advantages in immobilizing enzymes, among them, enzymes immobilized in solid matrices can be recycled, lowering their effective cost, and can be easily separated from their reaction mixture [16].

Enzymes have been immobilized in polymers, sol gels, surfactant films, hydrogels, and carbon paste, among other materials [13, 17–24]. The effect of the matrix surface on the immobilized proteins can affect the stabilization of the enzyme, improving activity and in few cases the selectivity of the enzyme is altered in a desirable way [25]. However, the

interaction of the protein and the matrix surface is not yet well understood [16].

One of the materials that has been used for protein immobilization are the layered zirconium phosphates (ZrP) [14, 16, 26, 27]. Zirconium phosphates are acidic inorganic ion exchangers with layered structures [28–30]. Cytochrome *c*, hemoglobin, myoglobin, and horseradish peroxidase, among other proteins, have been immobilized into ZrP and the hydrophilic nature of the phosphate groups are proposed to stabilize the protein [14, 16, 27].

Recently, we reported the construction of an amperometric ethanol biosensor using a carbon paste electrode (CPE) modified with ZrP that had intercalated in it the electron mediator bis(1,10-phenanthroline-5,6-dione)(2,2'-bipyridine)ruthenium(II) ([Ru(phen)<sub>2</sub>bpy]<sup>2+</sup>) [8]. In that previous biosensor yeast ADH (*y*-ADH) enzyme and its nicotinamide adenine dinucleotide (NAD<sup>+</sup>) cofactor were in solution. In the present study we report the construction of two new biosensors, one where *y*-ADH and NAD<sup>+</sup> are immobilized on the carbon paste electrode surface by immobilizing the enzyme in a polymer matrix, and a second one in which all components were drop-cast on a glassy carbon electrode surface.

## 2. Experimental

Mineral oil, Baker's yeast alcohol dehydrogenase (E.C. 1.1.1.1) and  $\beta$ -nicotinamide adenine dinucleotide were obtained from Sigma Chemicals. Graphite powder and copper wire were obtained from Fisher Co. All other reagents, at least 98% pure, were obtained from Aldrich. Nafion ethanolic solution was obtained from Sigma-Aldrich Chemicals. Nanopure water was obtained using a Barnstead purification train (17.5 M $\Omega$ /cm). UV-vis absorption spectra were obtained using a HP 8453 diode array spectrophotometer.

All electrochemical measurements were done with a BAS Model CV-50W potentiostat in a 5 mL cell containing the modified CPE, a Ag/AgCl (3 M NaCl) reference electrode and a Pt wire auxiliary electrode. The electrochemical results are reported as the average of five electrodes. Measurements of the stability of the self contained biosensor were done with a BASi Epsilon-EC-Ver. 1.60.70\_XP potentiostat in a 5 mL cell containing the modified glassy carbon electrode, a Ag/AgCl (3 M NaCl) reference electrode and a Pt wire auxiliary electrode.

The surface of a glassy carbon electrode (3 mm in diameter) was polished using a 1  $\mu$ m diamond polishing compound (Metadi II, Buehler) until a mirror-like surface was obtained. Then, the electrode was sonicated in a 1:1 acetone:distilled water solution for 15 minutes. The electrodes were allowed to dry in a desiccator at room temperature.

### 2.1. Immobilization of [Ru(phend)<sub>2</sub>bpy]<sup>2+</sup> into ZrP and Construction of Modified Carbon Paste Electrodes with [Ru(phend)<sub>2</sub>bpy]<sup>2+</sup> Intercalated into ZrP

The syntheses of ZrP and [Ru(phend)<sub>2</sub>bpy]<sup>2+</sup> and the immobilization of [Ru(phend)<sub>2</sub>bpy]<sup>2+</sup> appears elsewhere (the intercalated material is referred as Ru-ZrP) [8, 31–33]. The [Ru(phend)<sub>2</sub>bpy]<sup>2+</sup>:ZrP molar ratio used in this study was 1:2.3 which showed better stability and better catalytic current in comparison with other compositions tested. The construction of the carbon paste electrodes (CPEs) modified with Ru-ZrP has been previously reported [8].

### 2.2. Immobilization of $\gamma$ -ADH and NAD<sup>+</sup> on the Surface of Ru-ZrP Modified CPE

$\gamma$ -ADH and NAD<sup>+</sup> were immobilized on the surface of a Ru-ZrP modified CPE (1 mm diameter) using a procedure previously reported by Minter et al. [34–36]. A 5 wt% Nafion suspension was treated with quaternary ammonium bromide so that the concentration of quaternary ammonium bromide is in excess of the concentration of sulfonic acid sites in the Nafion suspension. The concentration of the quaternary ammonium bromide should be at least three times the concentration of the exchange sites of Nafion [34–36].

For the preparation of the mixture of the enzyme with the quaternary ammonium bromide/Nafion casting solution the volume ratio should be 2:1 (1200  $\mu$ L of 1.0  $\mu$ M enzyme: 600  $\mu$ L of 5% by wt. modified Nafion suspension). After the addition of 0.03 g of NAD<sup>+</sup> the mixture was vortexed for ca. 1 min in preparation for coating on electrodes. The solution (2  $\mu$ L) was pipetted onto the surface of the electrodes. The films were allowed to air dry for 20 min and cured overnight in a vacuum desiccator.

These electrodes need to be activated in a 0.1 mM NAD<sup>+</sup> solution before use to assure that NAD<sup>+</sup> is present inside the polymer matrix before alcohol sensing. This is expected, since the Nafion polymer is in an ethanolic solution (see Experimental Section), and the ethanol in the solvent in the presence of  $\gamma$ -ADH and NAD<sup>+</sup> in the intercalation solution, will produce NADH. If we use the electrodes without this pretreatment, the response is not reproducible. This procedure was designed to allow stability and reuse of the sensors.

### 2.3. Nanoencapsulation of $\gamma$ -ADH into ZrP Framework

A stock solution of  $\gamma$ -ADH (0.1 g of solid), with NAD<sup>+</sup> (1.0 mg) in 100 mL (using PBS,  $\mu = 0.1$ , at pH 7.0) was mixed with 0.2 g of the 10.3  $\text{Å}$  ZrP framework and stirred for two hours at room temperature. The nanoencapsulation was performed at a 1:1 (ADH:ZrP) molar ratio. The samples were filtered in vacuum and the solid was lyophilized for 48 hours. The resulting bone white solid was characterized using XRPD measurements, IR spectroscopy, and circular dichroism.

### 2.4. Enzyme Assay for the Determination of ADH Activity

The activity of the enzyme was determined as described in the literature [37]. Seven milligrams of ADH was added to a 10 mL volumetric flask using 0.1 M PBS at pH 7.0 as the solvent. The absorption at 340 nm of any NADH present was measured in a quartz cuvette filled with a solution containing 1.5 mL of a 0.1 M PBS at pH 8.0, 0.50 mL of 2 M ethanol and 1.00 mL of 25 mM NAD<sup>+</sup>. Afterwards, 150  $\mu$ L of the enzyme solution was added and the change in absorbance at 340 nm from NADH produced by the enzymatic reaction as a function of time was measured.

### 2.5. Construction of a Modified Glassy Carbon Electrode for Ethanol Sensing

A 2 mL aliquot from the suspension obtained in the synthesis of ZrP [31] was added to a test tube along with 5 mg of ADH, 30 mg of NAD<sup>+</sup>, and 10 mg of [Ru(phend)<sub>2</sub>bpy]<sup>2+</sup>. The suspension was vortexed for fifteen minutes. An aliquot of 5  $\mu$ L was added to the surface of a clean glassy carbon electrode and was allowed to dry overnight. Finally, 5  $\mu$ L of Nafion were dropped on the electrode surface. The

modified electrodes were allowed to dry and kept in a refrigerator before use. Calibration plots for ethanol sensing were constructed in the absence and presence of 5 mM ascorbate.

As controls, modified electrodes were also constructed following the same procedure as above, but in the absence of ZrP. The test tube was filled with 2 mL of nanopure water and subsequent immobilization steps were the same as explained before.

### 3. Results and Discussion

#### 3.1. Self-Contained Biosensor Based on CPE Modified with $[\text{Ru}(\text{phen})_2\text{bpy}]^{2+}$ -Intercalated ZrP

Previously, we reported the use of a Ru-ZrP modified CPE for ethanol sensing [8]. However, that biosensor was not self-contained; the enzyme and co-factor were not immobilized on the electrode surface; they were added to the substrate solution. To construct a self-contained device using a CPE modified with Ru-ZrP, we have now constructed a self-contained biosensor for ethanol sensing by using an approach pioneered by Minter et al. [35, 36, 38]. These authors were able to immobilize several dehydrogenases in a Nafion-modified electrode surface and study their activity in aqueous solution. Among the enzymes used was  $\gamma$ -ADH [36]. Following this precedent we decided to use Nafion to immobilize  $\gamma$ -ADH alcohol dehydrogenase and  $\text{NAD}^+$  on the surface of Ru-ZrP modified CPEs. Figure 1 shows a characteristic calibration plot for ethanol sensing for a self-contained CPE constructed using the Minter procedure incorporating Ru-ZrP,  $\gamma$ -ADH and the  $\text{NAD}^+$  cofactor. The electrodes show high sensitivity up to 0.07% v/v of ethanol concentration. The dynamic range was 0.01–0.07% ethanol (2–15 mM in ethanol concentration). How-

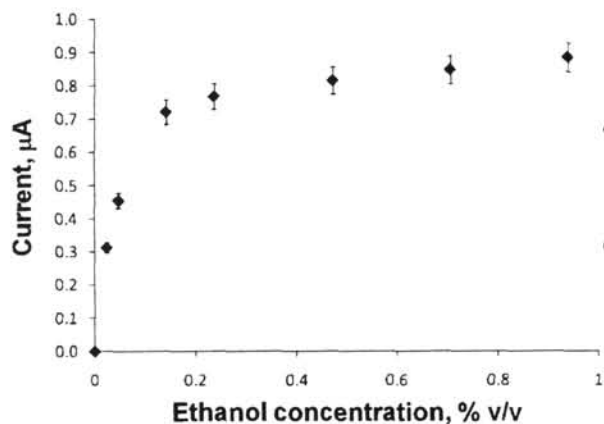


Fig. 1. Calibration plot for ethanol sensing using a Ru-ZrP-modified CPE that has on its surface  $\gamma$ -ADH and  $\text{NAD}^+$  immobilized with quaternary ammonium bromide-modified Nafion at the surface of a Ru-ZrP modified CPE ( $\mu = 0.1$ , pH 7.0). Error bars corresponds to  $\pm 1$  standard deviation.

ever, due to the low reproducibility of constructed CPEs we pursued a new approach to construct a chemically modified electrode using glassy carbon.

#### 3.2. Characterization of the ZrP Modified Glassy Carbon Electrode

Figure 2 shows a characteristic calibration plot for ethanol sensing using the modified glassy carbon electrode. A linear behavior is observed up to 6% (v/v) of ethanol concentration. The dynamic range was 0.01–6.0% ethanol (2 mM–1.0 M in ethanol concentration). Using cyclic voltammetry we observed that the sensitivity of the biosensor showed a 0.034  $\mu\text{A}$  change upon a change of 1% in ethanol concentration. All the components were immobilized and no leaching was detected as determined by Osteryoung square wave voltammetry and UV-vis spectrophotometry (data not shown).

Control experiments were performed in the absence of ZrP, while all the other components were immobilized in the electrode surface, and a catalytic current was also evident. Figure 3 shows characteristic calibration plot for ethanol sensing in the presence and in the absence of ZrP at the modified glassy carbon electrode surface. Although the catalytic current was also observed in the absence of ZrP the linearity of the calibration plot is affected.

In addition, we observed that the sigmoidal shape of the cyclic voltammograms of the modified glassy carbon electrode in the absence of ZrP were characteristic for an electrocatalytic process for solubilized components in solution. When we analyzed the PBS solution after the experiment using UV-vis spectrophotometry we observed a new absorption band at ca. 260 nm, which was not present in the PBS solution previous to the experiment. Figure 4 shows the UV-vis absorption spectra of the PBS before and after the calibration plot for ethanol sensing was obtained for the

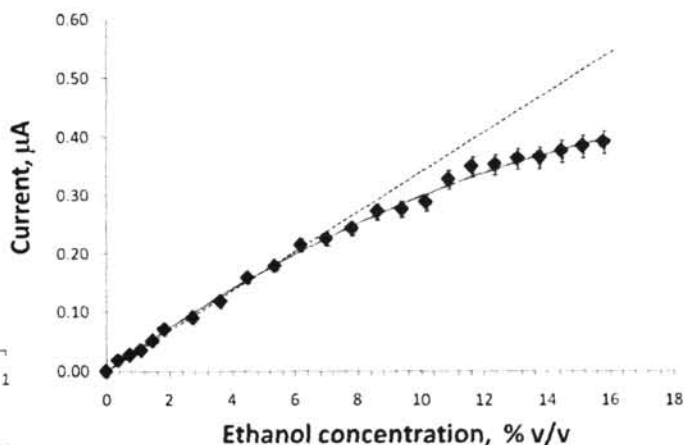


Fig. 2. Calibration plot for ethanol sensing in PBS ( $\mu = 0.1$ ) at pH 7.0 using a glassy carbon electrode modified with Ru-ZrP,  $\gamma$ -ADH and  $\text{NAD}^+$ . Error bars corresponds to  $\pm 1$  standard deviation.

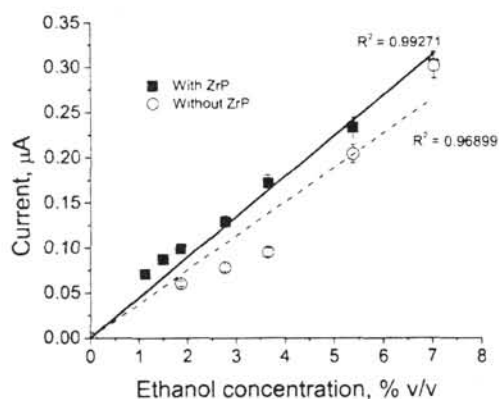


Fig. 3. Calibration plot for ethanol sensing using a glassy carbon electrode modified with  $[\text{Ru}(\text{phend})_2\text{bpy}]^{2+}$ ,  $\gamma$ -ADH and  $\text{NAD}^+$  (using concentrations that appear in Figure 1) in the presence and absence of ZrP (in PBS,  $\mu = 0.1$  at pH 7.0). Error bars corresponds to  $\pm 1$  standard deviation.

modified glassy carbon electrode in the absence of ZrP. The new band observed is due to the aromatic groups of the enzyme present in solution. Therefore, ADH is leaching out of the electrode surface. These findings are not surprising, Minter et al. demonstrated that in the presence of bulky quaternary amino molecules in Nafion, dehydrogenases do not leach out from an electrode surface [36].

In the presence of ZrP, leaching is not detected in the modified glassy carbon electrode due to the fact that ZrP is holding all the components ( $\text{ADH}$ ,  $\text{NAD}^+$ , and  $[\text{Ru}(\text{phend})_2\text{bpy}]^{2+}$ ), giving robustness to the biosensor, which can be used several times.

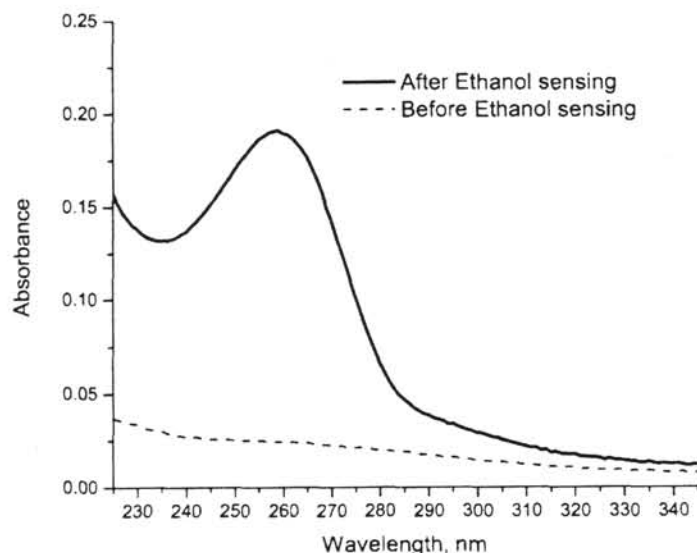


Fig. 4. UV-vis spectra of the PBS before and after obtaining the calibration plot for ethanol sensing in the absence of ZrP at the glassy carbon electrode modified with  $[\text{Ru}(\text{phend})_2\text{bpy}]^{2+}$ ,  $\gamma$ -ADH and  $\text{NAD}^+$  (using concentrations that appear in Figure 1).

To study the effect of ZrP on all the biocomponents of the sensor, we performed the nanoencapsulation of ADH in a buffered solution at pH 7.0. Figure 5 shows, the XRPD pattern of the ADH:ZrP composite material. The XRPD pattern shows the formation of a new phase with an interlayer distance of 85.0 Å. No peaks related to  $\alpha$ -ZrP (at 7.6 or 3.8 Å) were detected, in agreement with the results of Kumar et al. [16, 27]. The immobilization of ADH in the ZrP matrix expanded the interlayer spacing from 10.3 to 85.0 Å. From the crystal structure of  $\gamma$ -ADH, the approximate dimensions of the entire protein are  $144 \times 128 \times 72$  Å [39]. The smallest theoretical interlayer distance for the intercalated material should be 78.6 Å if the thickness of a ZrP layer (6.6 Å) is taken in consideration [40, 41]. The 6.4 Å difference between the theoretical minimum and the experimental interlayer distance can be attributed to the immobilization of counter ions, co-ions or water molecules in ZrP resulting in an additional expansion of the layers [16]. Different orientations of the enzyme inside ZrP can also be found, which can give different diffraction peaks. The peaks observed at 74.8 Å and 49.6 Å could be due to the second and third order diffraction peaks, respectively, of a first unobserved first order diffraction peak corresponding to the protein with the 144 Å dimension perpendicular to the layers ( $144 + 6.6 = 150.6$  Å).

Kumar and McLendon have nanoencapsulated cytochrome *c* into  $\alpha$ -ZrP. These authors observed an increase of the interlayer distance from 7.6 to 31.7 Å [27]. In addition, similar to our results, these authors observed other diffraction peaks at 24.0, 14.3 and 7.4 Å in the X-ray diffractogram. Kumar and McLendon reported that these peaks are due to different orientations of the protein inside the galleries of ZrP [27]. Our results showed that the  $\gamma$ -ADH protein can adopt different orientations inside ZrP, which can give different diffraction peaks at lower  $2\theta$  (e.g. the diffraction peak at 60.6 Å).

The IR-spectra of the immobilized enzymes provide information about the secondary structure of the enzyme. That information can help us elucidate whether the native form of a protein is lost due to an immobilization process. Figure 6 shows the FT-IR spectra of ZrP, free ADH and ADH nanoencapsulated in ZrP (ADH:ZrP) materials. The amide I and amide II vibrational bands of ADH are preserved in the ADH-intercalated protein suggested that the proteins is not denatured (inside ZrP) upon intercalation. The amide vibrational frequencies of proteins are sensitive to hydrogen bonding interactions of the amide with the solvent, and with neighboring functionalities. The IR spectra of ADH:ZrP showed that the amide I band at ca.  $1630 \text{ cm}^{-1}$  in solid state shifts to  $1640 \text{ cm}^{-1}$  in ADH:ZrP. This shift along with the broadness of the peak indicates some of the ADH secondary structure is affected due to restrict space of the microenvironment, but no denaturalization. The amide II band corroborated this finding, as it did not shift evidently in this environment. Therefore, it appears that a native-like secondary structure is preserved upon immobilization. These findings are consistent with the results reported by Kumar and Chaudhari [16].

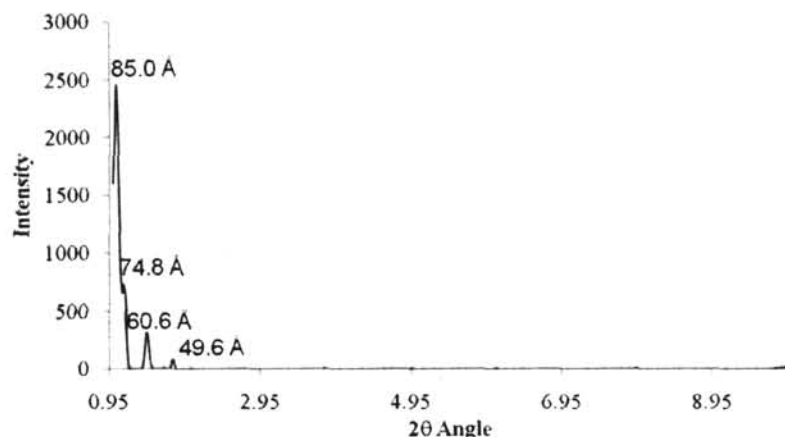


Fig. 5. X-ray powder diffractogram of ADH/ZrP composite material.

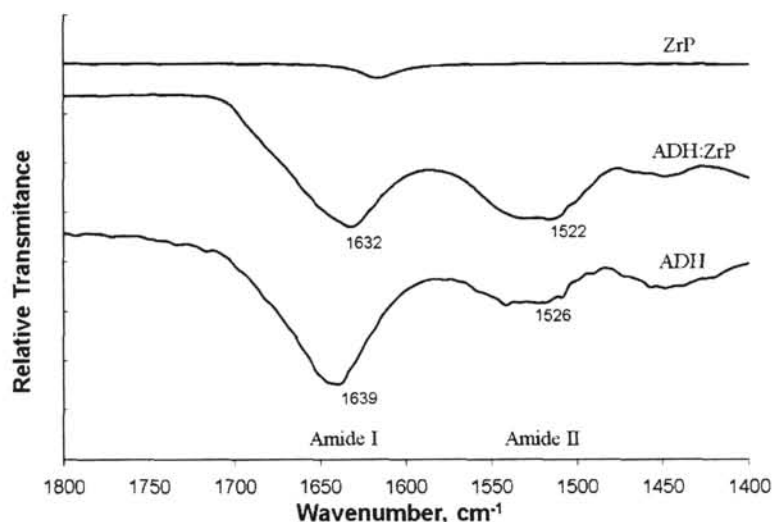


Fig. 6. FT-IR spectra of ZrP, free ADH and ADH:ZrP.

The secondary structure information obtained from IR spectroscopy can be corroborated using circular dichroism (CD) spectroscopy. In proteins, the electronic interactions between different residues contribute to a characteristic CD spectrum. The chromophores responsible for the absorption spectrum are the peptide bond, which absorbs below 240 nm; the aromatic amino acids, absorb between 260 to 320 nm; and disulphide bonds, which show a weak absorption at ca. 260 nm [42, 43].

The information obtained in a CD spectrum can also give insights of how the secondary structure is affected inside the ZrP matrix. The absorption below 240 nm, which is known as the far-ultraviolet CD, gives an idea of how the secondary structure is affected. The peptide bond has a weak but broad absorption at 220 nm due to an  $n \rightarrow \pi^*$  transition and a more intense absorption at 192 nm due to a  $\pi \rightarrow \pi^*$  transition [42]. Moreover, secondary structures such as  $\alpha$ -helices and

pleated- $\beta$  sheets, also have different absorptions in the CD spectra. The  $\alpha$ -helices have a negative absorption at 208 and 220 nm and the positive band at 192 nm [42–44]. The pleated- $\beta$  sheets contribute little to the CD spectra but show a broad negative absorption at 212 nm and a positive absorption at 195 nm [42–44].

The CD spectra of ADH at different pHs and of the ADH:ZrP material in water showed that the secondary structure of ADH in solution is dependent on pH (data not shown). The broadness of the absorption peaks at 208 and 220 nm due to the  $\alpha$ -helices broadens upon an increase in pH. Kumar and Chaudhari have observed that upon immobilization of enzymes inside the ZrP matrices little or no change in the secondary structure was evident in their CD spectra [16]. However, we observed that the secondary spectra of our enzyme nanoencapsulated in ZrP matrices is more consistent with the structure that this enzyme has at pH 8.0.

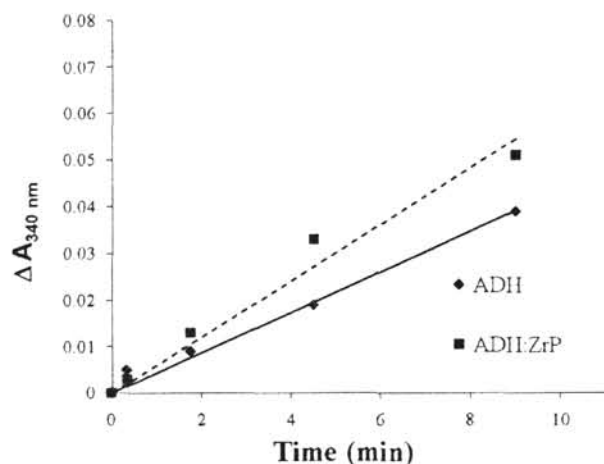


Fig. 7. NADH activity assay of free ADH and ADH:ZrP using ethanol as the substrate.

We must remember that the immobilization of the enzyme was performed at this pH to try to maintain the enzyme native structure inside ZrP.

Enzymes previously immobilized in ZrP retain their activity and are readily accessible by their substrates [16, 27]. Therefore, we studied the activity of ADH in ZrP. Figure 7

shows the NADH activity for the free ADH and ADH:ZrP material. The ADH:ZrP material showed that upon intercalation the ADH enzyme retained its activity and readily oxidizes ethanol to acetaldehyde. We observed an improvement on activity for the ADH:ZrP material. There is a 50% higher activity of the ADH:ZrP material in comparison with the free enzyme ( $\Delta A_{340}/\Delta min = 0.004$  for the free enzyme, 0.006 for ADH:ZrP). The 50% higher activity of ADH:ZrP tell us that the substrates can easily diffuse to the galleries of ZrP and a facile access to the active site is enhanced for the immobilized ADH.

Kumar and Chaudhari observed similar results when these two authors immobilized several proteins in  $\alpha$ -ZrP [16, 27]. For example, the activities of chymotrypsin and glucose oxidase were improved upon intercalation in ZrP from 25 thru 30% [16]. These authors explained that the large interlayer distance in protein-intercalated ZrP allow the substrate of interest to enter the layers of ZrP to reach the active site of the enzyme. In our case, ethanol can easily enter the cavities of ZrP and therefore when ethanol interacts with the active site of ADH it readily oxidizes to form formaldehyde. The fact that the ADH enzyme increases its activity upon intercalation in ZrP makes it suitable for the construction of an ethanol sensor.

To understand if NADH and/or NAD<sup>+</sup> can be immobilized into ZrP, we studied the intercalation reaction of NAD<sup>+</sup> and NADH in ZrP. Figure 8 shows the XRPD data

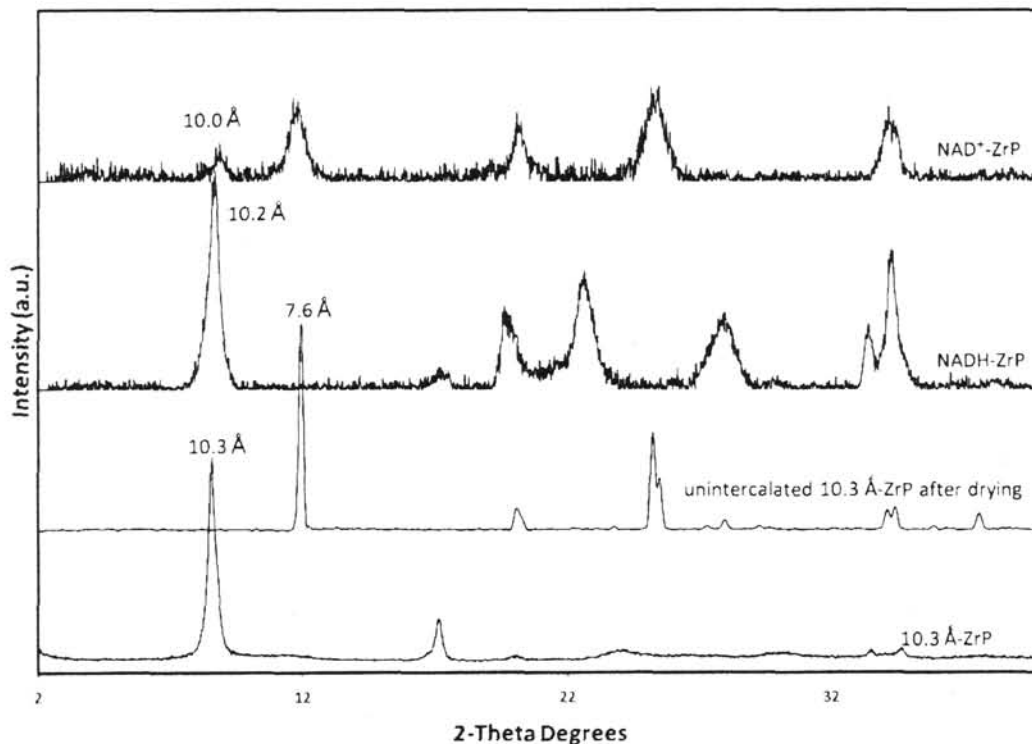


Fig. 8. XRPD patterns of a wet sample of 10.3 Å ZrP, a dried sample of 10.3 Å ZrP (upon drying 10.3 Å ZrP converts to  $\alpha$ -ZrP), a dried sample of NADH-intercalated ZrP and a dried sample of NAD<sup>+</sup>-intercalated ZrP.

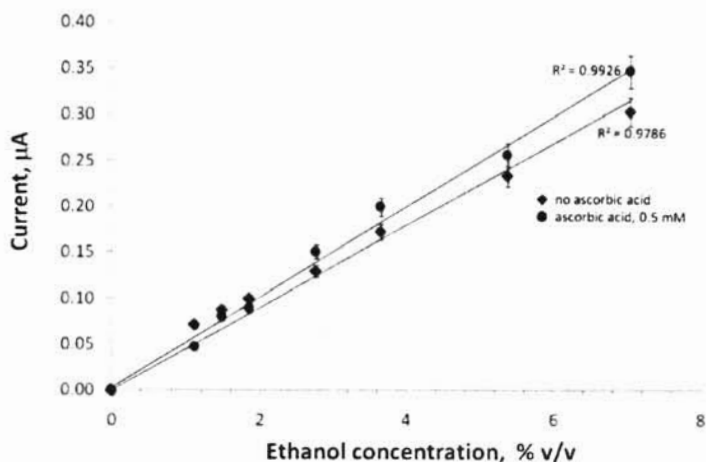


Fig. 9. Ethanol calibration plot for ethanol sensing in the absence and presence of ascorbic acid using a glassy carbon electrode modified with  $[\text{Ru}(\text{phen})_2\text{bpy}]^{2+}$ ,  $\gamma$ -ADH and  $\text{NAD}^+$  (using concentrations that appear in Figure 1; 0.5 mM in PBS  $\mu = 0.1$  at pH 7.0). Error bars corresponds to  $\pm 1$  standard deviation.

obtained for 10.3 Å wet phase of ZrP, for the dried phase of ZrP (which is the  $\alpha$ -phase), the dried phase of NADH-intercalated ZrP and the dried phase of  $\text{NAD}^+$ -intercalated ZrP. The XPRD pattern of the product of the intercalation of NADH within ZrP shows the formation of a new phase with a sharp diffraction peak corresponding to an interlayer distance of 10.2 Å. This expanded interlayer distance of the new phase indicates that NADH has been intercalated into ZrP, since unintercalated ZrP has an interlayer distance of 7.6 Å. Figure 8 also shows that for  $\text{NAD}^+$  intercalation a mixed phase forms, containing unintercalated ZrP and also  $\text{NAD}^+$ -intercalated ZrP since a diffraction peak at 10.0 Å indicates the formation of a new phase. This phase is less crystalline than the NADH-intercalated ZrP phase, as indicated by the broader diffraction peaks. These experiments show that whether NADH or  $\text{NAD}^+$  are present on the electrode surface, they both will be trapped by the ZrP framework.

Electrocatalytic sensing of NADH in clinical samples is plagued with problems due to interferences from ascorbic acid, uric acid, paracetamol and neurotransmitters [45]. Rotariu and Bala constructed a microbial ethanol biosensor by immobilizing yeast cells on the surface of an oxygen electrode and observed a well defined electrochemical signal for ethanol sensing [46]. However, these authors observed that glucose can act as an interfering agent.

Our ethanol sensor does not use living cells, instead it uses alcohol dehydrogenase which catalyzes a reaction that does not rely on oxygen concentration. In addition, since it uses  $\text{NAD}^+$  as a cofactor for the oxidation of ethanol to formaldehyde, we have used Ru-ZrP as an electron mediator since mediators with low potentials can avoid interfering reactions [45]. We performed experiments to test the selectivity of our modified glassy carbon ethanol biosensor in the presence of interferences such as ascorbic acid. Figure 9 shows the linear range for the calibration plot of ethanol sensing by the modified glassy carbon electrode

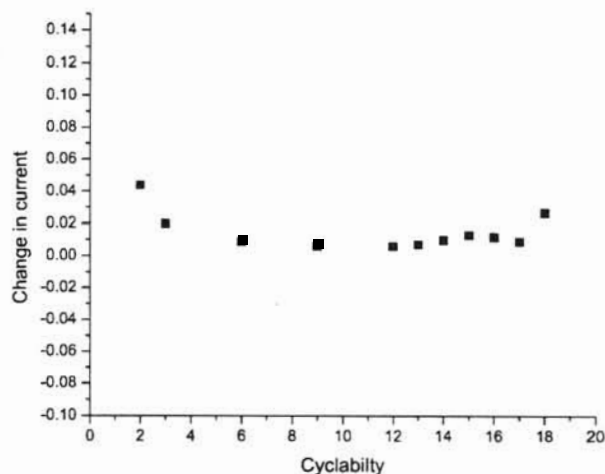


Fig. 10. Cyclability response of the ethanol sensor at  $-32.0$  mV vs. Ag/AgCl. Error bars corresponds to  $\pm 5\%$  of the reported value.

in the presence and in the absence of ascorbate. The slope of the two linear plots are nearly identical; in the presence of an interference such as ascorbate we did not observe a significant change of the sensor response signal. This result indicates that the oxidation of ascorbate does not interfere with the oxidation of NADH by  $[\text{Ru}(\text{phen})_2\text{bpy}]^{2+}$ .

To probe the stability of the sensor, we performed multiple current measurements at  $-32.5$  mV vs. Ag/AgCl as a function of time using a 7% v/v ethanol concentration. Figure 10 shows the cyclability response data from these multiple biosensor reuse measurements. Figure 10 shows that with a brand new sensor, after an initial partial loss in current, the current stabilizes after the fourth cycle.

Table 1 presents a comparison chart for the different ethanol sensors that we have constructed in our laboratory

Table 1. Comparison of the constructed ethanol biosensor constructed.

Type of sensor	Components in solution	Linear range (% v/v)
CPE modified with Ru-ZrP	$\gamma$ -ADH, and NAD <sup>+</sup>	15–80 mM (0.07–0.4%) [8]
Self-contained biosensor modified CPE	NONE	2–15 mM (0.01–0.07%)
Self-contained biosensor using glassy carbon electrode modified with Ru:ZrP, ADH, and NAD <sup>+</sup>	NONE	2 mM–1.0 M (0.01–6.0%)

using zirconium phosphate as the holding matrix. The immobilization of all components in the electrode surface enhances the linear range for the detection of ethanol concentration. Furthermore, the modified glassy carbon electrode gives the most extended linear range.

The amount of ethanol in human blood cannot exceed 0.5% before the person enters in a comatose state [47]. Most state laws have a 0.08% alcohol limit to determine if a person is intoxicated with alcohol [47, 48]. Recently, this limit has been under debate because at a 0.04% level it has been demonstrated that a person can also be intoxicated by this low amount [47, 48]. Therefore, the linear range of these Ru-ZrP modified ethanol biosensors make them suitable for forensic applications.

#### 4. Conclusions

We prepared two types of self-contained amperometric ethanol biosensors; the one using glassy carbon electrode modified with [Ru(phend)<sub>2</sub>bpy]<sup>2+</sup>, ZrP, ADH and NAD<sup>+</sup> immobilized in the electrode surface was able to detect ethanol concentrations up to 6.0% v/v of ethanol concentration. In addition, an interference in solution such as ascorbic acid did not affected ethanol sensing in these samples. We also constructed as controls modified glassy carbon electrodes with a mixture of [Ru(phend)<sub>2</sub>bpy]<sup>2+</sup>, NAD<sup>+</sup> and  $\gamma$ -ADH but no ZrP present and compared then to identically constructed electrodes with ZrP present. The electrodes that contain ZrP showed no leaching of the components into the electrolyte solution. We are now in the process of immobilizing other enzymes for biosensing applications, and the physical and chemical properties of these enzymes intercalated in ZrP are going to be discussed in detail in a future paper.

#### References

- [1] S. A. Kumar, S.-M. Chen, *Sensors* **2008**, *8*, 739.
- [2] P. Belenky, K. L. Bogan, C. Brenner, *Trends Biochem. Sci.* **2007**, *32*, 12.
- [3] N. Pollak, C. Dolle, M. Ziegler, *Biochem. J.* **2007**, *402*, 205.
- [4] Z.-H. Dai, F.-X. Liu, G.-F. Lu, J.-C. Bao, *J. Solid State Electrochem.* **2007**, *12*, 175.
- [5] W. W. Kubiak, J. Wang, *Anal. Chim. Acta* **1989**, *221*, 43.
- [6] M. Niculescu, R. Mieliauskiene, V. Laurinavicius, E. Csoregi, *Food Chem.* **2003**, *82*, 481.
- [7] A. M. Azevedo, M. F. Prazeres, J. M. S. Cabral, L. P. Fonseca, *Biosens. Bioelectron.* **2005**, *21*, 235.
- [8] M. B. Santiago, M. M. Vélez, S. Borrero, A. Díaz, C. A. Casillas, C. Hofmann, A. R. Guadalupe, J. L. Colón, *Electroanalysis* **2006**, *18*, 559.
- [9] W. J. Blaedel, R. C. Engstrom, *Anal. Chem.* **1980**, *52*, 1691.
- [10] J. Wang, E. Gonzalez-Romero, M. Oszos, *Electroanalysis* **1992**, *4*, 539.
- [11] A. S. Santos, R. S. Freire, L. T. Kubota, *J. Electroanal. Chem.* **2003**, *547*, 135.
- [12] Q. Chi, S. Dong, *Anal. Chim. Acta* **1994**, *285*, 125.
- [13] P. Bianco, *Rev. Mol. Biotech.* **2002**, *82*, 393.
- [14] L. N. Geng, N. Dai, X. F. Wen, F. L. Zhao, K. A. Li, *Colloids Surf. B, Biointerf.* **2003**, *29*, 81.
- [15] T. Zougrana, W. Norde, *Colloids Surf. B, Biointerf.* **1997**, *9*, 157.
- [16] C. V. Kumar, A. Chaudhuri, *J. Am. Chem. Soc.* **2000**, *122*, 830.
- [17] J. Wang, J. Liu, G. Cepra, *Anal. Chem.* **1997**, *69*, 3129.
- [18] A. K. Williams, J. T. Hupp, *J. Am. Chem. Soc.* **1998**, *120*, 4366.
- [19] *Analytical Uses of Immobilized Biological Compounds for Detection, Medical and Industrial Uses* (Eds: G. G. Guibault, M. Mascini), Reidel, Boston **1988**.
- [20] A. Guerrieri, G. E. De Benedetto, F. Palmisano, P. G. Zambonin, *Biosens. Bioelectron.* **1998**, *13*, 103.
- [21] Y. Degani, A. Heller, *J. Phys. Chem.* **1987**, *91*, 1285.
- [22] A. Heller, *J. Phys. Chem.* **1992**, *96*, 3579.
- [23] Y. Degani, A. Heller, *J. Am. Chem. Soc.* **1998**, *110*, 2615.
- [24] J. V. de Melo, S. Cosnier, C. Mousty, C. Martelet, N. Jaffrezic-Renault, *Anal. Chem.* **2002**, *74*, 4037.
- [25] *Protein at Interfaces II: Fundamentals and Applications* (Eds: T. A. Horbett, J. L. Brash), ACS Symposium Series 602, ACS, Washington, DC **1995**.
- [26] S. Park, T. D. Chung, S. K. Kang, R.-A. Jeong, H. Boo, H. N. Kim, *Anal. Sci.* **2004**, *20*, 1635.
- [27] C. V. Kumar, G. L. McLendon, *Chem. Mater.* **1997**, *9*, 863.
- [28] A. Clearfield, G. D. Smith, *Inorg. Chem.* **1969**, *8*, 431.
- [29] J. M. Troup, A. Clearfield, *Inorg. Chem.* **1977**, *16*, 3311.
- [30] C. V. Kumar, A. Bhambhani, N. Hnatiuk, in *Handbook of Layered Materials* (Eds: S. M. Auerback, K. A. Carrado, P. K. Dutta), Marcel Dekker, New York **2004**, pp. 313–372.
- [31] A. A. Martí, J. L. Colón, *Inorg. Chem.* **2003**, *42*, 2830.
- [32] C. A. Goss, H. D. Abruña, *Inorg. Chem.* **1985**, *24*, 4263.
- [33] N. Rivera-Vázquez, *Ph.D. Thesis*, University of Puerto Rico, Río Piedras, PR **2001**.
- [34] M. J. Schrenk, R. E. Villigam, N. J. Torrence, S. J. Brancato, S. D. Minteer, *J. Mem. Sci.* **2002**, *205*, 3.
- [35] T. J. Thomas, K. E. Ponnusamy, N. M. Chang, K. Galmore, S. D. Minteer, *J. Mem. Sci.* **2003**, *213*, 55.
- [36] C. M. Moore, N. L. Akers, A. D. Hill, Z. C. Johnson, S. D. Minteer, *Biomacromolecules* **2004**, *5*, 1241.

- [37] *Worthington Enzyme Manual* (Ed: C. C. Worthington), Worthington Biochemical Corporation, Freehold, NJ **1993**.
- [38] N. L. Akers, C. M. Moore, S. D. Minter, *Electrochim. Acta* **2005**, *50*, 2521.
- [39] B. V. Plapp, B. R. Savarimuthu, S. Ramaswamy, *Asymmetry in a Structure of Yeast Alcohol Dehydrogenase*, to be published, <http://www.rcsb.org/pdb/explore/explore.do?structureId=2HCY>.
- [40] C.-Y. Yang, A. Clearfield, *React. Polym., Ion Exch., Sorbents* **1987**, *5*, 13.
- [41] J. M. Troup, A. Clearfield, *Inorg. Chem.* **1977**, *16*, 3311.
- [42] S. M. Kelly, T. J. Jess, N. C. Price, *Biochim. Biophys. Acta* **2005**, *1751*, 119.
- [43] S. M. Kelly, N. C. Price, *Biochim. Biophys. Acta* **1997**, *1338*, 161.
- [44] W. B. Gratzer, D. A. Cowburn, *Nature* **1969**, *222*, 426.
- [45] L. Gorton, *Electroanalysis* **1995**, *7*, 23.
- [46] L. Rotariu, C. Bala, *Anal. Lett.* **2003**, *36*, 2459.
- [47] A. W. Jones, P. Holmgren, *J. Forensic Sci.* **2003**, *48*, 874.
- [48] M. E. Dennis, *The Chronicle of ADTSEA*, **2002**, *50*, 9.

# NADH Electrooxidation Using Bis(1,10-phenanthroline-5,6-dione) (2,2'-bipyridine)ruthenium(II)-Exchanged Zirconium Phosphate Modified Carbon Paste Electrodes

Mitk'El B. Santiago, Meredith M. Vélez, Solmarie Borrero, Agustín Díaz, Craig A. Casillas, Cristina Hofmann, Ana R. Guadalupe,\* Jorge L. Colón\*

Department of Chemistry, P. O. Box 23346, University of Puerto Rico, Río Piedras, P. R. 00931-3346, USA  
\*e-mail: a\_guadalupe@degi.rpp.upr.edu; jorgecr@caribe.net

Received: October 25, 2005  
Accepted: December 16, 2005

## Abstract

We present a carbon paste electrode (CPE) modified using the electron mediator bis(1,10-phenanthroline-5,6-dione) (2,2'-bipyridine)ruthenium(II) ( $[\text{Ru}(\text{phend})_2\text{bpy}]^{2+}$ ) exchanged into the inorganic layered material zirconium phosphate (ZrP). X-Ray powder diffraction showed that the interlayer distance of ZrP increases upon  $[\text{Ru}(\text{phend})_2\text{bpy}]^{2+}$  intercalation from 10.3 Å to 14.2 Å. The UV-vis and IR spectroscopies results showed the characteristic peaks expected for  $[\text{Ru}(\text{phend})_2\text{bpy}]^{2+}$ . The UV-vis spectrophotometric results indicate that the  $[\text{Ru}(\text{phend})_2\text{bpy}]^{2+}$  concentration inside the ZrP layers increased as a function of the loading level. The exchanged  $[\text{Ru}(\text{phend})_2\text{bpy}]^{2+}$  exhibited luminescence even at low concentration. Modified CPEs were constructed and analyzed using cyclic voltammetry. The intercalated mediator remained electroactive within the layers ( $E^{\text{red}} = -38.5$  mV vs. Ag/AgCl, 3.5 M NaCl) and electrocatalysis of NADH oxidation was observed. The kinetics of the modified CPE shows a Michaelis–Menten behavior. This CPE was used for the oxidation of NADH in the presence of Bakers' yeast alcohol dehydrogenase. A calibration plot for ethanol is presented.

**Keywords:** Zirconium phosphate, Modified carbon paste electrode, Ruthenium complex mediator, NADH electrooxidation

DOI: 10.1002/elan.200503432

## 1. Introduction

Considerable research efforts have been devoted to combine enzyme-catalyzed reactions with electrochemical transducers to produce highly selective and sensitive biosensors [1–9]. These sensors are attractive for several reasons [10–17]: 1) complex organic molecules can be determined with the convenience, speed and ease that characterize amperometric measurements; 2) biocatalysts permit reactions to occur under mild conditions of temperature, pH and minimal substrate concentrations; 3) the sensor response is analyte dependent as dictated by the specificity of most enzyme reactions; and 4) the measured signal is inherently amplified by the enzyme catalytic cycle.

A common type of amperometric biosensors is based on pyridine-nucleotide dependent dehydrogenase enzymes. Many dehydrogenase enzymes use the pyridine nucleotide cofactor, nicotinamide dinucleotide ( $\text{NAD}^+$ ) or nucleotide adenine dinucleotide phosphate ( $\text{NADP}^+$ ) [5, 18]. However, the electrochemical oxidation of NADH (or NADPH) requires a high overvoltage and suffers from side chemical reactions [18, 19]. The use of redox mediators has been demonstrated to substantially overcome these limitations, particularly in dehydrogenase sensors [4, 15, 20]. Ideal mediators should exhibit chemical and electrochemical

reversibility, stability under physiological conditions, a fast electron exchange reaction with the coenzymes, and a suitable redox potential, usually between  $-0.2$  to  $0$  V vs. SCE to avoid interferences in biological determinations [5, 18, 21].

NADH oxidation using electron mediators follows a Michaelis–Menten mechanism [18]. Typical second order rate constants values are below  $10^4 \text{ M}^{-1}\text{s}^{-1}$ ; very few mediators have second order rate constants in the range of  $10^4$  to  $10^6 \text{ M}^{-1}\text{s}^{-1}$  [5]. These values suggest that the electron transfer mechanism is mass transfer controlled. Several mediators have shown large second order rate constants but have required large overpotentials [18]. Many attempts have been done to build more efficient amperometric  $\text{NAD}^+/\text{NADH}$  biosensors that exhibit large second order rate constants, including preparing self-contained sensors [6, 17, 22–26].

To build self-contained sensors, the mediator, the cofactor and the enzyme must be incorporated within the sensor body. Important aspects to consider for the immobilization of these molecules are the preservation of their redox properties, chemical stability and retention within the chosen support. Immobilization methods include adsorption, covalent attachment, polymer entrapment and inclusion of the mediator in the electrode material [22–36].

Adsorption and inclusion are the simplest procedures for mediator immobilization; however, other elaborate procedures have shown better stability [11].

A material that shows promising for the immobilization of biological molecules is the layered  $\alpha$ -zirconium phosphate ( $\text{Zr}(\text{HPO}_4)_2 \cdot \text{H}_2\text{O}$ ,  $\alpha$ -ZrP) [20, 37]. Several authors have demonstrated the use of this material for the construction of NADH biosensors. Mediators previously immobilized in  $\alpha$ -ZrP are phenoxazines, phenothiazines, phenazines, fluorenes and flavines [15, 37–40]. These authors did not use enzymes in their studies nor provided X-ray powder diffraction (XRPD) evidence of the mediator intercalation into the layered material.

Ruan et al. showed that methylene blue-exchanged ZrP could be used for the electroreduction of hydrogen peroxide in the presence of horseradish peroxidase [39]. The authors presented XRPD and IR evidence that the mediator was intercalated between the layers of ZrP, not only exchanged on its surface. The interlayer distance of  $\alpha$ -ZrP increased upon intercalation from 7.6 Å to 16.1 Å, which demonstrates methylene blue incorporation within ZrP. The vibrational bands of  $\alpha$ -ZrP at 3593 and 3508  $\text{cm}^{-1}$  (assigned to the asymmetric and symmetric water stretching modes) disappeared upon methylene blue intercalation. This result indicates that methylene blue intercalation was accompanied by dehydration of  $\alpha$ -ZrP. These authors also observed that the intensity of the  $\text{P}=\text{OH}$  vibrational band at 3155  $\text{cm}^{-1}$  for methylene blue-intercalated ZrP diminished compared to that of unintercalated  $\alpha$ -ZrP [20]. This decrease in intensity occurs because some of the  $\text{H}^+$  in ZrP are exchanged by methylene blue, decreasing the number of protonated phosphate groups.

In our laboratory, we are interested in the immobilization of luminescent polypyridine complexes and other luminescent molecules by direct exchange into the layers of a highly hydrated ZrP material known as the 10.3 Å phase of ZrP for their use in artificial photosynthesis [41]. Tris(2,2'-bipyridine)ruthenium(II) ( $\text{Ru}(\text{bpy})_3^{2+}$ ), *fac*-tricarbonyl-chloro-1,10-phenanthroline-rhenium(I) ( $\text{Re}(\text{phen})(\text{CO})_3\text{Cl}$ ), and 1-aminomethylpyrene have been intercalated into the 10.3 Å phase of ZrP [41, 42]. Our current work involves the direct intercalation of bis(1,10-phenanthroline-5,6-dione)(2,2'-bipyridine) ruthenium(II) ( $[\text{Ru}(\text{phend})_2\text{bpy}]^{2+}$ ) within these layers. This complex is known to be a good redox mediator for the oxidation of NADH [43–45]. We report here the construction of a CPE modified with  $[\text{Ru}(\text{phend})_2\text{bpy}]^{2+}$ -exchanged ZrP (Ru-ZrP) for the mediated oxidation of NADH and the resultant electrode kinetics.

## 2. Experimental

### 2.1. Reagents

Mineral oil, Baker's yeast alcohol dehydrogenase (E. C. 1.1.1.1),  $\beta$ -nicotinamide adenine dinucleotide and  $\beta$ -nicotinamide adenine dinucleotide (reduced form) were obtained from Sigma Chemicals. Graphite powder and copper wire

were obtained from Fisher Co. All other reagents, at least 98% pure, were obtained from Aldrich. Nanopure water was obtained using a Barnstead purification train (17.5  $\text{M}\Omega/\text{cm}$ ). Capillary tubes were obtained from Kimble products.

### 2.2. Procedures

We used a hydrated form of ZrP, which has approximately six water molecules per formula unit and an interlayer distance of 10.3 Å [41, 46]. This material was synthesized as described previously [47]. A volume of 120 mL of 0.05 M  $\text{ZrOCl}_2 \cdot 8\text{H}_2\text{O}$  was mixed with 85 mL of 6 M  $\text{H}_3\text{PO}_4$  with constant stirring at 94 °C for 48 hours. The precipitated solid was filtered and washed three times with nanopure water. The wet precipitate was characterized using XRPD; the first diffraction peak gave the expected interlayer distance of 10.3 Å for this phase of ZrP.  $[\text{Ru}(\text{phend})_2\text{bpy}](\text{PF}_6)_2$  was synthesized as reported in the literature [43, 44] and the expected spectroscopic bands were observed (UV-vis (water)  $\lambda_{\text{max}}$  (nm): 288, 438; IR ( $\text{cm}^{-1}$ ):  $\nu_{\text{CO}} = 1695$ ,  $\nu_{\text{C-C}} = 1424$ ,  $\nu_{\text{CN}} = 1296$ ;  $^1\text{H-NMR}$  ( $\delta/\text{ppm}$ ,  $\text{CD}_3\text{CN}$ , 300 MHz):  $\delta$  8.55 (4 H, d), 8.15 (2 H, t), 8.08 (4 H, d), 8.00 (2 H, d), 7.87 (2 H, d), 7.64 (4 H, t), 7.46 (2 H, t)) HHH. Several suspensions with different solution molar concentration ratios (1:30, 1:20, 1:10, 1:1, and 5:1  $[\text{Ru}(\text{phend})_2\text{bpy}]^{2+}:\text{ZrP}$ ) were prepared from a  $1.0 \times 10^{-3}$  M  $[\text{Ru}(\text{phend})_2\text{bpy}]^{2+}$  aqueous stock solution adding different amounts of ZrP. These suspensions were maintained with constant stirring during five days until the pH stopped dropping. Afterwards, they were filtered, washed with water until a clear supernatant was obtained, and dried in air for four days. The obtained  $[\text{Ru}(\text{phend})_2\text{bpy}]^{2+}$ -intercalated ZrP materials are referred as Ru-ZrP. Elemental analysis was done by QTI Enterprises. The  $[\text{Ru}(\text{phend})_2\text{bpy}]^{2+}$  loading levels in ZrP obtained were: 1:21 (1:30), 1:12 (1:20), 1:10 (1:10), 1:2.3 (1:1), 2.2:1 (5:1), where the first ratio corresponds to the experimental loading level obtained from the elemental analysis of the intercalated materials and the second ratio (in parenthesis) is the  $[\text{Ru}(\text{phend})_2\text{bpy}]^{2+}:\text{ZrP}$  solution molar concentration ratios used in the intercalation experiments. XRPD measurements were performed to determine the interlayer distance after intercalation. Suspensions of the intercalated material in water were used for UV-vis absorption and luminescence measurements. IR spectroscopy was done on dried KBr pellets.

Modified CPEs were prepared mixing thoroughly 15 mg of Ru-Zr, 150 mg of graphite powder and 75  $\mu\text{L}$  of mineral oil to form a uniform paste suitable for molding the CPEs. Capillary tubes (2 mm diameter) were used to construct the modified CPEs. The electrical contact was done with a copper wire.

### 2.3. Instrumentation

UV-vis absorption spectra were obtained using a HP 8453 diode array spectrophotometer. XRPD measurements were

performed using a Siemens D5000 X-ray with Cu K $\alpha$  radiation ( $\lambda = 1.5406 \text{ \AA}$ ) with a filtered flat LiF secondary beam monochromator. The XRPD patterns were run on a  $2\theta$  range of  $1.2\text{--}45^\circ$ . IR spectroscopy measurements were performed using a MAGNA-IR Spectrometer model 750 from Nicolet with a deuterated triglycine sulfate (DTGS) detector, and the spectra were analyzed using OMNIC software, version 4.2. All electrochemical measurements were done with a BAS Model CV-50W potentiostat in a 10 mL cell containing the modified CPE, a Ag/AgCl (3 M NaCl) reference electrode and a Pt wire auxiliary electrode. Most of the electrolyte solutions were prepared using a phosphate buffer solution (PBS,  $\mu = 0.1$ ) at pH 8.0. When analyzing the dependence of the formal potential as a function of pH, PBS solutions with pHs of 4.0, 6.0, 7.0 and 8.0 were used. The electrochemical results were reported as the average of three electrodes. Kinetics studies were performed using a modified carbon paste rotating electrode using a constant sweep rate of 5 mV/s at different frequencies.

#### 2.4. Construction of the Calibration Plot for Ethanol Sensing

The current response of  $[\text{Ru}(\text{phend})_2\text{bpy}]^{2+}$ :ZrP modified CPE was measured using the following procedure. A stock solution of  $\gamma$ -ADH and NAD $^+$  (7.5 U/mL of  $\gamma$ -ADH and 10 mM of NAD $^+$  in PBS) was prepared. Known concentrations of ethanol were added and the current measured after each addition. All measurements were done at steady state.

### 3. Results and Discussion

#### 3.1. Characterization of Ru-ZrP

The elemental analyses results show that the ruthenium complex loading level in Ru-ZrP increases upon increasing the  $[\text{Ru}(\text{phend})_2\text{bpy}]^{2+}$ :ZrP solution molar concentration ratio used in the intercalation experiments. Figure 1 shows XRPD data of Ru-ZrP at several loading levels. The diffractograms show that the ZrP interlayer distance increases from 10.3  $\text{\AA}$  to 14.2  $\text{\AA}$  upon proton exchange with  $[\text{Ru}(\text{phend})_2\text{bpy}]^{2+}$ . This is a first indication that  $[\text{Ru}(\text{phend})_2\text{bpy}]^{2+}$  was intercalated into the ZrP interlayer space. This distance is smaller than that reported by Marti and Col3n for  $[\text{Ru}(\text{bpy})_3]^{2+}$  intercalation into ZrP (15.1  $\text{\AA}$ ) [41]. From the dimensions of  $[\text{Ru}(\text{phend})_2\text{bpy}]^{2+}$  the minimum distance that  $[\text{Ru}(\text{phend})_2\text{bpy}]^{2+}$  ions can separate the ZrP layers is 9.5  $\text{\AA}$ . The thickness of an  $\alpha$ -ZrP type layer is 6.6  $\text{\AA}$  [48, 49]; adding the expansion produced by  $[\text{Ru}(\text{phend})_2\text{bpy}]^{2+}$  ions would give an expected interlayer distance of 16.1  $\text{\AA}$ . There is a difference of 1.9  $\text{\AA}$  between the calculated and observed Ru-ZrP interlayer distance. Aside from the presence of water molecules, a possible explanation for this difference is that while the  $\alpha$ -ZrP is made of nearly perfect planes of Zr atoms having bridging  $\text{O}_3\text{PO}^-$  groups, above and below the Zr plane [46], nothing precludes intercalating molecules to penetrate slightly between the phosphate groups.

The IR and UV-vis spectra of Ru-ZrP (Supplemental Information) show no new bands. The IR bands observed are almost identical to those observed for unintercalated ZrP and for  $[\text{Ru}(\text{phend})_2\text{bpy}]^{2+}$  in solution, except for the

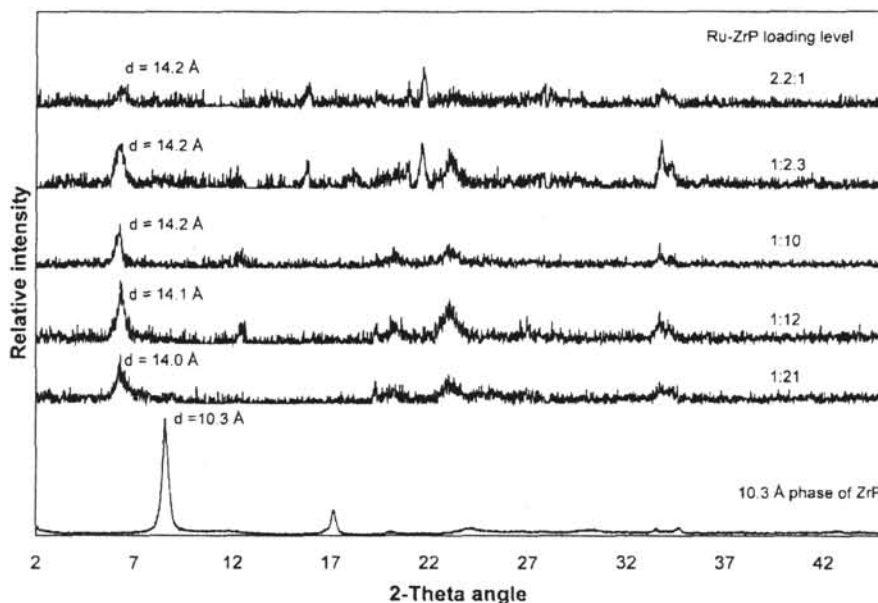


Fig. 1. XRPD patterns of the 10.3  $\text{\AA}$  phase of ZrP and of  $[\text{Ru}(\text{phend})_2\text{bpy}]^{2+}$ -exchanged ZrP materials at various loading levels. The interlayer distance is indicated next to the first order diffraction peak.

"lattice" water band at  $1630\text{ cm}^{-1}$  in unintercalated ZrP [50] which is dramatically reduced in the Ru-ZrP IR spectrum. This reduced intensity is expected since water is displaced in the intercalation process. In addition,  $\pi-\pi^*$  and MLCT bands are observed (at 288 nm and 438 nm, respectively) in the UV-vis spectra, as expected [43, 44], with an intensity proportional to the loading level.

### 3.2. Ru-ZrP Modified CPE

The cyclic voltammetry of Ru-ZrP modified electrodes at a 1:2.3 loading level was evaluated at different scan rates. The voltammograms show the dione/diol redox process indicating that the complex remains electroactive upon intercalation. The formal potential ( $E^0$ ) of  $[\text{Ru}(\text{phend})_2\text{bpy}]^{2+}$  exchanged into ZrP is  $-38.5\text{ mV}$  compared to  $-32.4\text{ mV}$  in buffered solution at pH 8.0 [43]. When compared to other loading levels we observe that the  $E^0$  shifts to more negative potentials as the concentration of  $[\text{Ru}(\text{phend})_2\text{bpy}]^{2+}$  increases inside ZrP (see Table 1). Since the dione/diol redox process is pH dependent, this behavior could be due to differences in the pH within the ZrP layers. ZrP layers are acidic ion exchangers. The intercalation process in ZrP materials is known to occur primarily by ion-exchange when cations from the bulk solution exchange with interlayer protons within the ZrP matrix [41, 51, 52]. When the concentration of  $[\text{Ru}(\text{phend})_2\text{bpy}]^{2+}$  is low, the microenvironment inside the layers is highly acidic. When the concentration of  $[\text{Ru}(\text{phend})_2\text{bpy}]^{2+}$  is high, most of the protons have been exchanged with  $[\text{Ru}(\text{phend})_2\text{bpy}]^{2+}$  and a slightly alkaline environment is expected. It is well known that the  $E^0$  of this complex (quinones in general) becomes more negative as the solution pH increases [43–45].

To determine the number of electrons responsible for the electron transfer process we evaluated the Ru:ZrP formal potential as a function of pH. Figure 2 shows the formal potential at two loading levels of Ru-ZrP; the potential drops as the solution pH increases. This result is different to that observed by Gorton et al. [15, 37, 38, 53]. These authors immobilized indophenol and *o*-quinones derivatives in amorphous ZrP to study their electrocatalytic properties for NADH oxidation. Gorton et al. showed that the organic compounds retained the electrocatalytic behavior upon immobilization. However, with many of the dyes, such as

methylene blue [37, 53], Nile blue [38], brilliant cresyl blue [38], lumichrome [38], toluidine blue [38], riboflavin [38, 53, 54], Meldola's blue [53], and indophenol and *o*-quinones derivatives [15], the formal potential was pH independent, contrary to our results. Gorton et al. attributed the pH-independent formal potential to the effect of having the organic dye bound to ZrP. Our pH-dependent  $E^0$  suggests that the dione functionality does not interact directly with the ZrP layer. The charge on the metal complex (from Ru(II)) is responsible for the electrostatic binding of the complex to ZrP. No binding occurs through the dione ligand. This explanation is further supported by the observation of the electrochemistry of the dione functionality. It is well known that the dione electroactivity is diminished or suppressed by direct interaction with other chemical species such as metal ions and protons [43, 45, 55].

In Figure 2, the slope of the linear plot is  $31.8\text{ mV/pH}$  for the 1:2.3 Ru-ZrP loading level. As reported previously, between pH 2.0 and 4.0 the dione/diol redox process is a  $2e^-$ ,  $3H^+$  process [43]. However, between pH 4.0 thru 7.0 it is a  $2e^-$ ,  $1H^+$  process and from 7.0 to 9.0 it is a  $1e^-$ ,  $1H^+$  process. The slope value of  $31.8\text{ mV/pH}$  shown in Figure 3 is consistent with a  $2e^-$ ,  $1H^+$  process, where the ideal slope should be  $29.5\text{ mV/pH}$ .

Further experiments were done using the 1:2.3 Ru-ZrP loading level ( $\Delta E_p = 62\text{ mV}$  and  $i_{pc}/i_{pa} = 1.18$ ), because at this loading level the intercalated  $[\text{Ru}(\text{phend})_2\text{bpy}]^{2+}$  electrochemical parameters resemble those of the complex in solution. The shape of the cyclic voltammograms suggests that the electron transfer is diffusion controlled. This result was further analyzed by looking at the dependence of the peak current on scan rate. Figure 3 shows that a plot of current as a function of the square root of the scan rate is linear. A slope of 0.6 was obtained from a  $\log i_p$  vs.  $\log v$  plot indicating that the process is mainly diffusion controlled with a small nondiffusional component.

To investigate the origin of the diffusional process, we studied whether leaching was occurring. No leaching of the electroactive species to the electrochemical cell was observed as monitored by UV-vis spectrophotometry (results not shown). We corroborated this result using a glassy carbon electrode to detect if  $[\text{Ru}(\text{phend})_2\text{bpy}]^{2+}$  was present in the buffer solution after withdrawing the modified CPE using Osteryoung square wave voltammetry (OSWV). Leaching of  $[\text{Ru}(\text{phend})_2\text{bpy}]^{2+}$  to the buffered solution was not detected with OSWV before and after 125 cycles between  $-300$  to  $300\text{ mV}$  using cyclic voltammetry (see Supplemental Information). The only signal detected was the oxidation of the phosphate groups around  $0.5\text{ V}$ . No leaching of  $[\text{Ru}(\text{phend})_2\text{bpy}]^{2+}$  was observed, as anticipated since leaching would occur in acidic solutions ( $\text{pH} < 3$ ), but not at the moderate pHs of our experiments ( $\text{pH} 4-8$ ), as has been shown for other mediators in ZrP by Gorton et al. [56].

The binding process of this metal complex to the ZrP matrix is controlled by electrostatic forces. Pessôa et al. suggested that when methylene blue is strongly adhered to ZrP, the mechanism of heterogenous electron transfer is

Table 1. Electrochemical parameters for modified CPEs at different loading levels. Scan rate =  $100\text{ mV/s}$ ,  $\mu = 0.1$  at pH 8.0 in PBS.

Ru:ZrP loading level	$E^0$ (mV)	$\Delta E_p$ (mV)	$i_{pa}/i_{pc}$
2.2:1	-42.5	61.0	1.20
1:2.3	-38.5	62.0	1.18
1:10	-27.5	54.0	0.90
1:12	-22.0	33.0	0.97
1:21	-23.0	28.0	1.05

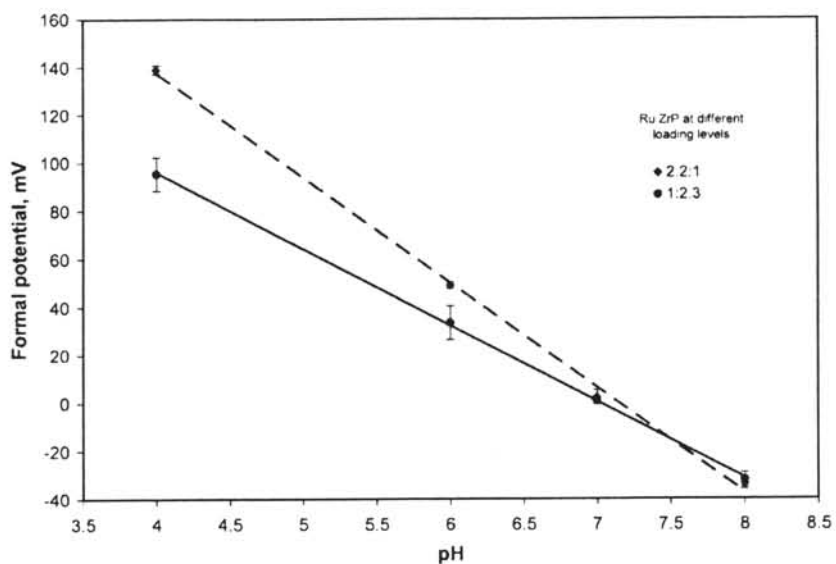


Fig. 2. Formal potential of Ru-ZrP as a function of pH. The measurements were made in PBS,  $\mu = 0.1$  at 100 mV/s.

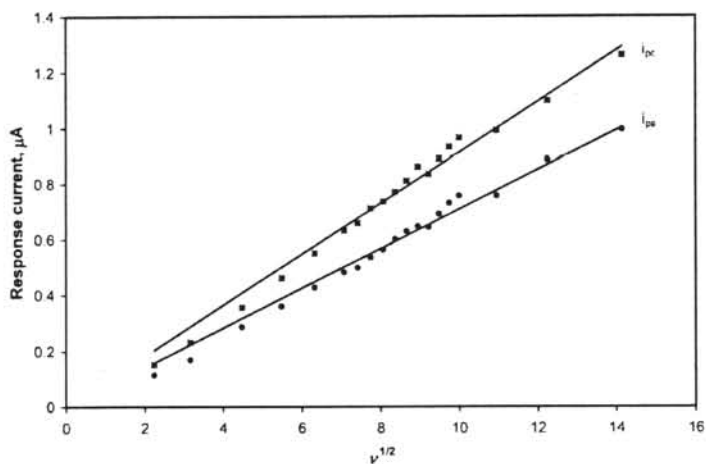


Fig. 3. Randles-Sévcik plot for the modified CPE at different scan rates.

affected by the transport of counter ions to and from the electrode interface to attain charge neutrality [37]. We observed (Supplemental Information) that upon an increase in the electrolyte concentration, the peak separation decreased and the peak current increased, demonstrating that charge transport is assisted by counter ion diffusion.

While counter ion diffusion is important in these materials, it is probable that the redox species in the modified CPE couple electronically through an electron-hopping mechanism. Electron hopping occurs via "electron self-exchange" whereby a reduced redox species simply gives an electron to its oxidized counterpart of the same species [34]. If this mechanism is occurring here a counter ion must come into the film from the contacting electrolyte solution to maintain electroneutrality. This type of mechanism has been pro-

posed for electroactive species covalently bound to a polymer chain or entrapped within zeolites [57–59].

### 3.3. Electrocatalysis of NADH

Guadalupe et al. [43] and Abruña et al. [44] have previously shown that  $[\text{Ru}(\text{phend})_2\text{bpy}]^{2+}$  is a mediator for the electro-oxidation of NADH with and without the presence of lactate dehydrogenase. Figure 4a shows the cyclic voltammetry of Ru-ZrP modified CPE without NADH present. When a known concentration of NADH is added to the electrolytic cell a catalytic current is observed (Figure 4b). As can be observed the onset of the catalytic current began at  $-100$  mV and reached a potential plateau above 50 mV.

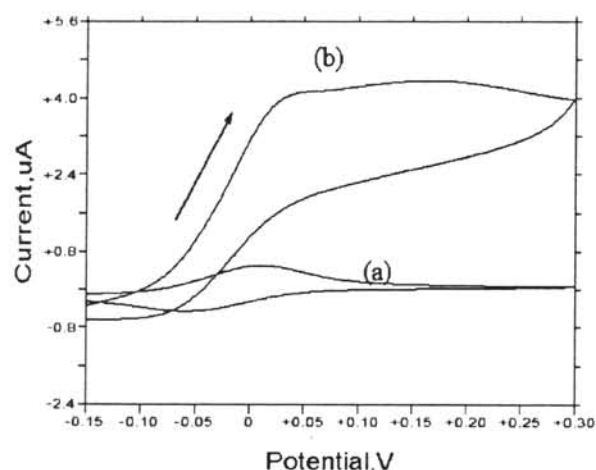


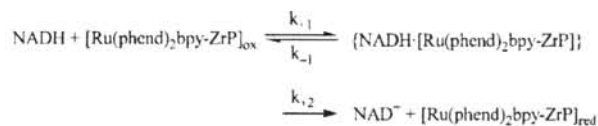
Fig. 4. a) Cyclic voltammogram at 5 mV/s of Ru-ZrP modified CPE (1:2.3 Ru-ZrP loading level) in PBS ( $\mu = 0.1$ , pH 8.0). b) Cyclic voltammogram at 5 mV/s showing electrocatalysis of 0.69 mM NADH using the Ru-ZrP modified CPE (1:1 Ru-ZrP loading level) in PBS ( $\mu = 0.1$ , pH 8.0).



Scheme 1. EC scheme for the reaction between NADH and  $[\text{Ru}(\text{phend})_2\text{bpy}]^{2+}$ -exchanged ZrP.

Also, the anodic peak current increases almost 5 times in the presence of NADH while almost no cathodic current is observed. These observations are consistent with a catalytic EC mechanism as illustrated in Scheme 1.

We prepared carbon paste rotating disk electrodes for the determination of the second order rate constant for the Process 2 in Reaction Scheme 1. To accomplish this process the NADH must reach the electrode surface. The formation of a complex between NADH and the surface is modeled as a Michaelis–Menten-like mechanism. This approach was introduced by Gorton and coworkers but criticized by Lyons [60]. Lyons indicated that this approach is only valid if the current is much less than the mass transport value. The kinetic data was fitted in the linear response range of the catalytic current as a function of NADH concentration. The 1:2.3 Ru-ZrP loading level material shows the highest catalytic current (Supplemental Information Figure S5) and



Scheme 2. Proposed Michaelis–Menten-like mechanism for the electrochemical reaction that occurs in the electrode surface.

therefore we model its behavior in the kinetics studies with a Michaelis–Menten-like mechanism (Scheme 2).

To determine the Michaelis–Menten constant ( $K_M$  in mM) we combine the rate constants to obtain:

$$K_M = \frac{k_{-1} + k_{+2}}{k_{+1}} \quad (1)$$

The second order rate constant ( $k_{\text{obs}}$  in  $\text{M}^{-1}\text{s}^{-1}$ ) can be obtained as a function of  $K_M$ :

$$K_{\text{obs}} = \frac{k_{+2}}{K_M + C_{\text{NADH}}} \quad (2)$$

where  $C_{\text{NADH}}$  is the NADH concentration in  $\text{mol}/\text{cm}^3$ .

Koutecky-Levich has developed an equation where we can determine the reaction rate by studying the reciprocal current as a function of the reciprocal square root of the angular frequency of rotation of the electrode [13–15, 38, 45, 60, 61]:

$$\frac{1}{i_{\text{cat}}} = \frac{1}{nFAk_{\text{obs}}\Gamma C_{\text{NADH}}} + \frac{1}{0.620nFAD_{\text{NADH}}^{2/3}\nu^{-1/2}kC_{\text{NADH}}} \cdot \frac{1}{\omega^{1/2}} \quad (3)$$

where  $\Gamma$  is the surface coverage in  $\text{mol}/\text{cm}^2$ ,  $F$  is the Faraday constant in  $\text{C}/\text{equiv}$ ,  $A$  is the area of the electrode in  $\text{cm}^2$ ,  $D_{\text{NADH}}$  is the NADH diffusion coefficient in  $\text{cm}^2/\text{s}$ ,  $\nu$  is the hydrodynamic viscosity of the medium ( $0.010 \text{ cm}^2/\text{s}$ ) and  $\omega$  is the angular frequency of rotation of the electrode in  $\text{s}^{-1}$ .

If Equation 1 and 2 are substituted in the Koutecky-Levich equation we obtain:

$$\frac{1}{i_{\text{cat}}} = \frac{1}{nFAk_{+2}\Gamma} + \left\{ \frac{K_M}{nFAk_{+2}\Gamma} + \frac{1.61\nu^{1/2}}{nFAD_{\text{NADH}}^{2/3}\omega^{1/2}} \right\} \times \frac{1}{C_{\text{NADH}}} \quad (4)$$

Equation 5 shows that a plot of  $1/i_{\text{cat}}$  vs.  $1/C_{\text{NADH}}$  will give a straight line if the  $[\text{NADH}\text{-(Ru-ZrP)}]$  complex is involved in

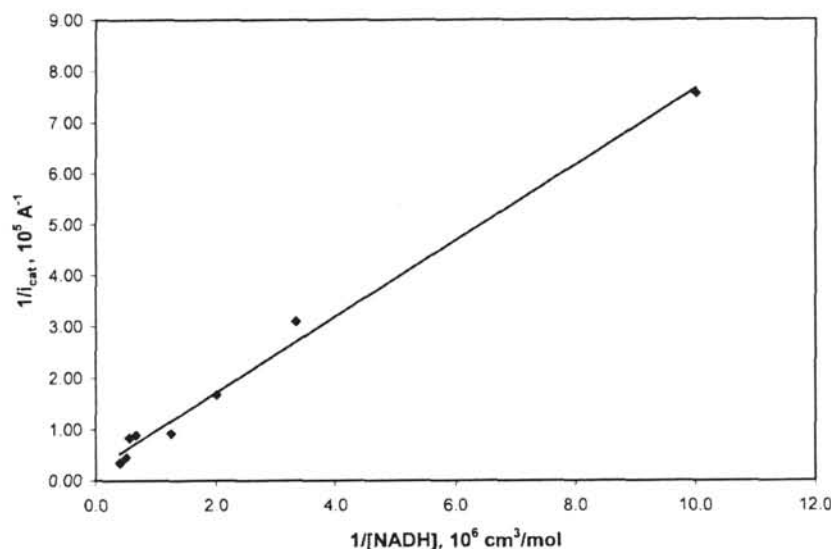


Fig. 5. Variation of  $1/i_{\text{cat}}$  as a function of  $1/[\text{NADH}]$  at pH 8.0 (PBS  $\mu = 0.1$ ,  $rpm = 200$ , scan rate = 5.0 mV/s).

the mechanism. From the intercept  $k_{+2}$  can be evaluated and from the slope  $K_M$ . Figure 5 shows the plot obtained for this mechanism at different NADH concentrations. The  $k_{+2}$  and  $K_M$  values from the intercept and the slope are  $503.3 \text{ s}^{-1}$  and  $1.98 \text{ mM}$ , respectively.

The second order rate constant  $k_{\text{obs}}$ , at different rotation frequencies was evaluated from the intercept using Equation 3. The  $k_{\text{obs}}$  value obtained,  $5.67 \times 10^4 \text{ M}^{-1} \text{ s}^{-1}$ , shows that the electron transfer kinetics is much faster than that of the complex in solution ( $2.0 \times 10^3 \text{ M}^{-1} \text{ s}^{-1}$ ) at the same experimental conditions [43, 45]. The difference in the catalytic activity observed between the dissolved and the immobilized mediator occurs since the immobilized mediators is an integral part of the electrode surface and therefore facilitates electron hopping between mediators inside the zirconium phosphate layers, compared to mediators diffusing in the bulk solution. This result along with the potential shift to positive potentials in the presence of NADH shows that the thermodynamic driving force is enhanced for the immobilized complex. This observation was also observed by Gorton et al. when they studied the immobilization of dyes in amorphous ZrP [4, 5]. These authors obtained higher  $k_{\text{obs}}$  values at pH 6 and pH 7. Table 2 summarizes the electrochemical and kinetic parameters of our modified CPE at different pHs. This table shows an increase in  $k_{\text{obs}}$  with an increase in the formal potential indicating that the thermodynamic driving force is responsible for the charge transfer and not the pH [15]. This result is in concordance with Marcus theory for an heterogeneous electron transfer mechanism [13–15, 22, 23, 25, 43, 53, 61].

These results suggest that a charge transfer (CT) complex is formed on the electrode surface. These findings also demonstrate that immobilizing inorganic complexes into ZrP can improve the kinetic parameters in comparison with the complex in solution.

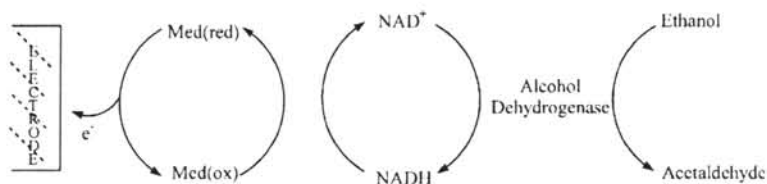
Table 2. Electrochemical and kinetic parameters of the modified CPE for NADH electrooxidation.

1 : 2.3 modified CPE	pH values		
	6	7	8
$E^{0'}$	33	0.83	-38.5
$K_M$ (mM)	3.40	5.27	1.98
$K_{+2}$ ( $\text{s}^{-1}$ )	586.3	1068.37	503.26
$k_{\text{obs}}$ ( $\text{M}^{-1} \text{ s}^{-1}$ )	$1.68 \times 10^5$	$1.24 \times 10^5$	$5.67 \times 10^4$

### 3.4. Calibration Curve for Ethanol Sensing

Having characterized our modified CPE we performed experiments where  $\text{NAD}^+$  and Bakers' yeast alcohol dehydrogenase ( $\gamma$ -ADH) were present in the electrochemical cell. In the absence of ethanol no electrocatalytic current was observed indicating that no NADH has been formed. When ethanol is added to the electrochemical cell, the monoenzymatic reaction cycle presented in Scheme 3 is completed and a catalytic current dependent on ethanol concentration is observed.

The steady state catalytic response of the modified CPE at various ethanol concentrations is shown in Figure 6. A linear range is observed from 10 to 80 mM ethanol concentration after which saturation occurs. The maximum catalytic current is dependent on enzyme and  $\text{NAD}^+$  concentration. Similar behavior was observed previously by Guadalupe et al. [43]. These authors reported that if we consider  $\text{NAD}^+$  as another enzyme substrate, the behavior can be explained as a saturation effect. A saturation effect occurs at  $\text{NAD}^+$  concentrations that are large enough so that  $\text{NAD}^+$  occupies all active sites reaching the maximum velocity at those conditions. This behavior is expected for a Michaelis–Menten-like mechanism. The saturation effect on ampero-



Scheme 3. A monoenzymatic reaction cycle for ethanol sensing.

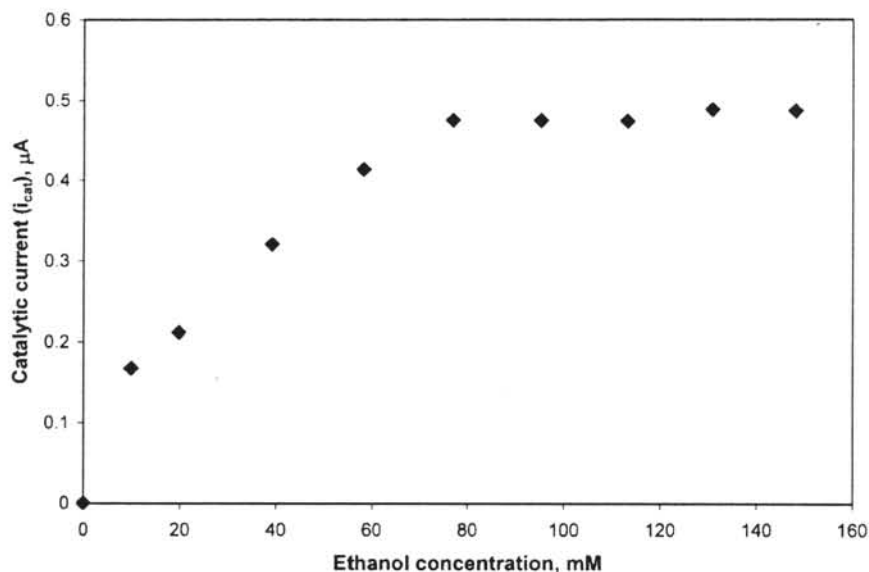


Fig. 6. Calibration plot for ethanol sensing using  $[\text{Ru}(\text{phend})_2\text{bpy}]^{2+}$ -exchanged ZrP modified CPE in the presence of 7.5 U/mL  $\gamma$ -ADH and 10 mM of  $\text{NAD}^+$  in PBS ( $\mu = 0.1$ ), at pH 8.0, 1 mV/s.

metric sensors has been observed previously in a wide range of sensors such as those for glucose [43], cholesterol [59], lactate [62].

#### 4. Conclusion

We have intercalated  $[\text{Ru}(\text{phend})_2\text{bpy}]^{2+}$  into the layers of ZrP increasing the interlayer distance from 10.3 Å in ZrP to 14.2 Å in Ru-ZrP. Ru-ZrP shows the spectral characteristics of intercalated complexes as shown by the UV-vis, luminescence and IR spectroscopic results. We have proven that  $[\text{Ru}(\text{phend})_2\text{bpy}]^{2+}$  remains electroactive within ZrP/CPE composites. The charge transfer process in the modified CPE is dependent on the electrolyte concentration. In addition, we observed that the formal potential of the electrode remains pH dependent, indicating that the dione ligand is not directly interacting with the ZrP matrix. We are currently evaluating the use of these modified CPEs in ethanol biosensors.

#### 5. Acknowledgements

We thank Dr. Antonio Martínez and the staff of UPR's Material Characterization Center for their help with the XRPD and IR spectroscopy measurements. The authors want to acknowledge Angel Martí for the molecular modeling analysis of  $[\text{Ru}(\text{phend})_2\text{bpy}]^{2+}$ . This work was supported by the NIH-RISE (grant R25GM061151), NIH-SCORE (grant 5S06GM08102), and PR-AGEP (NSF grant HRD-0302696) programs.

#### 6. Appendix: Supporting Information

IR and UV-vis spectra of the intercalated material are presented. Cyclic voltammograms of the Ru-ZrP modified CPE at various scan rates and at different ionic strengths in PBS. Successive cyclic voltammograms of the Ru-ZrP modified CPE at 1:2.3 loading level and OSWV of the buffer solution before and after these successive voltammograms.

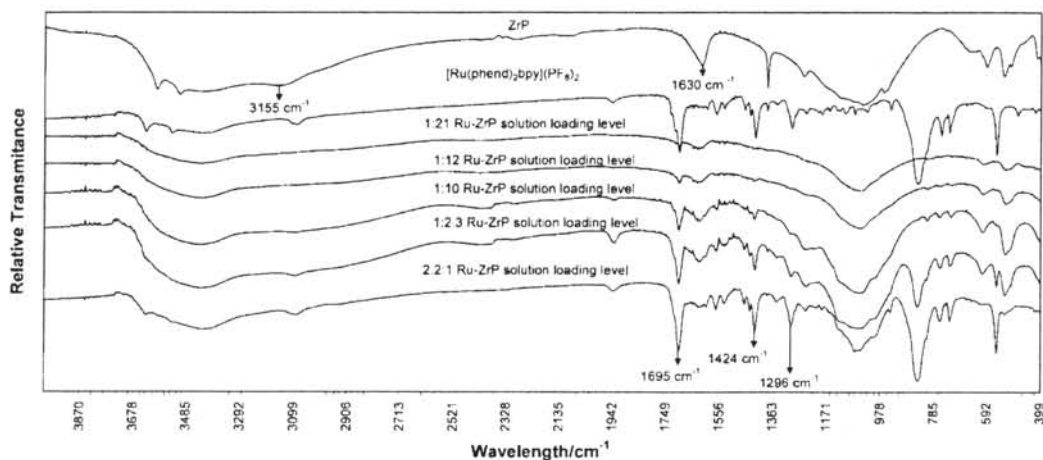


Fig. S1. IR spectra of ZrP,  $[\text{Ru}(\text{phen})_2\text{bpy}](\text{PF}_6)_2$  and Ru-ZrP materials at various solution loading levels.

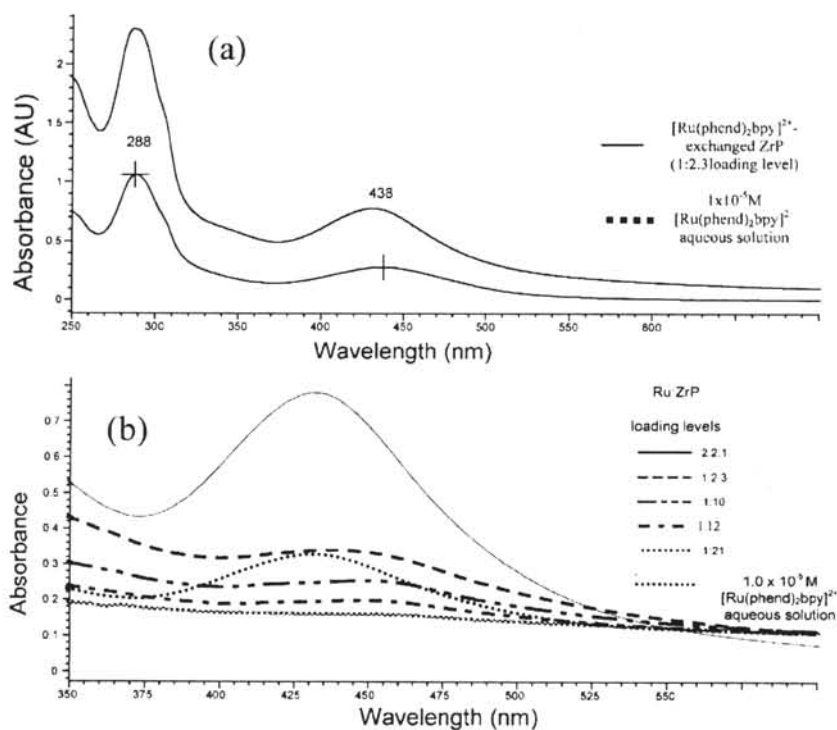


Fig. S2. a) UV-vis absorption spectra for a  $1.0 \times 10^{-5} \text{ M}$   $[\text{Ru}(\text{phen})_2\text{bpy}]^{2+}$  aqueous solution and a suspension of Ru-ZrP at a 1:1 loading level. b) UV-vis absorption spectra showing the MLCT band region for a  $1.0 \times 10^{-5} \text{ M}$   $[\text{Ru}(\text{phen})_2\text{bpy}]^{2+}$  aqueous solution and Ru-ZrP at different loading levels.

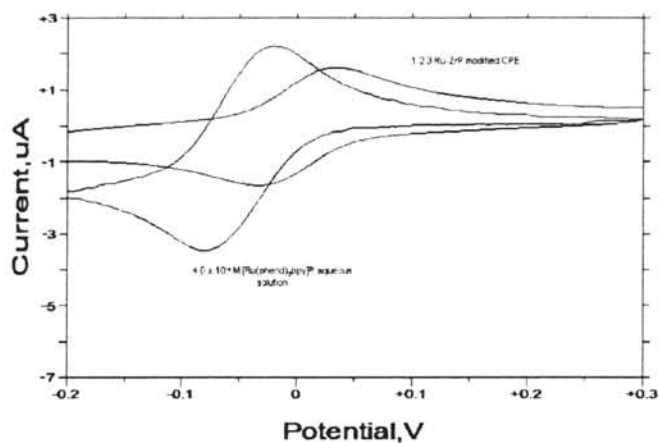


Fig. S3. Cyclic voltammograms of the 1:2.3 Ru-ZrP modified CPE and for the  $4.0 \times 10^{-4}$  M  $[\text{Ru}(\text{phend})_2\text{bpy}]^{2+}$  aqueous solution in a PBS ( $\mu = 0.1$ , pH 8.0), scan rate = 5 mV/s.

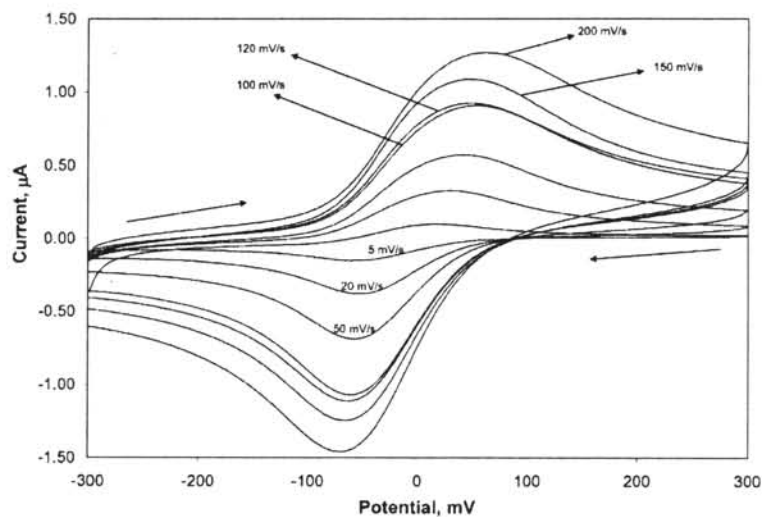


Fig. S4. Cyclic voltammograms of  $[\text{Ru}(\text{phend})_2\text{bpy}]^{2+}$ -exchanged ZrP modified CPE at a 1:2.3  $[\text{Ru}(\text{phend})_2\text{bpy}]^{2+}$ :ZrP loading level in PBS ( $\mu = 0.1$ , pH 8.0) at different scan rates.

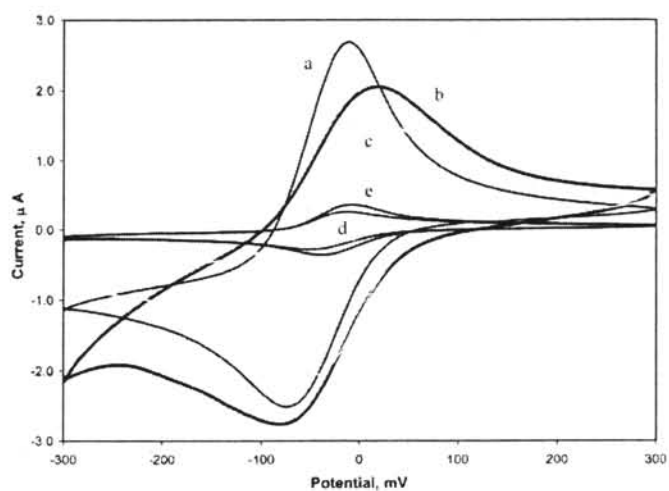


Fig. S5. Cyclic voltammograms of  $[\text{Ru}(\text{phend})_2\text{bpy}]^{2+}$ -exchanged ZrP modified CPE for the different materials in PBS,  $\mu = 0.1$  at pH 8.0. a) 2.2:1, b) 1:2.3, c) 1:2.3, d) 1:2.3, e) 1:2.3,

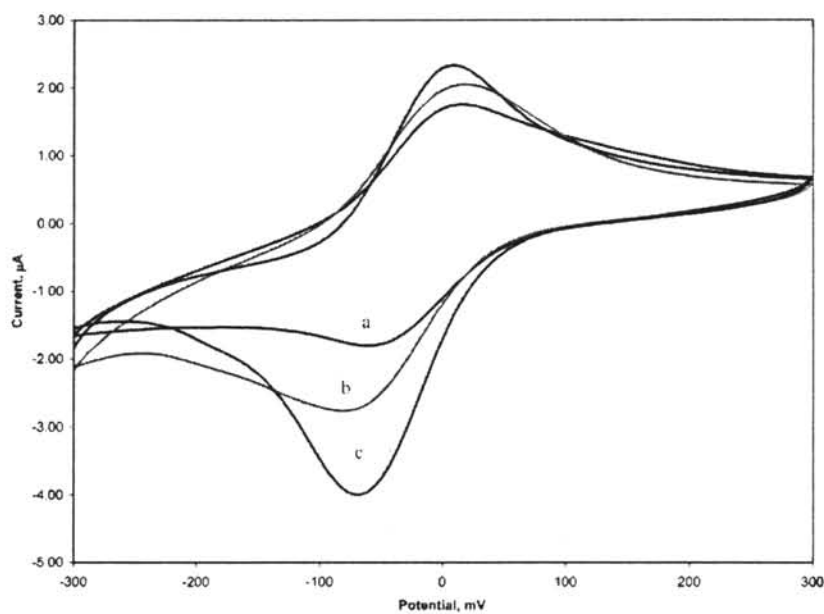


Fig. S6. Dependence of the peak current of  $[\text{Ru}(\text{phend})_2\text{bpy}]^{2+}$ -exchange ZrP (1:2.3 Ru-ZrP loading level) as a function of the ionic strength of the phosphate buffer solution at pH 8.0, scan rate = 50 mV/s. a)  $\mu = 0.05$ , b)  $\mu = 0.1$ , c)  $\mu = 0.3$ .

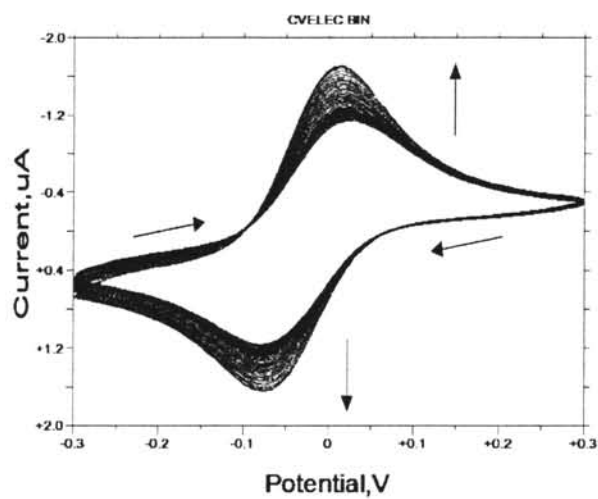


Fig. S7. Successive cyclic voltammograms of the 1:2.3 Ru-ZrP in PBS at pH 8.0, scan rate 100 mV/s, 150 cycles.

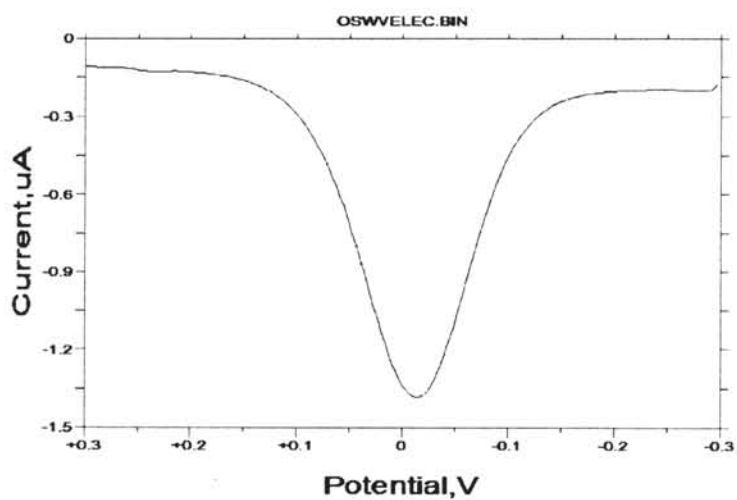


Fig. S8. OSWV of 1:2.3 Ru-ZrP modified CPE in PBS at pH 8.0 (potential peak = -20 mV).

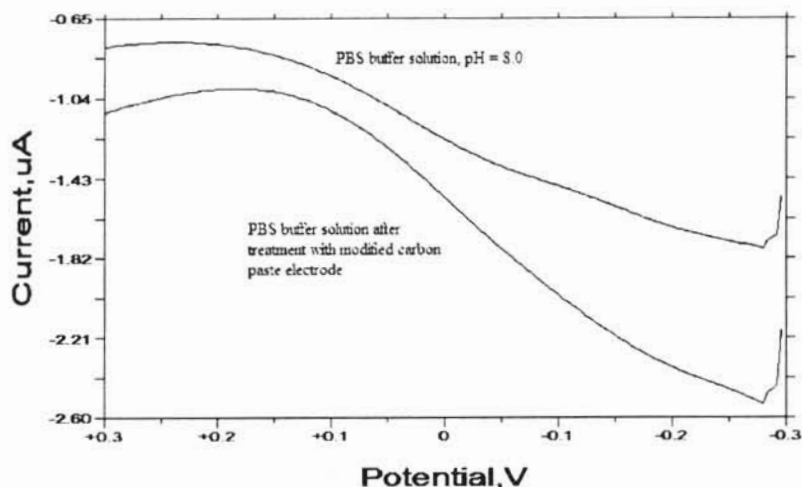


Fig. S9. OSWV of the buffer solution before and after the experiment that appears in Figure S2 using a glassy carbon electrode. The presence of leaching was not detectable in these conditions.

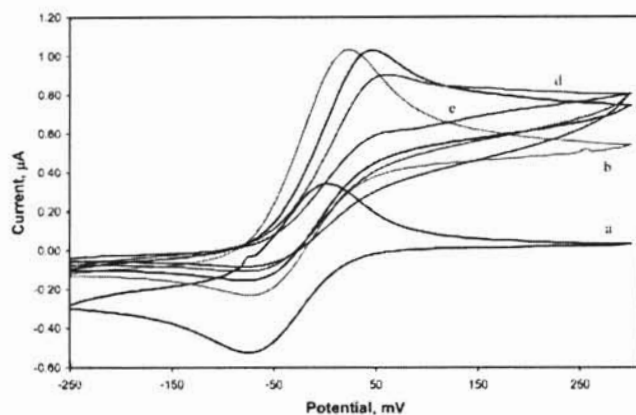


Fig. S10. Cyclic voltammograms of  $[\text{Ru}(\text{phen})_2\text{bpy}]^{2+}$ -exchanged ZrP modified CPE in the presence of 10 mM  $\text{NAD}^+$  and  $\gamma$ -ADH 45.1 U/mL at various ethanol concentrations (a: 0 mM, b: 19.8 mM, c: 58.25 mM, d: 76.9 mM, e: 113.2 mM) in PBS ( $\mu = 0.1$ , pH 8.0), 5 mV/s scan rate.

## 7. References

- [1] R. Wolfenden, M. J. Snyder, *Acc. Chem. Res.* **2001**, *34*, 938.
- [2] M. S. Alacjos, F. J. García Montelongo, *Chem. Rev.* **2004**, *104*, 3239.
- [3] G. S. Wilson, Y. Hu, *Chem. Rev.* **2000**, *100*, 2693.
- [4] L. Gorton, E. Domínguez, *Rev. Mol. Biotech.* **2002**, *82*, 371.
- [5] L. Gorton, E. Domínguez, in *Encyclopedia of Electrochemistry*, Vol. 9 (Eds: A. J. Bard, M. Stratmann, G. S. Wilson), Wiley-VCH, GmbH, Weinheim, Germany, **2002**, p. 67.
- [6] I. Willner, E. Katz, B. Willner, *Electroanalysis* **1997**, *9*, 965.
- [7] I. Willner, E. Katz, B. Willner, in *Sensor Updates*, Vol. 5 (Eds: H. Baltes, W. Göpel, J. Hesse), Wiley-VCH, Weinheim, Germany, **1999**, p. 45.
- [8] I. Willner, E. Katz, B. Willner, in *Biosensors and Their Applications* (Eds: V. C. Yang, T. T. Ngo), Kluwer, New York **2000**, p. 47.
- [9] I. Willner, E. Katz, *Angew. Chem. Int. Ed.* **2000**, *39*, 1180.
- [10] D. R. Thévenot, K. Toth, R. A. Durst, G. S. Wilson, *Biosens. Bioelectron.* **2001**, *16*, 121.
- [11] C. M. A. Brett, A. M. Oliveira-Brett, *Electrochemistry Principles, Methods and Applications*, Oxford University Press, New York **2002**.
- [12] S. Zhang, G. Wright, Y. Yang, *Biosens. Bioelectron.* **2000**, *15*, 273.
- [13] V. Laurinavicius, B. Kurtinaitiene, Boguslavsky, L. Geng, T. Skotheim, *Anal. Chim. Acta* **1996**, *330*, 159.
- [14] S. García Mullor, M. Sánchez-Cabezudo, A. J. Miranda Ordieres, B. López Ruiz, *Talanta* **1996**, *43*, 779.
- [15] D. Dicu, F. D. Munteanu, I. C. Popescu, L. Gorton, *Anal. Lett.* **2003**, *36*, 1755.
- [16] T. Gennett, W. C. Purdy, *Am. Lab.* **1991**, *23*, 60.
- [17] S. E. Creager, K. G. Olsen, *Anal. Chim. Acta* **1995**, *307*, 277.
- [18] M. J. Lobo, A. J. Miranda, P. Tuñón, *Electroanalysis* **1997**, *9*, 191.
- [19] J. Moiroux, P. J. Elving, *J. Am. Chem. Soc.* **1980**, *102*, 6533.

- [20] L. Gorton, *J. Chem. Soc., Faraday Trans.* **1986**, *1*, 1245.
- [21] A. Vasilescu, T. Noger, S. Andreescu, C. Calas-Blanchard, C. Bala, J. L. Marty, *Talanta* **2003**, *59*, 751.
- [22] F. A. Armstrong, H. A. Heering, J. Hirst, *Chem. Soc. Rev.* **1997**, *26*, 169.
- [23] F. A. Armstrong, G. S. Wilson, *Electrochim. Acta* **2000**, *45*, 2623.
- [24] J. D. Burgess, F. M. Hawkrige, in *Electroanalytical Methods for Biological Material* (Eds: A. Brajter-Toth, J. Q. Chambers), Marcel Dekker, New York **2002**, p. 107.
- [25] F. A. Armstrong, *J. Chem. Soc. Dalton Trans.* **2002**, 661.
- [26] D. H. Murgida, P. Hildebrandt, *Acc. Chem. Res.* **2004**, *37*, 854.
- [27] L. Goldstein, in *Methods in Enzymology* (Ed: K. Mosbach), Academic, New York **1976**, p. 397.
- [28] R. W. Murray, in *Electroanalytical Chemistry* (Ed: A. J. Bard), Marcel Dekker, New York **1984**, p. 191.
- [29] J. L. Brash, T. A. Horbett, (Ed: A. S. Series), American Chemical Society, Washington, DC **1987**.
- [30] P. N. Bartlett, in *Biosensors: Fundamental and Applications*, (Eds: A. P. F. Turner, I. Karube, G. S. Wilson), Oxford Science Publications, Oxford, **1987**, p. 211.
- [31] C. P. Andrieux, J. M. Saveant, in *Molecular Design of Electrode Surfaces* (Ed: R. W. Murray), Wiley, New York, **1992**, p. 207.
- [32] L. Gorton, G. Marko-Varga, E. Domínguez, J. Emnéus, in *Analytical Applications of Immobilized Enzyme Reactors* (Eds: S. Lam, G. Malikin), Blackie Academic & Professional, New York, **1994**, p. 1.
- [33] T. A. Horbett, J. L. Brash, (Ed: A. S. Series), American Chemical Society, Washington, DC **1995**.
- [34] C. R. Martin, C. A. J. Foss, in *Laboratory Techniques in Electroanalytical Chemistry* (Eds: P. T. Kissinger, W. R. Heineman), Marcel Dekker, New York **1996**, p. 403.
- [35] G. F. Bickerstaff, in *Methods in Biotechnology, Immobilization of Enzymes and Cells*, Vol. 1 (Ed: G. F. Bickerstaff), Humana, New Jersey **1997**, p. 1.
- [36] V. Erokhin, in *Protein Architecture: Interfacing Molecular Assemblies and Immobilization Biotechnology* (Eds: Y. Lyov, H. Mohwald), Marcel Dekker, New York **1999**, p. 99.
- [37] C. A. Pessoa, Y. Gushikem, L. T. Kubota, L. Gorton, *J. Electroanal. Chem.* **1997**, *431*, 23.
- [38] L. T. Kubota, L. Gorton, *Electroanalysis* **1999**, *11*, 719.
- [39] C. Ruan, F. Yang, J. Xu, C. Lei, J. Deng, *Electroanalysis* **1997**, *9*, 1180.
- [40] F. D. Munteanu, N. Mano, A. Kuhn, L. Gorton, *J. Electroanal. Chem.* **2004**, *564*, 167.
- [41] A. A. Martí, J. L. Colón, *Inorg. Chem.* **2003**, *42*, 2830.
- [42] R. A. Bermúdez, Y. Colón, G. Tejada, J. L. Colón, *Langmuir* **2005**, *21*, 890.
- [43] N. Rivera, Y. Colón, A. R. Guadalupe, *Bioelectrochem. Bioenerg.* **1994**, *34*, 169.
- [44] C. A. Goss, H. D. Abruña, *Inorg. Chem.* **1985**, *24*, 4263.
- [45] N. Rivera-Vázquez, *Ph. D. Thesis*, University of Puerto Rico (Río Piedras, Puerto Rico), **2001**.
- [46] G. Alberti, U. Constantino, J. S. Gill, *J. Inorg. Nucl. Chem.* **1976**, *36*, 1733.
- [47] G. Villemure, C. Detellier, A. G. Szabo, *J. Am. Chem. Soc.* **1986**, *108*, 4658.
- [48] C.-Y. Yang, A. Clearfield, *React. Polym., Ion Exch., Sorbents* **1987**, *5*, 13.
- [49] J. M. Troup, A. Clearfield, *Inorg. Chem.* **1977**, *16*, 3311.
- [50] S. E. Horsley, D. V. Nowell, D. T. Stewart, *Spectrochim. Acta* **1974**, *30 A*, 535.
- [51] A. Clearfield, J. M. Kalnins, *J. Inorg. Nucl. Chem.* **1976**, *38*, 849.
- [52] A. Clearfield, *Chem. Rev.* **1988**, *88*, 125.
- [53] F. D. Munteanu, L. T. Kubota, L. Gorton, *J. Electroanal. Chem.* **2001**, *509*, 2.
- [54] A. Malinauskas, T. Ruzgas, L. Gorton, *Bioelectrochem. Bioenerg.* **1999**, *49*, 21.
- [55] E. Katz, T. Lötzbeyer, D. D. Schlereth, W. Schuhmann, H. L. Shimidt, *J. Electroanal. Chem.* **1994**, *373*, 189.
- [56] F. D. Munteanu, M. Mosbach, A. Schulte, W. Schuhmann, L. Gorton, *Electroanalysis* **2002**, *14*, 1479.
- [57] B. R. Shaw, K. E. Creasy, C. J. Lanczycki, J. A. Saegent, M. Tirhado, *J. Electrochem. Soc.* **1988**, *135*, 869.
- [58] M. D. Baker, C. Senaratne, in *Electrochemistry of Novel Materials* (Ed: J. Lipkowski), VCH, New York **1994**, p. 339.
- [59] A. Walcarius, *Anal. Chim. Acta* **1999**, *384*, 1.
- [60] M. E. G. Lyons, *Sensors* **2002**, *2*, 473.
- [61] G. Hilt, T. Harbarwi, W. R. Heineman, E. Steckham, *Chem. Eur. J.* **1997**, *3*, 79.
- [62] M. J. Green, H. A. O. Hill, *J. Chem. Soc. Faraday Trans.* **1986**, *82*.

# Patentes



US006231920B1

(12) **United States Patent**  
Guadalupe et al.(10) **Patent No.:** US 6,231,920 B1  
(45) **Date of Patent:** May 15, 2001(54) **ELECTROANALYTICAL APPLICATIONS OF  
SCREEN-PRINTABLE  
SURFACTANT-INDUCED SOL-GEL  
GRAPHITE COMPOSITES**

- (75) Inventors:
- Ana R. Guadalupe; Yizhu Guo**
- , both
- 
- of San Juan, PR (US)
- 
- (73) Assignee:
- University of Puerto Rico**
- , San Juan,
- 
- PR (US)
- 
- (\* ) Notice: Subject to any disclaimer, the term of this
- 
- patent is extended or adjusted under 35
- 
- U.S.C. 154(b) by 0 days.

(21) Appl. No.: **09/181,875**(22) Filed: **Oct. 29, 1998****Related U.S. Application Data**

- (60) Provisional application No. 60/063,160, filed on Oct. 29,
- 
- 1997.
- 
- (51)
- Int. Cl.**
- <sup>7</sup>
- .....
- B05D 1/32**
- 
- (52)
- U.S. Cl.**
- .....
- 427/122; 427/282; 427/287**
- 
- (58)
- Field of Search**
- .....
- 427/2.11, 58, 122,**
- 
- 427/282, 287; 204/403, 294; 600/372; 252/510,**
- 
- 511**

(56) **References Cited****U.S. PATENT DOCUMENTS**

4,229,490	10/1980	Frank et al. .
5,160,418	* 11/1992	Mullen .
5,403,462	4/1995	Lev et al. .
5,494,562	* 2/1996	Maley et al. .
5,529,676	6/1996	Maley et al. .
5,573,647	11/1996	Maley et al. .
5,582,698	12/1996	Flaherty et al. .
5,601,694	2/1997	Maley et al. .
5,616,222	4/1997	Maley et al. .
5,711,868	1/1998	Maley et al. .
5,770,028	6/1998	Maley et al. .

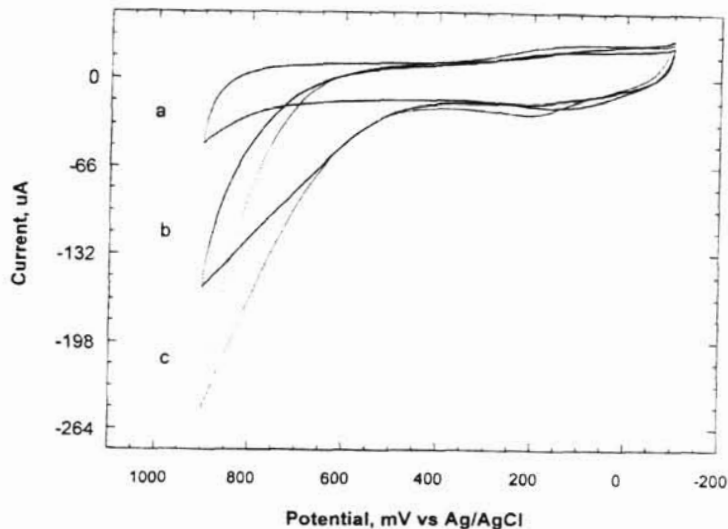
**OTHER PUBLICATIONS**

Kalcher, K.; Kaufmann, J. M.; Wang, J.; Vytras, K.; Neuhold, C.; Yang, Z. *Electroanalysis* 1995, 7, No. 1, pp. 5-22.  
Bilitewski, U.; Ruger, P.; Schmid, R. D., *Biosens. & Bioelectron.* 1991, 6, pp. 369-373.  
Ikegami, A.; Arima, H.; Iwanaga, S.; Kaneyasu, M., *Proceedings of the 4th European Hybrid Microelectronic Conference*, Copenhagen, May 18-20, 1983, pp. 211-218.  
Alvarez-Icaza, M.; Bilitewski, U., *Anal. Chem.* Jun. 1993, vol. 65, No. 11, pp. 525A-533A.  
Kalcher, K., *Electroanalysis* 1990, 2, pp. 419-433.  
Tsionsky, M.; Lev, O., *Anal. Chem.* 1995, 67, pp. 2409-2414.  
Tsionsky, M.; Gun, G.; Glezer, V.; Lev, O. *Anal. Chem.* 1994, 66, pp. 1747-1753.  
Sampath, S.; Lev, O. *Anal. Chem.* 1996, 68, pp. 2015-2021.  
Iosefzon-Kuyavskaya, B.; Gigozin, I.; Ottolenghi, M.; Avnir, D.; Lev, O., *J.Non-Cryst. Solids* 1992, 147 & 148, pp. 808-812 (North Holland).

(List continued on next page.)

*Primary Examiner*—Fred J. Parker(74) *Attorney, Agent, or Firm*—Patent Law Office of Heath W. Hoglund(57) **ABSTRACT**

A process for preparing sol-gel graphite composite electrodes is presented. This process preferably uses the surfactant bis(2-ethylhexyl) sulfosuccinate (AOT) and eliminates the need for a cosolvent, an acidic catalyst, a cellulose binder and a thermal curing step from prior art processes. Fabrication of screen-printed electrodes by this process provides a simple approach for electroanalytical applications in aqueous and nonaqueous solvents. Examples of applications for such composite electrodes produced from this process include biochemical sensors such as disposable, single-use glucose sensors and ligand modified composite sensors for metal ion sensitive sensors.

**8 Claims, 10 Drawing Sheets**

10 AUG 16 P 1:15

RECIBIDO  
SERVICIO ACADÉMICO  
RECINTO 900 PIEDRAS UPR

## OTHER PUBLICATIONS

- Dunuwila, D.C.; Torgerson, B.A.; Chang, C.K.; Berglund, K.A., *Anal. Chem.* 1994, 66, pp. 2739-2744.
- Dunbar, R.A.; Jordan, J.D.; Bright, F.V. *Anal. Chem.* 1996, 68, pp. 604-610.
- Petit-Dominguez, M.D.; Shen, H.; Heineman, W.R.; Seliska, C.J., *Anal. Chem.* 1997, 69, pp. 703-710.
- Wang, J.; Pamidi, P.V.A.; Park, D.S., *Anal. Chem.* 1996, 68, pp. 2705-2708.
- Avnir, D., *Acc. Chem. Res.* 1995, 28, pp. 328-334.
- Avnir, D.; Braun S.; Lev, O.; Ottolenghi, M., *Chem. Mater* 1994, 6, pp. 1605-1614.
- Zink, J. I.; Yamanaka, S. A.; Ellerby, L. M.; Valontine, J. S.; Nishida, F.; Dunn, B. J., *Sol-Gel Sci. Technol.* 1994, 2, pp. 791-795.
- Hench, L. L.; West, J. K., *Chem. Rev.* 1990, 90, pp. 33-72.
- Brinker, C. J.; Hurd, A. J.; Schunk, P. R.; Frye, G. C.; Ashley, C. S., *J. Non-Cryst. Solids* 1992, 147 & 148, pp. 424-436.
- Cardosi, M.F.; Birch, S.W., *Anal. Chim. Acta* 1993, 276, pp. 69-74.
- Avnir, D.; Kaufman, V. R.; Feisfeld, R., *J. Non-Cryst. Solids* 1985, 74, pp. 395-406.
- Green, M.I.; Hilditch, P.I., *Anal. Proc.* 1991, 28, pp. 374-376.
- Turner, A.D.F., *Anal. Proc.*, 1991, 28, pp. 376-377.
- Adams, R.N., *Anal. Chem. Sep.* 1958, 30, p. 1576.
- Gorton, L., *Electroanalysis* 1995, 7, No. 1, pp. 23-45.
- Creasy, K.E.; Shaw, B.R., *Anal. Chem.* 1989, 61, pp. 1460-1465.
- Wang, J.; Golden, T.; Varughese, K. El-Reyes, I., *Anal. Chem.* 1981, 61, pp. 508-512.
- Wang, J.; Varughese, K., *Anal. Chem.* 1990, 62, pp. 318-320.
- Shaw, B.R.; Creasy, K.E., *Anal. Chem.* 1988, 60, pp. 1241-1244.
- Alegret, S.; Cespedes, F.; Martinez-Fabregas, E.; Martorell, D.; Morales, A.; Centelles, E.; Munoz, J., *Boisens. & Bioelectron.*, 1996, 11, pp. 35-44.
- Alegret, S., *Analyst* 1996, 121, pp. 1751-1758.
- Wring, S.A.; Hart, J.P.; Birch, B.J., *Analyst* 1989, 114, pp. 1563-1570.
- Wring, S.A.; Hart, J.P.; Birch, B.J., *Electroanalysis* 1992, 4, p.299-309.
- Wring, S.A.; Hart, J.P.; Birch, B.J. *Analyst*, Feb. 1991, 116, pp. 123-129.
- Baldwin, R.; Christensen, J.; Kryger, L., *Anal. Chem.* 1986, 58, pp.1790-1798.
- Brinker, C.J.; Scherer, G.W., *Sol Gel Science*, Academic Press, San Diego, 1990, pp.vii-x.
- Kasem, K.K.; Abruna, H.D. *J. Electroanal. Chem.* 1988, 242, pp. 87-96.
- Gao, Z.; Wang, G.; Li, P.; Zhao, Z., *Anal. Chem.* 1991, 63, pp. 953-957.
- Guadalupe, A.R.; Abruna, H.D., *Anal. Chem.* 1985, 57, pp. 142-149.
- Wier, L.M.; Guadalupe, A.R.; Abruna, H.D., *Anal. Chem.* 1985, 57, 2009-2011.
- Neuhold, C.; Wang, J.; Cai, X.; Kalcher, K., *Analyst* 1995, 120, pp. 2377-2380.
- Nehould, C.; Wang, J.; Nascimento, V.; Kalcher, K., *Talanta*, 1995, 42, pp. 1791-1798.
- Wang, J.; Nascimento, V.B.; Lu, J.; Park, D.S. Angnes, L., *Electroanalysis* 1996, 8, No. 7, pp. 635-638.
- Prabhu, S.V.; Baldwin, R.P., *Anal. Chem.* 1987, 59, pp. 1074-1078.
- Rohm, I.; Kunnecke, W.; Bilitewski, U. *Anal. Chem.* 1995, 67, pp. 2304-2307.
- Guo, Yizhu, Guadalupe, Ana R., *Sensors and Actuators B* 46 (1998) pp. 213-219.
- P. V.A. Pamidi, "Structurally and Chemically Modified Sol-Gel Carbon Thick Film Glucose Sensors", *Polymeric Materials Science and Engineering*, Spring Meeting, Apr. 1997, vol. 76, Apr. 1997, pp. 513-514.
- J. Gun, "Sol-Gel Derived Ferrocenyl-Modified Silicate-Graphite Composite Electrode: Wiring of Glucose Oxidase", *Analytica Chimica ACTA*, vol. 336, No. 1-3, 1996, pp. 95-106.

\* cited by examiner

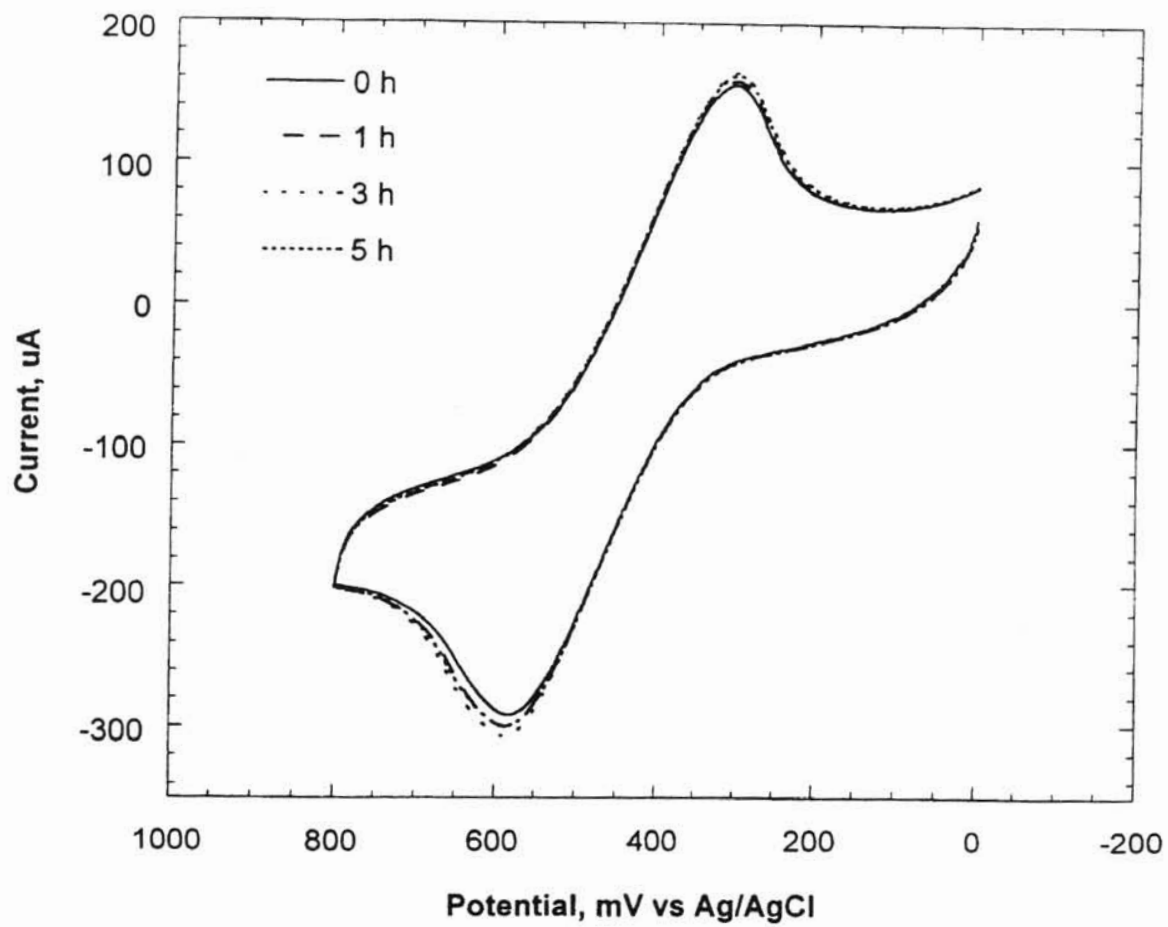


FIG. 1

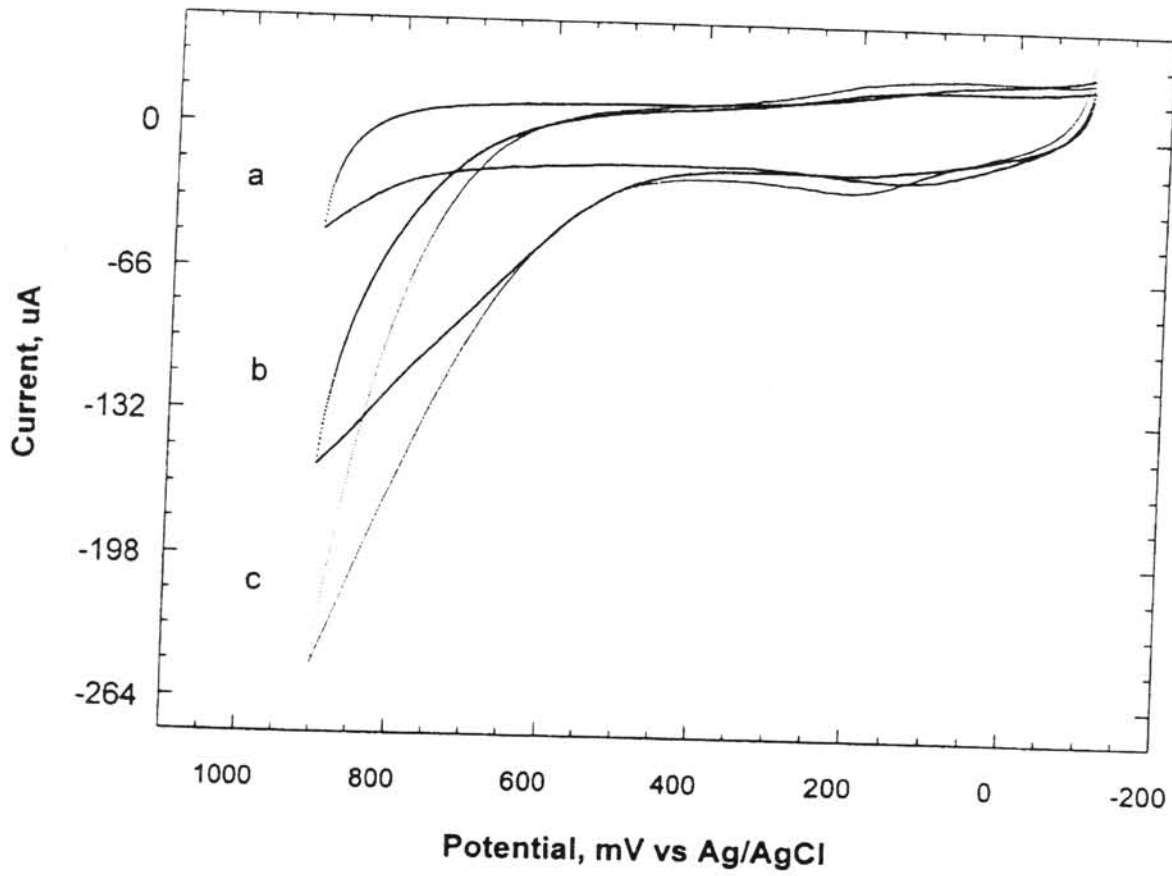


FIG. 2

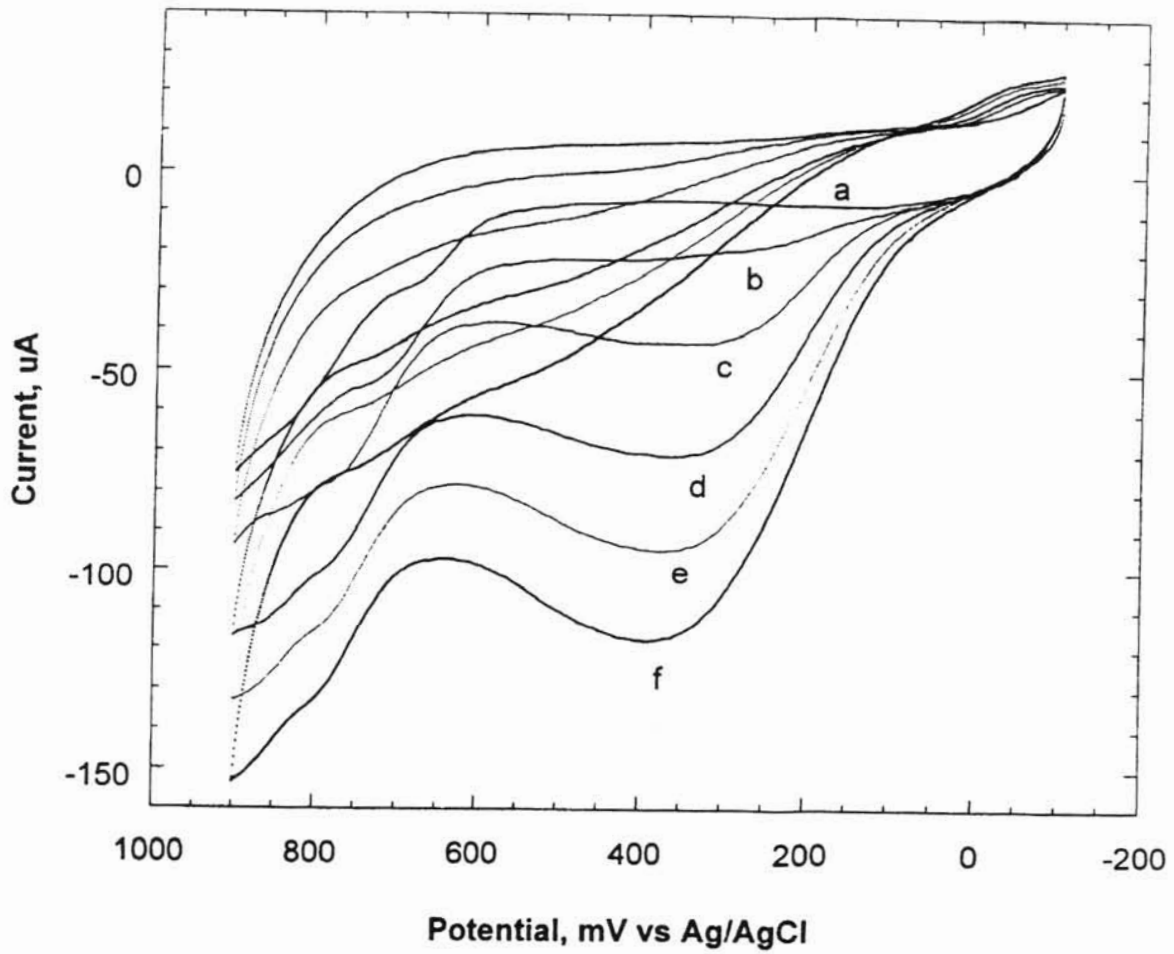


FIG. 3

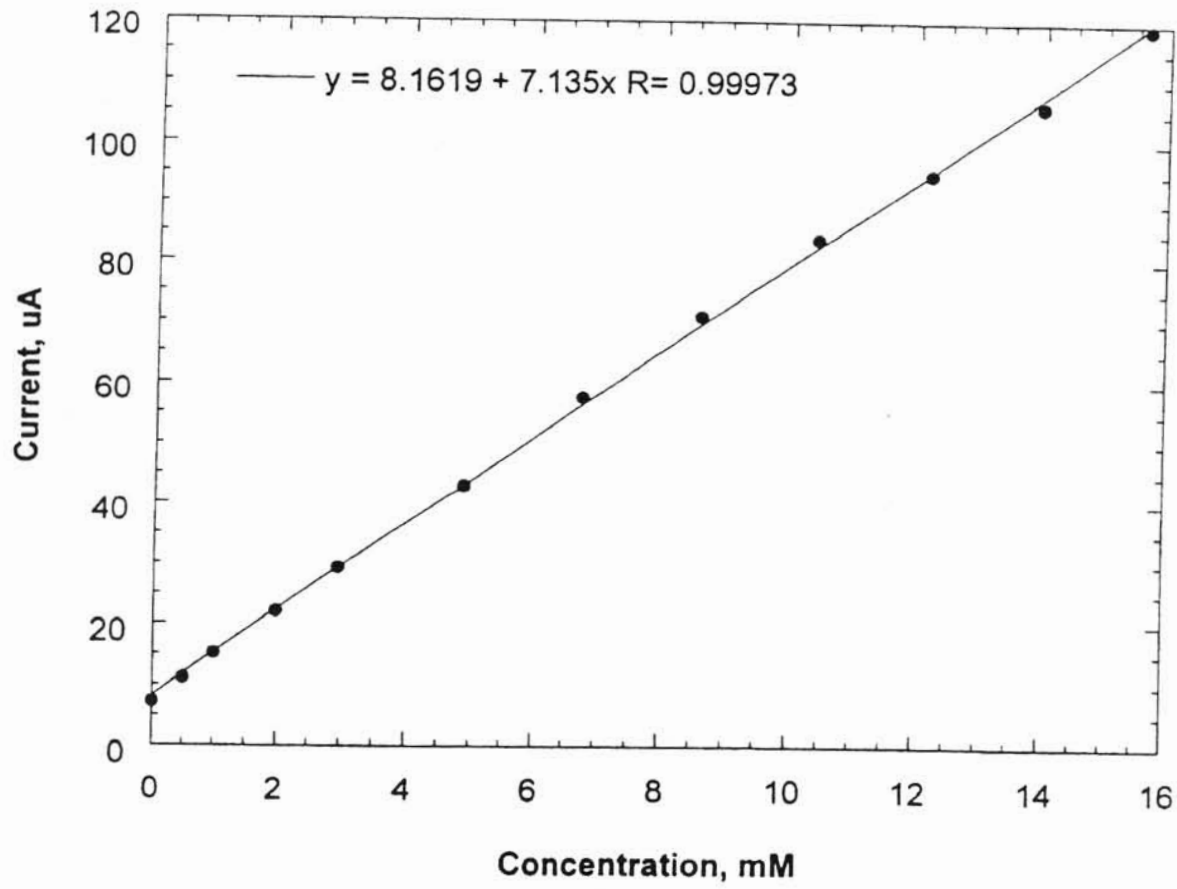


FIG. 4

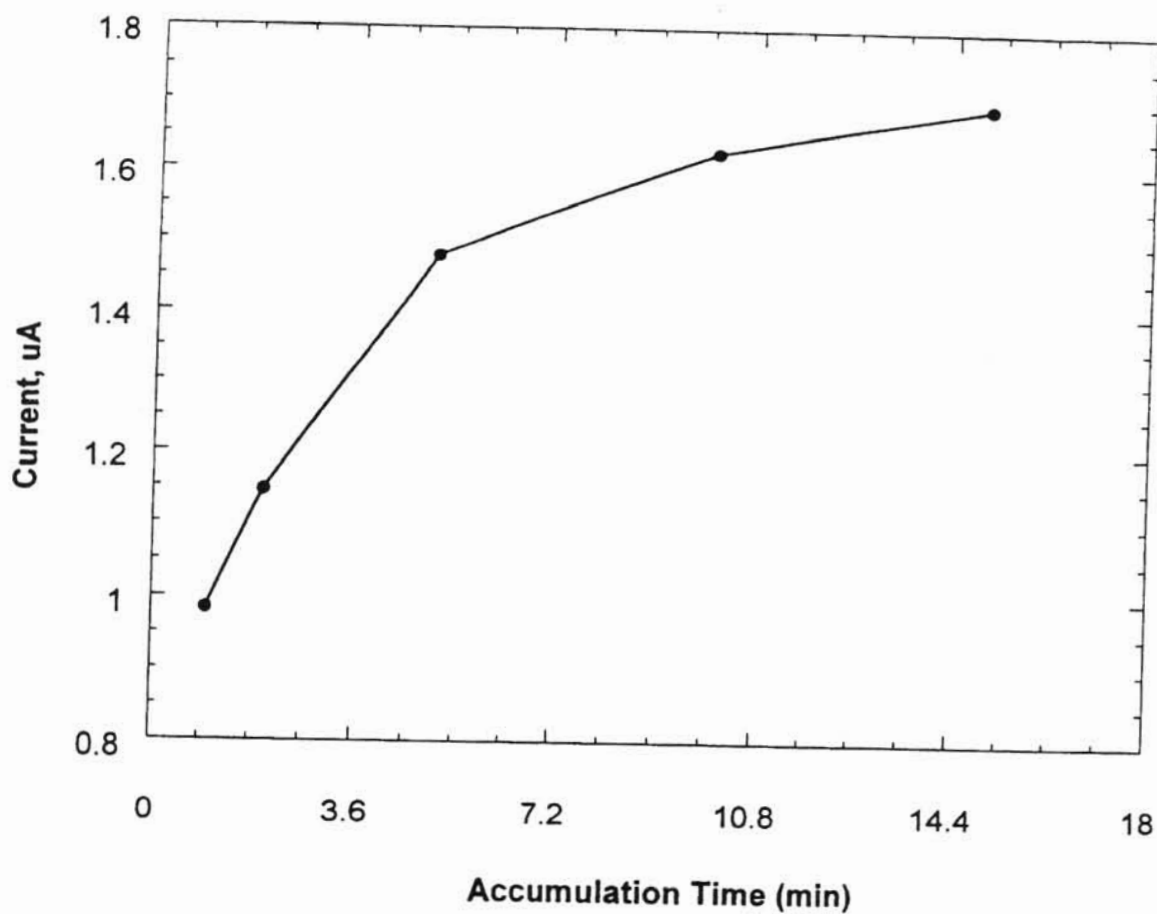


FIG. 5

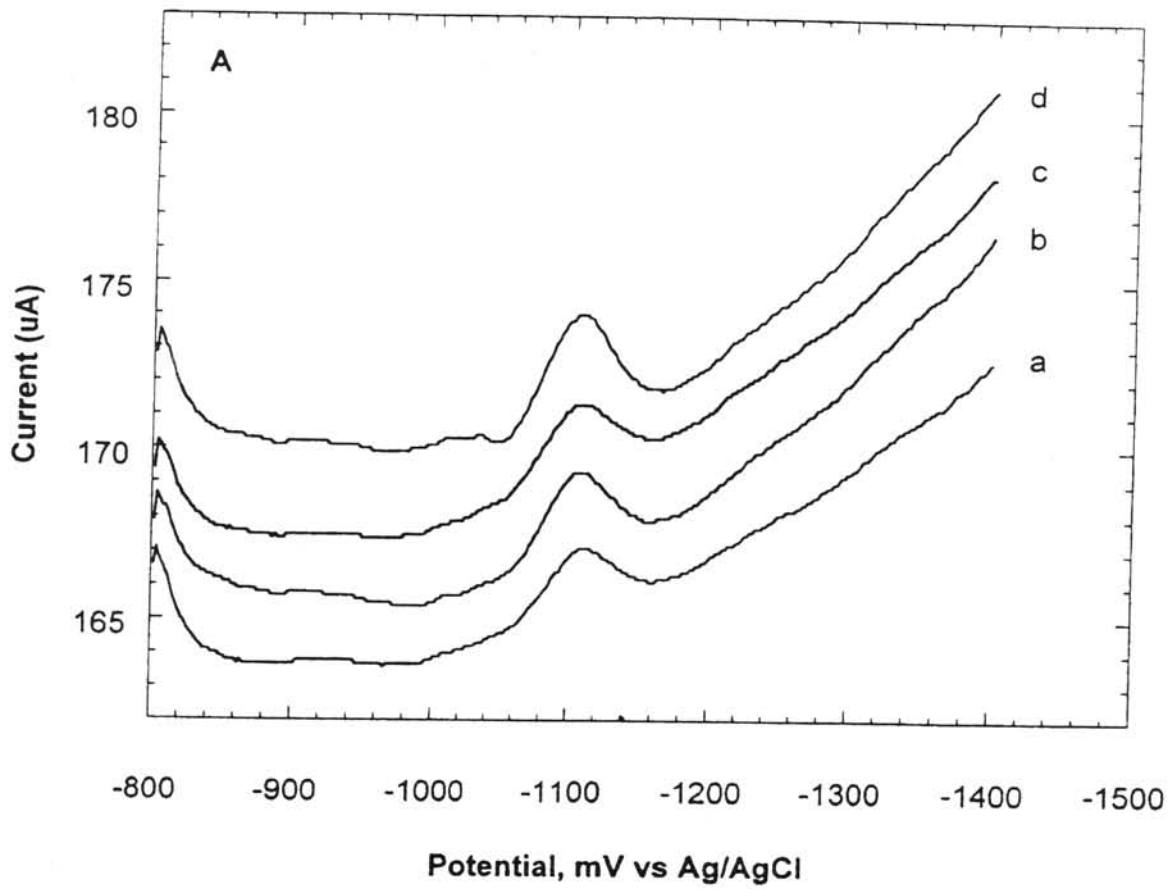


FIG. 6A

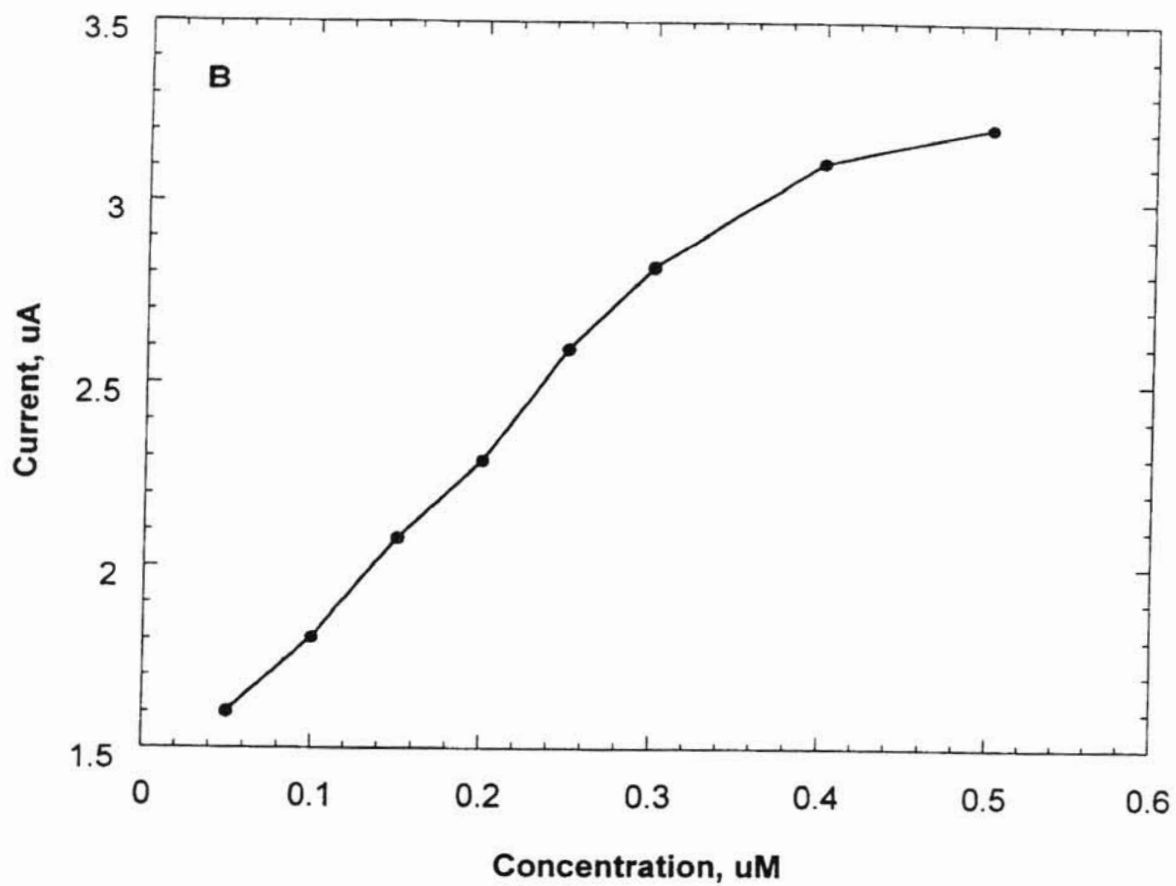


FIG. 6B

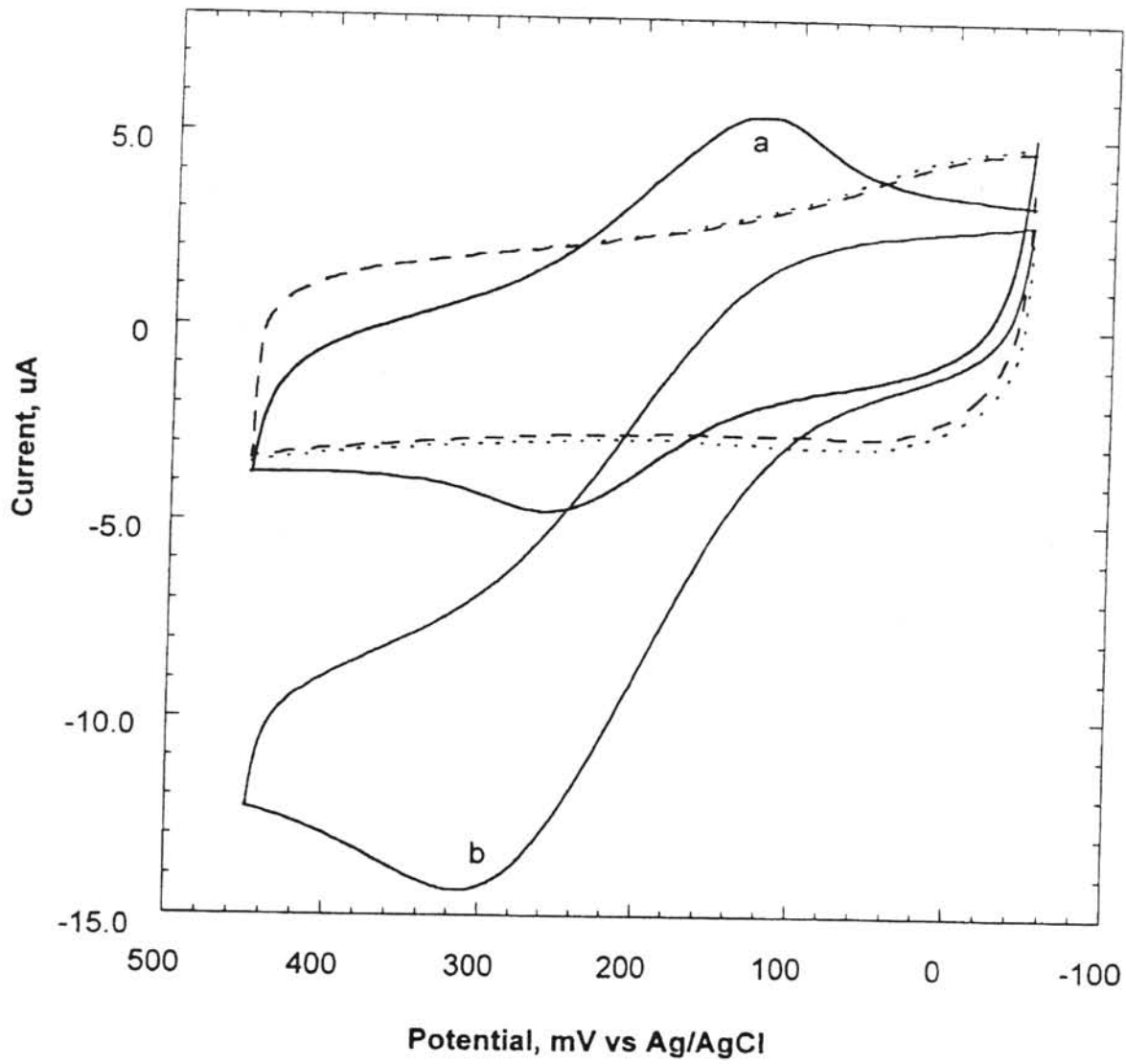


FIG. 7

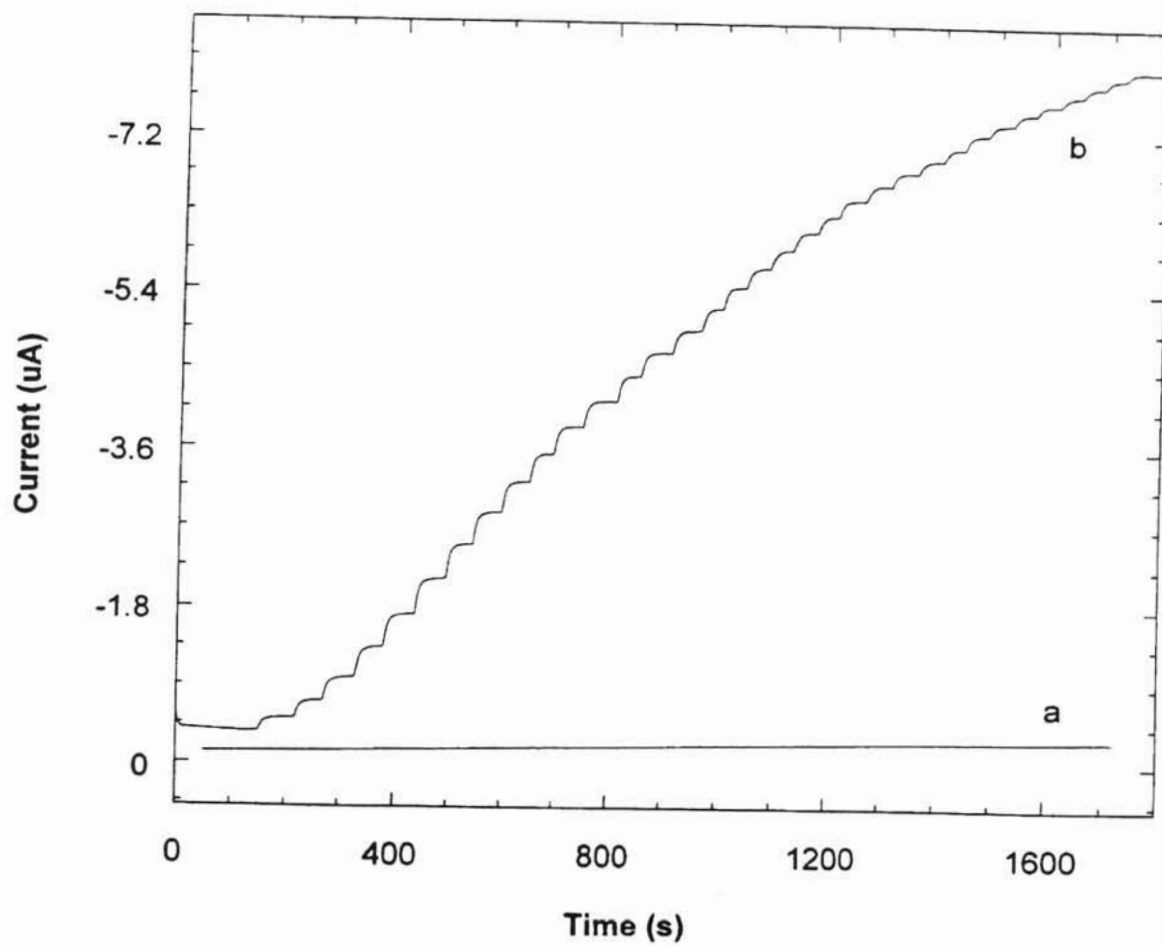


FIG. 8

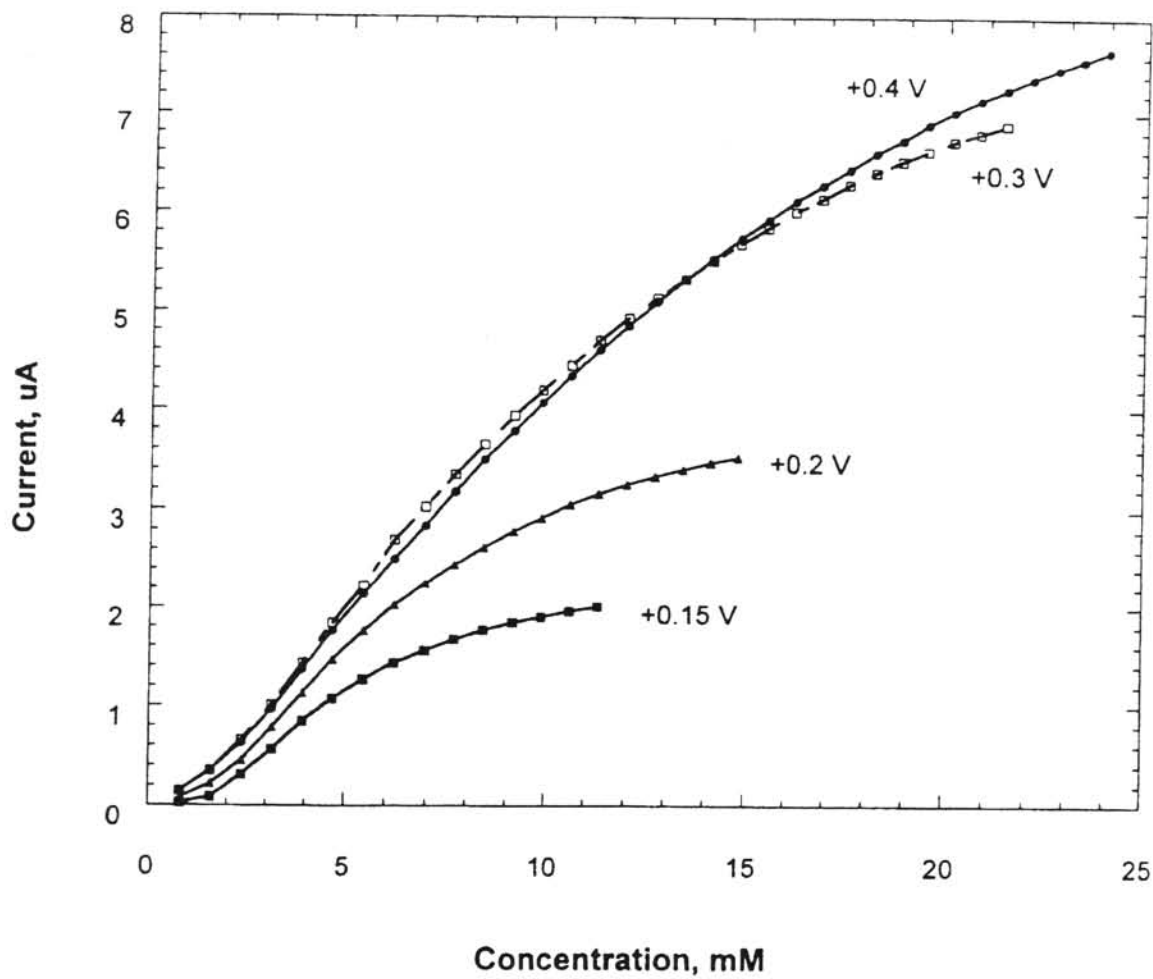


FIG. 9

**ELECTROANALYTICAL APPLICATIONS OF  
SCREEN-PRINTABLE  
SURFACTANT-INDUCED SOL-GEL  
GRAPHITE COMPOSITES**

This application claims the benefit under 35 USC 119(c) of provisional patent application No. 60/063,160, filed Oct. 29, 1997.

The subject matter of this invention was made with the financial support of the U.S. government, under the following grants: DOE-EPSCOR (Grant number 046138) and NIH-MBRS Program (Grant Number S06 GM 08102). The U.S. government has certain rights in this invention.

This invention relates to a novel process for preparing sol-gel graphite composite electrodes, and to the composite electrodes produced therefrom.

Carbon paste and graphite composites with their unique properties of easy and bulk modification, renewable surface and low background currents have found wide applications in electrocatalysis and electroanalysis. Carbon inks are commonly and commercially used for the microfabrication of electrochemical sensors and biosensors based on thick-film technologies. The selectivity of these surfaces is enhanced by their modification with a recognition entity chosen according to the analytes to be determined. The simple mixing of the surface modifier with the graphite before the electrode assembly has always presented the problem of modifiers leaching with concomitant detrimental effects on the electrochemical response. Recently, sol-gel graphite composite electrodes have been reported for biosensors and chemical sensors and procedures for screen-printed electrodes with these composites. Sol-gel networks are promising encapsulation matrices because mild polymerization conditions and low gelation temperatures can be used allowing the encapsulation of fragile biological molecules. Furthermore, properties such as porosity, hydrophilicity and matrix chemical modification can be controlled in the preparation process to avoid the leaching problem and enhance the analyte diffusion and selectivity.

Generally, sol-gel reactions proceed by hydrolysis of an alkoxide precursor under acidic or basic conditions, and subsequent condensation of the hydroxylated monomers to form a porous gel. The addition of a co-solvent is necessary to mix the alkoxide with water.

**SUMMARY OF THE INVENTION**

To avoid the previously discussed problems, the present invention is directed to a novel process for preparing sol-gel graphite composite electrodes, which comprises introducing a surfactant into the process and thus avoiding the need for a co-solvent, a catalyst, a cellulose binder and thermal curing. This process is more environmentally friendly and compatible for organics and biomolecules immobilization, and offers an economical one-step fabrication of screen-printed modified electrodes. Additionally, composite electrodes produced from this novel process exhibit improved properties previously not taught in the prior art. Specifically, the resulting composite electrodes have a fine texture, and exhibit excellent adhesion and mechanical strength when exposed to both aqueous and non-aqueous solutions.

Because composites generally have low electrical resistance and good adhesion to various substrates (e.g., PVC, ceramics, metals, glass), this procedure offers an economical, one-step and low cost fabrication of screen-printed modified electrodes. Therefore, a further object of the present invention is to demonstrate electroanalytical applications of this composite in electrocatalysis and

electroanalysis, specifically for composite electrodes in chemical sensors and biosensors.

Biosensors have been in the market place for several years, of which glucose sensors have prevailed, creating a large and stand-alone business. Disposable single-use sensors are one of the main products used by diabetic patients. However, to be more competitive with the existing methodologies on a large scale, many aspects should be improved to make them less expensive, user and environment friendly, and more easily manufactured (less complex to readily control quality and cut costs). Printing inks are obviously one of the critical components determining the products' performance and acceptance. And many efforts have been made in this field. UV-polymerizable screen-printable composites have been produced for more durable enzyme sensors. Screen-printable sol-gel enzyme-containing carbon inks offer a one-step fabrication of disposable enzyme strips obviating the need for thermal curing.

Besides the low cost and easy fabrication, the mediated glucose sensor that can be prepared in accordance with the present invention possesses excellent characteristics such as low operation potential (+0.3 V) and therefore less interferences, a wide working range (up to 30 mM) with a linear range up to 15 mM, a short response time (around 10 seconds) and long-term stability and shelf time.

In accordance with the present invention, disposable complexing (pre-concentrating) screen-printed strip electrodes for trace nickel have been fabricated by doping a sol-gel graphite composite with ligand dimethylglyoxime. Optimum quantitation procedures and parameters have been identified. A short (1 minute) accumulation period using open-circuit condition yielded a detection limit of 2  $\mu\text{g/L}$  nickel. Fabrication of screen-printed environmental sensors by incorporation of ligands into carbon inks holds promise in routine trace metal speciation and quantitation based on the conventional pre-concentration/voltammetric strategy. For example, cobalt phthalocyanine (CoPC) modified composite electrode shows a behavior different from previous studies, indicating differences in charge and mass transport of species in these composite electrodes compared to traditional carbon paste electrodes. In addition, the surfactant-induced sol-gel polymerization that occurs in accordance with the present invention allows the encapsulation of fragile molecules under relatively mild conditions. This polymerization beneficially results in a mechanically and chemically stable surface for organic solvents.

Additional features and advantages of the present invention will be set forth in part in the description that follows, and in part will be apparent from the description, or may be learned by practice of the invention. The objectives and other advantages of the present invention will be realized and attained by means of the elements and combinations particularly pointed out in the written description and appended claims.

**BRIEF DESCRIPTION OF THE DRAWINGS**

FIG. 1. FIG. 1 illustrates a cyclic voltammogram of ferrocene in acetonitrile at the unmodified SSCEs when the solution comprises 5 mM Fc, 0.1M TEATS, wherein the scan rate is 20 mV/s.

FIG. 2. FIG. 2 illustrates a cyclic voltammogram of reduced glutathione at the unmodified SSCEs when the solution comprises (a) pH5.5 PBS; (b) a+6.76 mM GSH; (c) a+15.67 mM GSH, wherein the scan rate is 10 mV/s.

FIG. 3. FIG. 3 illustrates a cyclic voltammogram of reduced glutathione at the CoPC modified SSCEs when the

3

solution comprises pH 5.5 PBS containing (a) 0.0, (b) 1.98, (c) 4.88, (d) 8.16, (e) 12.21, (f) 15.67 mM GSH, and the scan rate is 10 mV/s.

FIG. 4. FIG. 4 illustrates the corresponding calibration plot from FIG. 3.

FIG. 5. FIG. 5 illustrates the dependence of the OSW peak current on the accumulation time in a quiescent  $\text{Ni}^{2+}$  solution (2.0  $\mu\text{M}$ ) at open circuit.

FIG. 6. FIG. 6A illustrates Osteryoung square wave voltammetric responses of the DMG modified SSCEs for various nickel concentrations when the solution is ammonia buffer (pH 9.2) containing (a) 0.1, (b) 0.2, (c) 0.3, and (d) 0.4  $\mu\text{M}$   $\text{Ni}^{2+}$ , the scan ratio is 10 mV/s, the amplitude is 25 mV, the accumulation condition is a 1 min in-stirred solution. FIG. 6B represents a corresponding calibration plot.

FIG. 7. FIG. 7 illustrates a cyclic voltammograms of (Ferrocene+GOx) modified (solid curves) and unmodified (dashed and dotted curves) SSCEs in PBS (pH 6.95) containing 0.0 mM glucose (curve a and dashed curve) and 10.0 mM glucose (curve b and dotted curve), with a scan rate of 5 mV/s.

FIG. 8. FIG. 8 illustrates chronoamperometric responses of (ferrocene+GOx) modified (b) and unmodified (a) SSCEs to successive addition of 0.8 mM glucose when the solution comprises PBS (pH 6.95), uses a stirring rate of 250 rpm, and an applied potential of +0.3 V.

FIG. 9. FIG. 9 illustrates calibration plots for the (ferrocene+GOx) modified SSCEs at different applied potentials.

#### DETAILED DESCRIPTION OF THE INVENTION

This invention as broadly described above is directed to a method of producing surfactant-induced, sol-gel graphite composite electrodes by mixing an aqueous solution of a silane or a siloxane with a surfactant to get a clear and homogeneous sol solution. Specifically, Applicants have discovered that by incorporating a surfactant into the sol solution, the need for a co-solvent, a catalyst, or a cellulose binder is eliminated. Elimination of these components in turn eliminates the need for a thermal curing process that has been required until now when producing such electrodes.

Once a homogeneous sol solution is achieved, it is mixed with a graphite powder to form a uniform and free-flowing paste and applied to a substrate to form at least one electrode. Preferably, several electrodes can be formed at one time. While screen printing has been used to produce advantageous electrodes, this step may be performed using other traditional thick-film techniques.

This invention is further directed to a surfactant-induced, sol-gel graphite composite electrode. Applicants have discovered that such surfactant-induced electrodes can be fabricated into smooth films that exhibit high adhesion, mechanical strength and stability on the substrate to which they are applied. Such electrodes have the unexpected property of being stable in both aqueous and non-aqueous solutions.

Surfactant-induced sol-gel graphite-composites were prepared and analyzed using a variety of materials in accordance with the invention. Various silanes and siloxanes, including tetramethyl orthosilicate (TMOS), methyltrimethoxysilane, tetraethoxysilane, and methyltriethoxysilane, and different surfactants, including bis(2-ethylhexyl) sulfosuccinate, i.e., Aerosol OT (AOT), an octylphenol ethylene oxide condensate, i.e., Triton X-100,

4

cetyltrimethylammonium bromide (CTAB), and sodium dodecylsulfate (SDS) were tested as components of the sol solution. Advantageous and unexpected results were obtained for the (AOT+TMOS) systems, with respect to the viscosity, gelation time, mechanical strength, and compatibility with the graphite powder.

AOT in the system may act as a catalyst for the sol-gel formation, and a dispersing agent for homogenizing the carbon particles and incorporated reagents. Addition of surface active agents during sol-gel process are known to result in greatly improved homogeneity, remarkably smooth surface texture, and high adhesion between gel film and substrates. The introduction of AOT eliminates the use of such additives as alcohol cosolvents, acid catalyst, and cellulose binders, which simplifies the fabrication processes. For example, the elimination of such additives reduces the parameters influencing the final products' performances. In turn, the complexity and cost are reduced.

The following materials are advantageously used in accordance with the present invention: Ferrocene from Alfa Chemicals; Acetonitrile (water content less than 0.001%) from Burdick and Jackson; Glucose, glucose oxidase (GOx, EC 1. 1.3.4, from *Aspergillus niger*, 166,100 units/g), and glutathione (reduced form, GSH) from Sigma; Cobalt phthalocyanine (CoPC), bis(2-ethylhexyl) sulfosuccinate (sodium salt, AOT) from Fluka; Graphite powder (Grade #38) from Fisher Scientific; Tetramethyl orthosilicate (TMOS) from Aldrich; Dimethylglyoxime (DMG) from Matheson Coleman and Bell; Nickel ammonium sulfate from J. T. Baker; Tetraethylammonium 4-toluenesulfonate (TEATS) from Acros. The reagents should be at least analytical reagents and can be used as received. All aqueous solutions were prepared using nanopure water (18  $\Omega$ .cm). PVC (48"×96"×1 mm, Sintra sheet-white) from United States Plastic Corp. Ceramic sheets (4.5 inch×4.5 inch×0.45 mm) obtained from Coors Ceramics Company.

#### Apparatus Used for Electrode Measurements

Voltammetric (cyclic and Osteryoung square wave (OSWV)) and amperometric measurements were carried out at room temperature with a Bioanalytical Systems Model 100 B/W potentiostat in a 10-ml cell containing a SSCEs working electrodes, a Ag/AgCl (3M NaCl) reference electrode and a Pt wire auxiliary electrode. All potentials in the text are referred to the Ag/AgCl electrode without regard for the liquid junction. pH measurements were made with a  $\phi$ 50 pH meter (Beckman).

#### Preparation of Sol-gel Graphite Mixtures

Sol-gel graphite mixtures were prepared using the following procedures. The mixing of AOT:TMOS:H<sub>2</sub>O (1:50:200, molar ratio) readily gave a clear and homogeneous solution. Immediately prior to use, 1 ml of the sol solution prepared above was added to 0.6 g graphite powder in a small glass vial and well mixed for about 3 minutes to give a uniform free-flowing paste.

For the modified electrodes, a modifier or recognition entity that included ferrocene was used. The ferrocene was first dissolved in ethanol. After the solvent evaporated, an enzyme was added. More specifically, prior to addition of the sol, the graphite powder was mixed with ferrocene (2.5%, w/w expressed as ferrocene with respect to graphite) which was first dissolved in ethanol, glucose oxidase (5%) buffer solution or cobalt phthalocyanine (5%), dimethylglyoxime (10%) ethanol solution, and then dried at room temperature.

#### Preparation of Electrodes by Screen Printing

After the sol-gel step, a preferred method of screen-printing the modified and non-modified graphite electrodes

5

proceeded in the following manner. A home-made screen-printer was used to fabricate the surfactant-induced sol-gel derived carbon working electrodes (SSCEs). Pretreated PVC or ceramic sheets were used as substrates. Pretreatment preferably included coating the substrate with a clear nail polish. The paste was printed onto the pretreated PVC substrates (2.5×4.0 cm) to yield eight strips of 2.5×0.5 cm with 2.0×0.15 cm working electrode pattern. A portion of the electrode surface was covered with nail-polish insulating layer, leaving 0.1 cm<sup>2</sup> area on both ends for defining the working electrode and the electrical contact. For applications in organic solvents, the insulating layer was wrapped with Parafilm (American National Can).

#### Preparation of Buffered Solutions

Buffered solutions were subsequently prepared for further studies. Phosphate buffer (PBS) was used for glucose determinations (pH 6.95) and glutathione (GSH) determinations (pH 5.5). A 0.1M ammonia buffer solution (pH 9.2) served as the supporting electrolyte for nickel quantitation. Acetonitrile containing 0.1M TEATS was employed for the non-aqueous electrochemical studies.

#### Evaluation of Electrodes

Electrodes fabricated from the surfactant-induced sol-gel composites prepared in accordance with the present invention were evaluated and found to be mechanically strong. They also possessed a high adhesion to ceramics, glass and metal sheets, and weighing paper except PVC, on which the coated film was readily cracked and peeled off. However, due to its low cost and better processing characteristics, PVC is one of the most commonly and commercially used substrates in the fabrication of screen-printed strips. It was found that excellent performance (high adhesion, mechanical strength and stability, and smooth film) was obtained with slightly pretreated PVC substrates. Therefore, the pretreated PVC was used as substrate in the examples presented herein.

#### Evaluation of Electrical and Microstructural Properties

The screen-printed carbon strips were evaluated and found to have low electrical resistance. They gave resistance values of approximately 100 Ω over a 1-cm electrode length, obviating the need for a conducting metal layer and thermal curing. They thus provide a rapid and economical one-step fabrication of screen-printed electrodes. Scanning electron micrograph studies revealed a microporous structure of the electrode surface with particles of different size, reflecting a high surface area.

#### Evaluation of Stability in Organic Solvent

The stability of the inventive sol-gel graphite composite electrodes in organic solvent was evaluated. Carbon paste electrodes or robust carbon composite electrodes are usually made of carbon powder dispersed in organic polymers, e.g., wax, epoxy, poly(chlorotrifluoroethylene) or organic liquids, e.g., paraffin oil, silicone, Nujol, grease. The use of organic binders has generally hindered their applications in nonaqueous solutions due to their dissolution. Sol-gel graphite composite electrodes in accordance with the present invention are a reasonable alternative to this problem, because the inorganic matrices thereof are stable in both aqueous and nonaqueous media. To investigate the stability of the surfactant-induced sol-gel graphite composite electrodes of the present invention in organic solvents, the electrochemistry of ferrocene (Fc) in acetonitrile (AN) was studied with the SSCEs. FIG. 1 shows the cyclic voltammograms of Fc in AN at unmodified SSCEs after 1, 3 and 5 hours of immersion in stirred AN solution. There was a slight increase in the peak current after 1 hour immersion.

6

This may have been due in part to some dissolution of the surfactant, which increased the electrode area. Another possibility is the dissolution of the insulating nail-polishing layer, which would also expose a greater electrode surface area. There were no obvious differences between the second, the third and the fourth cycles; thereby demonstrating a high stability of the composite electrodes in organic solvents.

The invention is illustrated in greater detail in the following, non-limiting examples.

#### EXAMPLE 1. Electrodes for Electrocatalytic Applications

To demonstrate the potential use of the electrode surfaces of the electrodes prepared in accordance with the present invention for catalyst immobilization, cobalt phthalocyanine (CoPC) was immobilized into the SSCEs and used in the electrocatalytic determination of GSH. FIG. 2 shows the cyclic voltammograms of GSH at the unmodified SSCEs. The onset potential for the direct oxidation of GSH at this electrode was about +0.4 V, as demonstrated by an anodic current increase as a function of GSH concentration when the applied potential exceeded +0.6 V. Meanwhile, at the CoPC modified electrodes, the electrocatalytic current started rising at potentials +0.05 V, and an anodic peak was observed around +0.35 V (see FIG. 3). The peak current was found to be proportional to the GSH concentration up to 15 mM, as shown in FIG. 4. The immobilized CoPC acted as a mediator, accelerating the rate of GSH oxidation at low overpotentials. On these experiments, two anodic waves were observed, e.g., ca.+0.3 V and +0.78 V at a CoPC modified electrode. The peak at +0.3 V, occurring only in the presence of GSH, was assigned to the oxidation of Co<sup>I</sup> to Co<sup>II</sup> and the peak at +0.78 V, occurring in the absence and presence of GSH, was considered to be the oxidation of Co<sup>II</sup> to Co<sup>III</sup>. The current at +0.78 V was about 3 times higher than that at +0.3 V previously discussed in the art while the anodic wave at +0.3 V was better developed on SSCEs. The higher efficiency of the Co<sup>I</sup>/Co<sup>II</sup> center may have been due to more accessibility of the catalyst incorporated in the porous SSCEs and higher conductivity of the SSCEs matrix, which appeared to facilitate the mass transport and electron transfer.

#### EXAMPLE 2. Metal Ion Sensitive Electrodes

While most electroanalytical applications of chemically modified electrodes have been focused on electrocatalysis, a few have employed pre-concentration/voltammetric strategy based on immobilized ion exchangers, organic coordinating ligands, clays, etc., which have shown great analytical promise, especially for the speciation and quantitation of trace metals in environmental monitoring and control. For example, complexation and quantitation of lead was performed with DPT modified SSCEs. In addition, to demonstrate the feasibility to construct disposable metal ions sensitive electrodes with SSCEs, dimethylglyoxime (DMG) was incorporated into the SSCEs for the detection of trace nickel.

The quantitation procedure comprised three steps: the accumulation, measurement, and cleaning steps. For the Ni<sup>2+</sup> pre-concentration, the electrode was immersed in the stirred or quiescent sample solution for a few minutes at an open circuit or at an applied potential. Then, the accumulated nickel was measured by Osteryoung Square Wave Voltammetry (OSWV) in pH 9.2 ammonia buffer. Last, following each measurement, the electrode was immersed in 0.1M HCl solution for a 30 seconds cleaning step and then rinsed with water.

The accumulation conditions advantageously influence, and/or optimize, sensor response time, sensitivity and the detection limit. Accumulation in stirred or quiescent solution at open circuit or a certain applied potential was investigated.

Table 1 shows the electrode response under different accumulation conditions.

TABLE 1

Electrode Responses Under Different Accumulation Conditions with the DMG Modified SSCEs				
conditions*	1	2	3	4
unstirred	✓			✓
stirred		✓	✓	
open circuit	✓	✓		
applied potential (-0.5 V)			✓	✓
current (μA)	0.96	1.39	1.18	0.92

\* Accumulation time: 1 min; Accumulation solution:  $[Ni^{2+}] = 5 \times 10^{-7}$  M.

As can be seen from the results presented in Table 1, accumulation in a stirred solution at an open circuit gave the highest sensitivity, which was comparable to the response observed in the unstirred solution or under an applied -0.5 volts. These results suggest that the use of an applied potential may be unnecessary. FIG. 5 shows the dependence of response current on accumulation time in quiescent solutions at an open circuit. FIG. 5 shows that 5 minutes accumulation in quiescent solution gave comparable results with the 1 minute in stirred solution.

One minute accumulation in stirred solution was used in the following evaluation. FIG. 6 shows the Osteryoung square wave voltammetric responses of the DMG-modified SSCEs for various nickel concentrations and the corresponding calibration plot. Well-defined peaks were obtained over this low concentration range. Linear responses were attained between 0.05 and 0.3 μM. A detection limit of 0.02 μM (about 2 μg/L) was achieved under these quantitation conditions.

### EXAMPLE 3. Mediated Glucose Biosensor

A mediated glucose biosensor was prepared and evaluated by incorporating mediator ferrocene and enzyme glucose oxidase into the composite. Cyclic voltammograms in FIG. 7 (solid curves a and b) show the mediated biocatalysis of glucose on the FcGOx modified SSCEs. Curve a shows the redox process of the immobilized Fc in PBS background solution. As shown, the anodic current increased with the addition of glucose (curve b). However, no obvious change occurred on the unmodified electrodes (dashed and dotted curves in FIG. 7). FIG. 8 shows the chronoamperometric responses of glucose on the modified (b) and unmodified (a) SSCEs. No response was observed on the unmodified electrodes, while rapid and sensitive responses occurred on the modified electrodes. Steady-state currents were obtained within 10 seconds, with linearity up to 15 mM and a useful working range from 0.05 mM to 30 mM. Such fast response may be attributed to the absence of any covering membrane and the porous character of the composite surface. FIG. 9 shows the calibration plots for the Fc-GOx modified SSCEs at different applied potentials.

The potential-dependent performances of the modified electrodes are summarized in Table 2.

TABLE 2

Potential-Dependent Performances of the (Ferrocene + GO <sub>x</sub> ) Modified Carbon Strips				
applied potential (mV)	+150	+200	+300	+400
$K_M^{app}$ (mM)	8.5	9.5	16.2	22.9
$I_s^{max}$ (μA)	3.5	5.8	12.1	15.0
linear range (mM)	0-5	0-8	0-15	0-15
sensitivity (μA/mM)	0.33	0.42	0.52	0.39

<sup>a</sup>, <sup>b</sup>calculated from  $I_s = I_s^{max} - K_M^{app} (I_s/C_s)$

<sup>c</sup>calculated from the linear portion of the calibration curve.

As shown in Table 2, quick background stabilization, rapid response, high sensitivity, and wide linearity were obtained at an applied potential of +0.3 V. Although designed for disposable single-use sensors, these biosensors are very durable and robust. No obvious deterioration in responses were observed for a period of three months with intermittent uses for these sensors kept at room temperature.

It is to be understood that both the foregoing general and detailed description are exemplary and explanatory only and are intended to provide further explanation of the invention, as claimed.

What is claimed is:

1. A method for preparing a surfactant-induced, sol-gel graphite composite electrode, said method comprising the steps of:

25 mixing an aqueous solution of the surfactant with a silane or a siloxane to obtain a clear and homogeneous sol solution, wherein said mixing is performed in the absence of a co-solvent, a catalyst, or a cellulose binder;

30 mixing said sol solution with graphite powder to form a uniform and free-flowing paste; and

35 applying said paste onto a substrate to form at least one electrode;

wherein a thermal curing process step is not required.

40 2. The method of claim 1, wherein the graphite powder is mixed with a buffer solution or an alcohol solution containing a modifier or recognition entity for an analyte, wherein said modifier or recognition entity is chosen according to the analyte to be determined, and dried prior to being mixed with the sol solution.

45 3. The method of claim 2, wherein the buffer solution or alcohol solution comprises ferrocene and glucose oxidase.

4. The method of claim 2, wherein the alcohol solution is an ethanol solution.

50 5. The method of claim 1, wherein the substrate is PVC, a ceramic, a metal, or a glass.

6. The method of claim 1, wherein the silane or siloxane is tetramethyl orthosilicate, methyltrimethoxysilane, tetraethoxysilane, or methyltriethoxysilane, and the surfactant is surfactant bis(2-ethylhexyl) sulfosuccinate, octylphenol ethylene oxide condensate, cetyltrimethylammonium bromide, or sodium dodecylsulfate.

7. The method of claim 6, wherein the siloxane is tetramethylorthosilicate and the surfactant is surfactant bis(2-ethylhexyl) sulfosuccinate.

8. The method of claim 1, wherein the paste is applied onto the substrate to form at least one electrode by screen printing.

\* \* \* \* \*